TU Delft

Technische Universiteit Delft

Faculteit der Civiele Techniek
Vakgroep Waterbouwkunde

Suspended-load experiments in a curved flume, run no. 2

A.M.Talmon

report no. 4-89, August 1989

part of:
STW-project; River bend morphology with suspended sediment.

Delft University of Technology
Faculty of Civil Engineering
Hydraulic Engineering Division

ABSTRACT

A laboratory experiment in a 180 degree curved flume with a mobile bed and suspended sediment transport is described. The flow is steady.

The aim the of experiment is to obtain data on the axi-symmetrical region.

The bed topography is measured by means of a profile indicator. Downstream of the bend entrance a pool and a submerged point-bar are present, here the radial bed slope is maximal. Further downstream the transverse bed slope decreases and converges to a constant transverse slope (constant with streamwise direction), here the bed topography is axi-symmetrical.

Suspended sediment concentrations are determined by the method of siphoning. Concentration verticals are measured throughout the whole bend (at 1/4, 1/2 and 3/4 of the channel width). In the region were the bed topography is axi-symmetrical a denser measuring grid is used. The measurements indicate that the concentration field is also axi-symmetrical.

CONTENTS

LIST OF TABLES

LIST OF FIGURES

LIST OF SYMBOLS

a	local ensemble mean water depth	[m]
a'	local fluctuation of bed level	[m]
a_0	mean water depth of cross-section 1	[m]
$\hat{a}$	complex amplitude of bed oscillation	[-]
A	critical mobility number	[-]
B	mobility parameter; $B = \tau_{cr}/(\mu\tau)$	[-]
c	local concentration	[g/l]
c_r	concentration at reference level	[g/l]
$\bar{c}$	local depth averaged concentration	[g/l]
$\bar{c}_{tr}$	total transport concentration; $\bar{c}_{tr} = Q_s/Q_w \ 10^{-3}$	[g/l]
$\bar{c}_{trb}$	transport conc. of bed-load; $\bar{c}_{trb} = S_{s\ bed}/(\bar{u}a_0) \ 10^{-3}$	[g/l]
$\bar{c}_{trs}$	transport conc. of suspended-load; $\bar{c}_{trs} = S_{s\ sus}/(\bar{u}a_0) \ 10^{-3}$	[g/l]
C	parameter in Ackers White formula	[-]
C	Chézy coefficient, with $d=a_0$; $C = \bar{u}/\sqrt{(di)}$	[$m^{0.5}/s$]
C_r	Chézy coefficient, with $d=r_b$; $C_r = \bar{u}/\sqrt{(di)}$	[$m^{0.5}/s$]
d	a representative water depth	[m]
D_{gr}	dimensionless grain diameter; $D_{gr} = D_{50}(\Delta g/\nu^2)^{1/3}$	[-]
D_g	geometric mean grain diameter; $D_g = \sqrt{(D_{84}/D_{16})}$	[m]
D_p	grain size for which p% of the grains is smaller than D_p	[-]
D_{50}	median grain size	[m]
D_s	sedimentation diameter	[m]
F_g	grain Froude number	[-]
F_{g0}	critical grain Froude number	[-]
F_{gr}	grain mobility number	[-]
Fr	Froude number, with $d=a_0$; $Fr = \bar{u}/\sqrt{(gd)}$	[-]
Fr_r	Froude number, with $d=r_b$; $Fr_r = \bar{u}/\sqrt{(gd)}$	[-]
G	coefficient in gravitation term	[-]
H	depth of the flume	[m]
i	water surface slope	[-]
k	complex wave number	[1/m]
k_b	wave number in transversal direction	[1/m]
k_{sn}	secondary flow convection factor	[-]
L_c	arc length of the bend	[m]
L_{cs}	length scale of adaptation of concentration	[m]
m	parameter in Ackers White formula	[-]
n	parameter in Ackers White formula	[-]
n	coordinate in transverse direction	[m]

P	wetted perimeter	[m]
Q_w	water discharge	[m^3/s]
Q_s	sediment discharge	[g/s]
r_b	hydraulic radius of the bed	[m]
r_u	profile function of the velocity profile	[-]
r_c	profile function of the concentration profile	[-]
R_c	radius of curvature of axis of flume	[m]
R_g	grain Reynolds number; $R_g = \sqrt{(gD_{50}^3)}/\nu$	[-]
s	coordinate in streamwise direction	[m]
$S_{s\ sus}$	transport rate of suspended sediment, per unit width, in s-direc.	[g/m/s]
$S_{n\ sus}$	transport rate of suspended sediment, per unit width, in n-direc.	[g/m/s]
S_{tot}	total transport rate, per unit width	[g/m/s]
T	water temperature	[^{0}C]
u	local depth averaged mean flow velocity	[m/s]
$\bar{u}$	overall averaged mean flow velocity: $\bar{u} = Q_w/(Wa_0)$	[m/s]
u_{cr}	critical depth averaged velocity	[m/s]
u_*	bed friction velocity, based on C : $u_* = (u\sqrt{g})/C$	[m/s]
u_{*r}	bed friction velocity, based on C_r: $u_{*r} = (\bar{u}\sqrt{g})/C_r$	[m/s]
W	width of the flume	[m]
w_s	fall velocity of sediment	[m/s]
Z	the Z parameter: $Z = w_s/(\beta\kappa u_*)$	[-]
z_r	reference level	[m]
z_s	surface level	[m]
β	ratio of exchange coefficients of sediment and momentum	[-]
β	coefficient in the bed shear-stress direction model	[-]
κ	von Karman constant	[-]
λ_c	adaptation length of concentration	[m]
λ_s	adaptation length of bed level	[m]
λ_{sf}	adaptation length of bed shear-stress	[m]
λ_w	adaptation length of velocity	[m]
μ	efficiency factor	[-]
ρ	density of water; ρ =1000 kg/m^3	[kg/m^3]
ρ_s	density of sediment; ρ_s=2650 kg/m^3	[kg/m^3]
σ_g	gradation of sediment; $\sigma_g = D_{84}/D_{16}$	[-]
τ	total drag	[N/m^2]
τ'	effective grain-shear stress; $\tau' = \mu\tau$	[N/m^2]

τ_{cr}	critical bed-shear stress	[n/m^2]
ν_{tm}	turbulent diffusion coefficient of momentum	[m^2/s]
ν_{tc}	turbulent diffusion coefficient of mass	[m^2/s]
θ	Shields number, with d=a_0: θ = di/(ΔD_{50})	[-]
θ_r	Shields number, with d=r_b: θ_r= di/(ΔD_{50})	[-]
θ_{cr}	critical Shields number	[-]
Δ	relative density of the sediment; Δ = 1.65	[-]

1. INTRODUCTION

The project at hand is directed towards the computation of river bend morphology in case of alluvial rivers transporting a significant part of their bed material in suspension.

In this report an experiment is described which will serve to calibrate and test morphological models for river bend flow with suspended sediment. The aim of the experiment is to obtain data on the axi-symmetrical region. The experiment is performed in the curved flume of the Laboratory of Fluid Mechanics. It is the second of a number of successive runs. The steady state bed topography and local concentrations of suspended sediment are measured.

In chapter 2 the laboratory equipment is described briefly. In chapter 3 the properties of the sediment and the overall flow conditions are given. In chapter 4 the results of the measurements of bed topography and concentration are reported. In chapter 5 the results are discussed, attention is being paid to implications regarding the mathematical and numerical simulation of the experiment. In chapter 6 the conclusions are presented.

This research is a part of the project: 'River bend morphology with suspended sediment', project no. DCT59.0842. The project is supported by the Netherlands Technology Foundation (STW).

2. LABORATORY EQUIPMENT

2.1 The flume

The layout of the LFM curved flume is shown in figure 1. Water is pumped from an underground reservoir to an overhead tank and led to the flume. The water discharge is controlled by a valve in the supply pipeline. Sand is supplied to the model 2 m downstream of the entrance of the flume. The sand supply is effectuated by two small holes, 2.5 mm diameter, in the bottom of a container located 0.5 m above the water surface.
After passing the tailgate of the flume, by which the water level is adjusted, the water pours in a settling tank. After passing this tank the water flows back into the underground reservoir.
The dimensions of the flume are:

inflow section length	11.00 m
outflow section length	6.70 m
arc length of the bend	L_c = 12.88 m
radius of the bend	R_c = 4.10 m
width of the flume	W = 0.50 m
depth of the flume	H = 0.30 m

The bottom of the flume is made of glass and the side walls are made of perspex.

2.2 Measuring equipment

2.2.1 Discharge measurement

The discharge is controlled by a valve in the supply pipeline.
The discharge is measured by a volumetric method. A 150 liters barrel is partly filled during about 25 seconds at the downstream end of the flume. The volume is measured and divided by the filling time.

2.2.2 Slope and depth measurements

The measurements of the bottom and water level are performed with an electronic profile indicator (PROVO). From these measurements the longitudinal slope of the water level and the local depth are calculated. This device is traversed in cross-sectional direction. In each cross-section 9 equidistant measuring points are used. The carriage in which the PROVO is mounted is also traversed in longitudinal direction. In longitudinal direction 48 cross-sections are situated, they are indicated in figure 5. The distance between these cross-sections at the flume axis is 0.32 m. The profile indicator is continuously moved in cross-sectional direction, this is achieved by specially developed electronic hardware. The position of the profile indicator is measured electronically. The carriage is moved manually in longitudinal direction.

2.2.3 Concentration measurement by siphoning

Throughout the whole bend sediment concentrations are measured. The sediment concentration is determined from samples siphoned by a tube-pipette of stainless steel (Outside diameter 5 mm, inside diameter 3 mm) shaped much like a pitot tube. The tip of the sampler is flattened in order to minimize the vertical extended of the measuring volume.
To prevent sand to accumulate in the plastic tube it is necessary to increase the sampling velocity. This yields a non-isokinetic sampling velocity slightly higher then the local flow velocity. This does not seriously affect measurements (Talmon and Marsman, 1988).
Measuring periods of about 45 minutes are employed.

2.2.4 Optical measurement of concentration

The optical concentration meter OPCON has not been used.
Although, according to the manual, concentrations are within the measurement range, an electronic drift excluded practical application of the OPCON.
The sensitivety of the OPCON is obtained by calibration:

$E = 2.24\ c$, c[g/l], E[V] at output 10x amplifier
The sensitivety of the OPCON to ambient temperature has been investigated under controlled conditions ($20^0 < T < 22^0$):
$\Delta E = -0.025\ \Delta T$, T^0, E[V] at output 10x amplifier
In the laboratory the ambient temperature gently increases from 16^0 at 8 p.m. toward 19^0 at 5 a.m. This yields an temperature effect of:
$\Delta E \approx -0.075$ V.
Concentrations are within 0.02 ... 0.15 g/l, this corresponds to: E= 0.045 ... 0.37 V. Provided that care is being taken when the smallest concentrations are measured, the OPCON should be applicable. In the laboratory, however, electronic drift up to 0.2 V (from 8 p.m. to 5 a.m.) is measured. This yields the conclusion that under the present conditions a zero concentration adjustment has to be made prior to each measurement. This very laborious.
Because of these problems and because much data had already been collected by siphoning it was decided not to use the OPCON.

2.2.5 Temperature measurements

Temperatures are measured by inserting a thermometer into the flow near the downstream end of the flume. The water temperature during the measurements was 20 ± 0.5 ^{0}C .

2.3 Measuring procedures

The flume is partly filled up with sand. The thickness of the sand bed at the entrance of the flume is 0.11 m, at the exit the bed thickness is about 0.08 m. The sieve curve of the sand is given in figure 2.
The sand supply is measured daily. The sand settled in the settling tank is gathered at regular intervals (about 14 to 22 hours) and is weighed under water. The results are converted to equivalent weights of dry sand. The supply rate is adjusted such that the supply rate and the discharge rate balance approximately.
The water surface slope in longitudinal direction is measured daily. After about 200 hours of flow, measurement of the bed topography and the concentration are started when steady conditions are established. At

that stage no significant changes of the water surface slope and differences between in and outflow of sand are measured.
The stationary bed topography is obtained by ensemble averaging of 11 measuring sessions. A measuring session consists of a water level - and a bed level measurement. The water level is measured during flow conditions. After closing the tailgate and filling the flume with water (about 100 mm above the bed level), the bottom is measured. This procedure to measure the bed topography is necessary, because the PROVO needs a minimal water depth of 25 mm. One measuring session takes about one hour. The average time interval between each session is about 5 hours, consequently the measuring sessions can be considered as independent.
Each session consists of 2 * 48 cross-sectional traverses (one bed and one water level measurement). Within a cross-section 9 measuring points are used. The data are digitized and stored at a local data-acquisition system which uses a HP1000 mini computer. Next, the data are processed by a central main frame IBM computer of the Delft University. From the mean water level in each cross-section the longitudinal slope is determined. Comparing the results of each measuring session, only local differences in the water level slope are noticed.

Most sediment concentration profiles are taken at the cross-section numbers 1, 5, 10, 15, 20, 25, 30, 35, 40, 45 (see figure 5).
In a vertical, depending on the local water depth, 5 to 40 samples are taken. The samples are siphoned into buckets. With a measuring time of 45 minutes about 9 liters water are gathered. The sample is weighed to determine the volume. Then the water is separated from the sediment. The sediment is weighed under water with an electronic balance (Mettler PE 360). Weights are read with an accuracy of 10 mg. The results are converted to equivalent weights of dry sand.

Near the bed it is not possible to take samples, because of propagating bedforms.

3. FLOW AND SEDIMENT CONDITIONS

3.1 The sediment

3.1.1 Sieve curve

The sediment used in the flume is prepared in a sieve-installation of the Laboratory of Fluid Mechanics. Figure 2 shows the cumulative probability distribution of the grain sizes of the sand, included are the parameters which describe size and grading of the sand. The quantity D_p is described as the grain size for which is p % of the total mixture volume, smaller then D_p. Characteristic diameters are:
D_{10}= 69 μm, D_{16}= 72 μm, D_{50}= 88 μm, D_{84}= 112 μm, D_{90}= 122 μm
The gradation of the sediment is: $\sigma_g = D_{84}/D_{16}$= 1.56
The geometric mean diameter is: $D_g = \sqrt{(D_{84}D_{16})}$= 90 μm

3.1.2 Fall velocity

The fall velocity of the suspended sediment is determined in a settling tube.
A settling tube is a device to determine the fall velocity distribution of particles in a sample. The analysis are made using the layer method. At the lower end of the settling tube the sediment particles accumulate on a very sensitive weighing device. A cumulative weight distribution of the sample as a function of the measuring time is obtained. This distribution is converted into the fall velocity distribution of the sample using the height of the settling tube (Slot and Geldof, 1986). The samples are siphoned 1.9 m upstream of cross-section 1 at respectively 10, 20, 30 mm below the water level. The probe is moved continuously in cross-sectional direction during the measuring period (30 minutes). Samples siphoned at the same height during several measuring periods are put together. The samples are dried and split into amounts that can be used in the settling tube.
Figure 3 shows the probability distribution of the fall velocity.
The mean fall velocity is: w_s = 0.0076 m/s.
The sedimentation diameter is calculated by the formula given by Slot (1983). The sedimentation diameter is: D_s= 100 μm.

3.2 Flow conditions

The flow conditions are given in table 3.1a and 3.1b. The values of parameters determined by measurement are given in table 3.1a. The values of parameters obtained by calculation are given in table 3.1b. In table 3.1b, Chézy, Froude and Shields parameters are given both based on the mean flow depth and the hydraulic radius related to the bed. The latter is based on the Vanoni and Brooks (1957) correction method for side wall effects.

Table 3.1a Measured parameters

Q_w	= 0.0077	$[m^3/s]$
W	= 0.50	[m]
a_0	= 0.072	[m]
i	= $1.7\ 10^{-3}$	[-]
D_{50}	≈ 88	[μm]
w_s	≈ $7.6\ 10^{-3}$	[m/s]
Q_s	= 1.08	[g/s] (output)
T	= 19.5	[°C]

Table 3.1b Calculated parameters

$\bar{u}$	$= Q_w/(Wa_0)$	= 0.214	[m/s]		
$\bar{c}_{tr}$	$=(Q_s/Q_w)10^{-3}$	= 0.140	[g/l]		
r_b	=	= 0.069	[m]		
<u>C, Fr, θ related to</u> a_0				<u>C, Fr, θ related to</u> r_b	
C	$= \bar{u}/\sqrt{(a_0 i)}$	= 19.4	$[m^{0.5}/s]$	$C_r = \bar{u}/\sqrt{(r_b i)}$	= 19.8 $[m^{0.5}/s]$
Fr	$= \bar{u}/\sqrt{(ga_0)}$	= 0.25	[-]	$Fr_r = \bar{u}/\sqrt{(gr_b)}$	= 0.26 [-]
θ	$= a_0 i/(\Delta D_{50})$	= 0.84	[-]	$\theta_r = r_b i/(\Delta D_{50})$	= 0.84 [-]
u_*	$= (\bar{u}\sqrt{g})/C$	= 0.035	[m/s]	$u_{*r} = (\bar{u}\sqrt{g})/C_r$	= 0.034 [m/s]
D_s	≈ 100 [μm]		(sec. 3.1.2.)		
Z	$= w_s/(\beta\kappa u_*)$	= 0.37	(sec. 4.2.2.)		

4. RESULTS

4.1 Depth measurements

4.1.1 Mean depth

The ensemble relative water depth of the 11 measuring sessions are tabulated in appendix A. Figure 5 shows the ensemble averaged contour line map of the relative water depth (normalized with the mean water depth of cross-section 1). The contour lines are drawn at intervals of $\Delta a/a0 = 0.2$. The relative depth, at 0.3 W, 0.5 W and 0.7 W, as a function of longitudinal distance is depicted in figure 6. Figures 7a to 71 show the ensemble averaged flow depths of each cross section.

A maximum of the transversal bed slope occurs at cross sections 15 to 17. A minimum of the transversal bed slope occurs at cross sections 24 to 27. In the region of cross-section 35 ... 45 the lateral bed slope does not vary significantly with streamwise direction. In this region the bed topography is axi-symmetrical.

4.1.2 Dune statistics

The bed consists of dunes moving downstream. The dimensions of the dunes are rather large in comparison with the flow depth. These dunes cause a significant form drag. This is reflected in the low Chézy value; $C \approx 20$ $m^{0.5}/s$. The large dimensions of the dunes also affect the choice of reference level, i.e. the level above which the sediment is considered to be transported as suspended load and below which the sediment is considered to be transported as bed-load transport.
To guide the choice of reference level the probability distribution of dune height is calculated. This is achieved as follow: In a selected region of the flume, the data of all individual local depth measurements is gathered and normalized with their local ensemble averaged value: a'/a. (at each location 11 data points are available.)
Two regions have been selected, each possessing local ensemble averaged water depths about equal to a_0.

- The inflow section, cross section 1 to 5; 495 data points
- The centerline of the channel ; 528 data points

The probability distributions of the water depth of both regions are shown in fig. 8. Both distributions are very similar. These distributions, assuming steady state of the bed, equal the dune height distributions. In fig. 8 also the 5% and 10% exceedance levels of dune height are indicated. These are within the range: 0.125 a to 0.175 a.

4.2 Concentration measurements

4.2.1 Mean concentration

The mean concentrations are tabulated in appendix B.
The figures 9a - 9i show the concentration profiles of respectively the cross-sections 1, 5, 10, 15, 20, 30, 35, 40, 45.

4.2.2. Curve fit of equilibrium concentration profile

The straight reach prior to the bend entrance serves to establish flow and sediment conditions which are in equilibrium with the local conditions, i.e. the flow and concentration fields are independent of streamwise coordinates. The length of this reach is sufficient (Talmon and Marsman, 1988).

In the straight reach concentrations have been measured 1.28 m upstream of the bend entrance (cross section 1). To establish the values of parameters of the concentration vertical at equilibrium conditions, the measurements at this location are used. The Rouse concentration profile is fitted with the measurements. This profile is based on the parabolical function for the turbulent exchange coefficient over the vertical.
The parameters of the concentration vertical are:

- the choice of reference height z_r/a
- the concentration at reference height c_r

- The Z parameter, $w_s/(\beta\kappa u_*)$

The concentration profile is given by:

$$c = c_r\left(\frac{z_r}{a_0-z_r}\,\frac{a_0-z}{z}\right)^Z \qquad (4.1)$$

Curve fitting has been performed with the aid of a computer program which, given z_r, estimates the Z and c_r parameters of eq.(4.1). A least squares method is employed. Results are given in table 4.1. About 5% of the time the dune height is larger than 0.175 a, see fig. 8. Therefore a reference height of $\gtrapprox$ 0.15 a should be appropriate. An example of a fitted curve is given in fig. 10 (for z_r/a_0=0.20, Z=0.37 and c_r=0.20 g/l).

Table 4.1 Parameter sets of the equilibrium concentration profile

z_r/a_0[-]	c_r[g/l]	Z [-]	$\bar{c}$ [g/l]
0.1	0.277	0.370	0.095
0.15	0.223	0.370	0.093
0.2	0.205	0.370	0.100
0.25	0.184	0.370	0.101

The estimated Z parameter of the concentration vertical is: Z=0.37. The standard deviation is: σ_Z= 0.033. The reference concentration varies with the choice of reference level. (Applying a parabolical-constant turbulent exchange coefficient, as reported by van Rijn (1982), yields; Z=0.40)

In table 4.1 also the depth-averaged concentration is given. This value is the integral of the concentration curve eq. (4.1) divided by a_0-z_r, see section 4.2.3.

4.2.3. Depth-averaged concentrations

The results of the experiment will be used to test depth-averaged mathematical models. To that purpose depth-averaged values of concentration have to be computed. The depth-averaged value of the concentration is defined by:

$$\bar{c} = \frac{1}{a-z_r} \int_{z_r}^{a} c \, dz \qquad (4.2)$$

with: a = local flow depth

z_r = reference level, close to the bed

The choice of reference level is uncertain. This level will be located near the top of the dunes. Concentration measurements below $z/a \lesssim 0.10$ were troubled by the presence of dunes. Consequently depth-averaged concentrations have been computed for $z_r/a = 0.10$, 0.15 and 0.20
The depth-averaged concentration of a vertical is computed by:

$$\bar{c} = \frac{1}{j_{max}} \sum_{j=1}^{j_{max}} c_j \qquad (4.3)$$

with j_{max} the number of measurements above z_r

For a very large number of data points, uniformly distributed over the depth, the summation series converge to the definition (4.2). The available number of data points is, however, limited. Measurements are taken with a vertical increment in vertical direction of 5 mm. At each x,y,z location two or more measurements have been performed. For small values of z_r data points are absent, especially in the outer part of the bend (fig. 9b ... 9i).
Considering these limitations, the accuracy of the computed depth-averaged values will be limited. The depth-averaged concentration fields, for $z_r/a = 0.10$, 0.15, and 0.20 are given in table 4.2. The depth-averaged concentration as function of the longitudinal coordinate, for $z_r/a = 0.15$ is given in figure 12.

Table 4.2 Depth-averaged concentrations in the 180 degree bend

cross-sec. no.	$\bar{c}$ (1/4 W)	$\bar{c}$ (2/4 W)	$\bar{c}$ (3/4 W)	
1	0.000	0.128	0.000	reference level at:
5	0.000	0.122	0.000	$z_r/a = 0.10$
10	0.176	0.107	0.108	
15	0.043	0.109	0.132	
20	0.054	0.193	0.146	
25	0.051	0.166	0.156	
30	0.057	0.150	0.123	
35	0.046	0.125	0.150	
40	0.066	0.174	0.137	
45	0.038	0.129	0.163	
1	0.000	0.128	0.000	reference level at:
5	0.000	0.122	0.000	$z_r/a = 0.15$
10	0.176	0.107	0.101	
15	0.050	0.109	0.131	
20	0.054	0.193	0.146	
25	0.051	0.166	0.156	
30	0.057	0.136	0.123	
35	0.043	0.116	0.150	
40	0.066	0.158	0.132	
45	0.038	0.118	0.152	
1	0.000	0.128	0.000	reference level at:
5	0.000	0.122	0.000	$z_r/a = 0.20$
10	0.153	0.107	0.098	
15	0.050	0.101	0.122	
20	0.054	0.192	0.133	
25	0.046	0.166	0.156	
30	0.043	0.125	0.123	
35	0.043	0.116	0.139	
40	0.066	0.158	0.127	
45	0.038	0.118	0.147	

4.2.4 Concentrations in the axi-symmetrical region

The bed topography in the region of cross section 35...45 is axi-symmetrical, sec. 4.1.1. Extended measurements of the concentration field at cross sections 40 and 45 are performed in order to investigate whether the concentration field is also axi-symmetrical.

In fig. 11a and 11b the concentration verticals of cross section 40 are given. In fig. 11c and 11d the concentration verticals of cross section 45 are shown. The concentration verticals have been measured at 1/8, 2/8, 3/8, 4/8, 5/8, 6/8 and 7/8 of the channel width.

An iso-concentration contour representation of the concentration field at cross-sections 40 and 45 is given in figure 11e. These contour plots are made by lineair interpolation between the data points. A contour interval of 0.02 g/l has been chosen for concentrations less than 0.1 g/l. For c > 0.1 g/l the interval is 0.05 g/l.

Concentration distributions in both cross sections are very similar. The lowest concentrations are found in the inner part of the bend. In the upper part of the flow the concentrations increase with the Y-coordinate (up to Y = 0.75 W). In the region Y > 0.75 W the concentrations decrease with Y. The highest concentrations are found close the bed in the region 0.5 < Y/W < 0.8. The near bed concentration in the innerpart of the bend is circa 1/4 of the concentration near the bed at Y/W = 0.6.

The measurements indicate that the concentration field is by approximation axi-symmetrical in the region of cross section 40...45.

5 DISCUSSION

The general purpose of the experiment is to provide data on which numerical and analytical morphological models, including suspended sediment transport, can be calibrated and verified.

The specific aim of this experiment is to include a region which is axi-symmetrical. This yields the possibility to test morphological models by means of their axi-symmetrical solution.

Important input parameters of morphological models are:

- The percentage of suspended sediment transport
- The shape of the equilibrium concentration profile
- A transport formula

These subjects are discussed in sections 5.1, 5.2, 5.3 and 5.4. Adaptation lengths of flow, bed level and concentration are calculated in sec. 5.5. The bed topography is discussed in sec. 5.6. Also a mathematical approximation of the bed topography is given. In section 5.7. the concentration field in the axi-symmetric region is discussed. When a depth averaged morphological model is used, which will be the case at the present state (1989) of computer facilities, depth averaged concentrations are of interest. The depth averaged values of concentration are calculated in sec. 5.8.

5.1. The Z parameter

Curve fitting of the concentration profile prior to bend entrance yields a Z parameter of 0.37 (sec. 4.2.2.). The Z parameter is defined by: $Z = w_s/(\beta\kappa u_*)$. The Z parameter is a measure of the ratio of the downward flux by the fall velocity w_s and the upward flux by turbulent diffusion. Turbulent diffusion of sediment is modelled by:

$\nu_{tc} = \beta\, \nu_{tm}$, with ν_{tm} = turbulent diffusion of momentum

ν_{tc} = turbulent diffusion of mass (sediment)

It is generally accepted that the turbulent diffusion coefficient of mass is greater than of momentum (Csanady 1973). Consequently $\beta>1$. In the experiment, upward of the bend entrance the wall shear velocity is equal to u_*= 0.035 m/s while w_s= 0.0076 m/s (sec. 3.1.2.) This yields $\beta \approx 1.5$

Based on a large data set van Rijn (1982) has calculated β by fitting the data with concentration verticals which are based on a parabolical-constant profile for the turbulent diffusion coefficient ν_{tc}. (The present curve fitting is based on a parabolical profile for ν_{tc}). For w_s/u_*= 0.0076/0.035 = 0.22 van Rijn reports effective β values of 1.0 and 1.7 for the experiments of Coleman (1970).
Hinze (1959) reports values of the turbulent Prandtl number $Pr_{turb}= 1/\beta$ of 0.65 to 0.72 (β=1.4 to 1.5) for various measurements on the distribution of heat and matter in pipe flow and two-dimensional channels.

5.2. Percentage of suspended sediment transport

The percentage of suspended sediment transport upstream of the bend is an important physical parameter in the experiment.
The division between bed and suspended load transport is somewhat arbitrary and is effected by the choice of reference level. The amount of suspended sediment transport per unit width is defined by:

$$S_{s\ sus} = \int_{z_r}^{z_s} u\ c\ dz \qquad (5.1)$$

Two methods will be employed to estimate the suspended sediment transport:

1 - Based on curve fitting of the concentration profile upstream of the bend entrance. By integration of the product of the mathematical functions of u and c, over the suspended load region, the suspended sediment transport is calculated.
2 - Based on an estimate of the depth-averaged concentration, multiplied by the depth-averaged velocity.

Method 1

The suspended sediment transport rate per unit width is equal to:

$$S_{s\ sus} = \bar{u}\,\bar{c} \int_{z_r}^{z_s} r_u r_c\,dz = (a_0 - z_r)\bar{u}\,\bar{c} \int_0^1 r_u r_c\,d\zeta = (a_0 - z_r)\bar{u}\,\bar{c}\,\alpha_s \qquad (5.2)$$

with: r_u, r_c shape functions of velocity and concentration
The total transport rate per unit width is equal to:

$$S_{tot} = a_0 \bar{u}\,\bar{c}_{tr} \qquad (5.3)$$

in which: $\bar{c}_{tr}$ = the transport concentration defined by eq.(5.3)

The results for $0.1 < z_r/a_0 < 0.2$ are given in table 5.1.

Table 5.1 Fraction of suspended sediment transport in cross section 1, by method 1

	Z=0.37		
z_r/a_0	$\bar{c}$ [g/l]	$S_{s\ sus}/S_{tot}$	$S_{s\ sus}/S_{tot}$
0.10	0.095	0.61	0.67
0.15	0.093	0.57	0.63
0.20	0.100	0.57	0.63
		$\alpha_s = 1$	$\alpha_s = 1.1$ (Z=0.35, C=20 $m^{0.5}/s$)

Method 2

The suspended sediment transport per unit width is approximated by:

$$S_{s\ sus} \approx \frac{1}{z_s - z_r} \int_{z_r}^{z_s} u\,dz \int_{z_r}^{z_s} c\,dz \approx (z_s - z_r)\,\bar{u}\,\bar{c} \qquad (5.4)$$

The depth-averaged concentration $\bar{c}$ is computed by the method outlined in subsection 4.2.3. Dividing the suspended sediment transport by the total sediment discharge at channel exit, yields the fraction of suspended sediment transport (table 5.2).

Table 5.2 Fraction of suspended sediment transport, in cross section 1, by method 2

z_r/a	$\bar{c}$[g/l]	$S_{s\ sus}/S_{tot}$
0.10	0.128	0.82
0.15	0.128	0.78
0.20	0.128	0.71

Both methods involve some disadvantages.
Method 1 is based on curve fitting of the concentration profile. This fitting will be affected by the non-homogeneous distribution of measuring points in the vertical. Consequently the integral of the concentration profile will be affected also, even though by integrating the profile all points in the vertical are weighed equally.
Method 2, which yields a rough estimate of the depth-averaged concentration, favourables the region were many measuring points are taken. In computing the depth integrated suspended transport the shape of the concentration and velocity profiles are neglected.
Based on the results given in table 5.1 and 5.2 it is concluded that the percentage of suspended transport is within the range: 60...70 % .

5.3 Transport formulae

To simulate the experiment numerically or analytically a transport formula is necessary to predict concentration and sediment transport rates. In this section the overall transport rate of the experiment is compared with some transport formulae known from literature. The purpose is to judge the suitability of these formulae for use in the simulations. Also insight could be gained in the choice of transport formula to be employed in the design of new experiments.
It is common practice to express the total sediment transport rate in the transport concentration: $\bar{c}_{tr} = Q_s/Q_w$ ($S_{tot} = \bar{c}_{tr} \bar{u}\ a_0$ [g/m/s]). The measured transport concentration is equal to: $\bar{c}_{tr} = 0.14$ g/l.
The transport formulae of Engelund and Hansen (1967), Ackers and White (1973), Brownlie (1981) and Van Rijn (1984c) will be evaluated.
These formulae are often employed outside their range of applicability, yielding reasonable results. The Ackers White and Brownlie formulae are

based on data sets which include data of laboratory flumes with fine sediments.

The Engelund Hansen formula reads:

$$\phi = \frac{0.05}{1-\Gamma} \frac{C^2}{g} \theta^{2.5}, \quad \text{with } \theta = \frac{di}{\Delta D_{50}}, \; \phi = \frac{S}{\sqrt{(\Delta g D^3)}}, \tag{5.6a}$$

$$\text{or: } \bar{c}_{tr} = \rho_s \frac{1}{\bar{u} a_0} 0.05 \sqrt{(\Delta g D_{50}^3)} \frac{C^2}{g} \theta^{2.5} \tag{5.6b}$$

Depending on the choice of d ($d=a_0$ or $d=r_b$) the transport concentration is within the range of: $0.71 < \bar{c}_{tr} < 0.73$ g/l

The Ackers White formula reads:

$$\bar{c}_{tr} = \rho_s \frac{D_{50}}{a_0} \left(\frac{\bar{u}}{u_*}\right)^n C \left(\frac{F_{gr}}{A} - 1\right)^m \tag{5.7}$$

with:
$$F_{gr} = \frac{1}{\sqrt{(\Delta g D_{50})}} u_*^n \left(\frac{\bar{u}}{\sqrt{32} \log (10 a_0/D_{50})}\right)^{1-n} = 0.73$$
$$A = 0.23/\sqrt{D_{gr}} = 0.294$$
$$n = 1.00 - 0.56 \log D_{gr} = 0.806$$
$$m = 9.66/D_{gr} + 1.34 = 5.69$$
$$C = 10^{(2.86 \log D_{gr} - \log^2 D_{gr} - 3.52)} = 0.0022$$
$$D_{gr} = D_{50} (\Delta g/\nu^2)^{1/3} = 2.22$$

According to White (1972) the formula is fitted to data for which no side wall correction method has been employed, i.e. $d=a_0$. In the publication of Ackers and White (1973), however, d is defined by d=A/P, while the same transport formula is reported. (P = wetted perimeter) Following the original work of White (1972) $d=a_0$ is used in eq.(5.7). This yields a transport concentration equal to: $\bar{c}_{tr} = 0.29$ g/l

The Brownlie formula reads:

$$\bar{c}_{tr} = 7115 (F_g - F_{g0})^{1.978} i^{0.6601} (r_b/D50)^{-0.3301} \quad [mg/l] \tag{5.8}$$

with:
$$F_g = \frac{\bar{u}}{\sqrt{(\Delta g D_{50})}} \quad \text{grain Froude number}$$
$$F_{g0} = 4.596 \theta_{cr}^{0.5293} i^{-0.1405} \sigma_g^{-0.1606} \quad \text{critical grain Froude number}$$
$$\theta_{cr} = 0.22 Y + 0.06 (10)^{-7.7 Y} \quad \text{critical Shields number}$$
$$Y = (\sqrt{\Delta} R_g)^{-0.6}$$

$R_g = \sqrt{(gD_{50}^3)}/\nu$ grain Reynolds number

$r_b = 0.069$ [m], hydraulic radius related to the bed according to Vanoni and Brooks (1957)

Prediction with this formula yields: $\bar{c}_{tr} = 0.069$ g/l

The Van Rijn (1984c) formulae read:

bed-load: $$\bar{c}_{trb} = \rho_s \, 0.005 \left(\frac{u-u_{cr}}{\sqrt{(g\Delta D_{50})}}\right)^{2.4} (D_{50}/a_0)^{1.2} \qquad (5.9a)$$

suspended-load: $$\bar{c}_{trs} = \rho_s \, 0.012 \left(\frac{u-u_{cr}}{\sqrt{(g\Delta D_{50})}}\right)^{2.4} D_{50}/a_0 \, d_*^{-0.6} \qquad (5.9b)$$

total load: $\bar{c}_{tr} = \bar{c}_{trb} + \bar{c}_{trs}$

with: $d_* = D_{50}\sqrt[3]{(\Delta g/\nu^2)}$

$u_{cr} = 0.19 \, D_{50}^{0.1} \log (12r_b/(3D_{90})) = 0.251$ m/s

The transport predicted with these formulae is equal to: $\bar{c}_{tr} = 0$

This is caused by: $u_{cr} > u$

Unfortunate none of these transport formulae predicts the actual transport concentration of the experiment. It can be argued that Engelund Hansen and Van Rijn are applied outside their ranges of applicability. The Ackers White and Brownlie formulae, however, are applied within their ranges of application.

The Ackers White formula overpredicts the transport concentration by a factor 2, whereas the Brownlie formula underpredicts the transport concentration by a factor 0.5.

Prediction of the ratio of suspended-load and total-load can be accomplished by the equations of Van Rijn eq.(5.9a,b). Due, however, to $u_{cr} > u$ this is impossible.

Van Rijn (1984b) has calculated the ratio of suspended-load and total-load of measurements reported by Guy et.al. (1966). It is noticed that for $u_*/w_s > 3$ more than 50% suspended-load is present. This is in accordance with the results of the experiment: $u_*/w_s = 4.6$, $S_{s\,sus}/S_{tot} \approx 0.65$

The performance of the transport formulae with regard to this experiment is comparable to the performance of the formulae in case of the suspended load experiment run no 1 (Talmon and Marsman, 1988).

5.4. Bed-shear stress and sediment transport

In case of a dune covered bed the bed resistance consist of bed shear stress (friction drag) and of a pressure gradient generated by the dunes (shape drag). The total drag (which actually consist of friction and shape drag) is defined by: $\tau=\rho gai$

The process of sediment transport is caused by the shear stress acting on the grains. The shear stress related to sediment transport is given by: $\tau'=\mu\tau$

in which: μ - efficiency factor

τ' - effective grain-shear stress

τ - total drag.

To initiate sediment transport the shear stress has to exceed a critical value: τ_{cr}.

In the experiment both μ and τ_{cr} are unknown.

One of the reasons of the poor performance of the transport formulae could be caused by the relatively high resistance ($C\approx 20\ m^{0.5}/s$). The data on which the transport formulae have been developed generally relate to less resistance ($C\gtrsim 30\ m^{0.5}/s$). The transport formulae implicitly, or explicitly, contain the ratio of friction and total drag. This ratio could differ under the present conditions (the relatively large dune height is quite exceptional). Consequently the effective grain-shear stress will differ also.

In the following sediment transport related parameters μ and θ_{cr} are estimated with the aid of some empirical formulae known from literature.

The transport formulae which incorporate the critical bed-shear stress are generally proportional with:

$$\left(\frac{\mu\tau-\tau_{cr}}{\tau_{cr}}\right)^b = \left(\frac{\mu\theta-\theta_{cr}}{\theta_{cr}}\right)^b = \left(\frac{1-B}{B}\right)^b \qquad (5.10a)$$

or:

$$(F_g - F_{g0})^b = \left(\frac{u - u_{cr}}{\sqrt{(g\Delta D_{50})}}\right)^b = (1-\sqrt{B})^b \left(\frac{C}{\sqrt{g}}\sqrt{\theta}\right)^b \qquad (5.10b)$$

in which: $B = \frac{\tau_{cr}}{\mu\tau}$, mobility parameter (5.10c)

Both unknown parameters are now incorporated in the B parameter.

Three methods are used to estimate B. The methods are:

1)- The set of transport formulae by Van Rijn (1984c), eq.(5.9a,b), is used to relate the total transport concentration c_{tr} and the B parameter. Substitution of the calculated c_{tr} value yields B.

2)- The bed load transport formula by Van Rijn (1984a), eq.(5.10) is used to relate the bed-load transport concentration and the B parameter. Substitution of the calculated c_{trb} value yields B.

$$c_{trb} = \frac{\rho_s}{a\ u}\ 0.053\ \sqrt{(\Delta g)}\ \frac{D_{50}^{1.5}}{d_*^{0.3}}\ \left(\frac{1-B}{B}\right)^{2.1} \quad [g/l] \qquad (5.11)$$

3)- A relation to estimate the critical Froude grain number by Brownlie (1981) is used.

$$F_{g0} = 4.596\ \theta_{cr}^{0.5293}\ i^{-0.1405}\ \sigma_g^{-0.1606} \qquad (5.12)$$

This relation has been obtained by Brownlie by manipulation of an empirical function which was derived to predict the flow depth. (The Brownlie depth prediction for this experiment is 30 % too large). With the aid of eq.(5.10b) B is calculated.

According to the Shields diagram the critical Shields number of the sediment is: $\theta_{cr} = 0.11$ (smaller θ_{cr} values have also been reported; Mantz(1977), $D_{50} = 77,\ 93\ \mu m$, $\theta_{cr} = 0.096$).

The methods are applied to the data of the present experiment and of the previous experiment run no. 1. The results are given in table 5.3.

Table 5.3 The mobility number B

run no. 1	method 1	method 2	method 3
B	0.29	0.29	0.20
μ (at θ_{cr}=0.11)	0.33	0.33	0.48
remark		60 % susp. transp.	depth prediction 60 % too large

run no. 2	method 1	method 2	method 3
B	0.44	0.32	0.30
μ (at θ_{cr}=0.11)	0.29	0.41	0.43
remark		65 % susp. transp.	depth prediction 30 % too large

The results of the three methods are comparable. The B parameter of run no. 1 is smaller than of run no. 2. This corresponds with a smaller total shear stress of run no. 2. The μ parameter is calculated by eq.(5.10c). The μ parameter of both experiments is within the range: $0.3 < \mu < 0.5$. The Van Rijn (1984a) model for μ, which is applied in the Van Rijn transport formulae, yields a distinct result: $\mu = (C/C')^2 = (20/60)^2 = 0.11$. These results indicate that the estimate of μ, implicitly or explicitly contained in the transport formulae, could be erroneous.
The estimated value of μ indicates that about 40 % of the total drag is available for sediment transport.

5.6 Adaptation lengths

In order to formulate mathematically the interaction of flow and sediment adaptation lengths of flow velocity, bed level and concentration have been defined: Struiksma et.al. (1986) and Olesen (1987). These adaptation lengths are defined as follows:

adaptation length of flow: $\lambda_w = \frac{C^2}{2g} a_0$ (5.13a)

adaptation length of bed level: $\lambda_s = \frac{1}{\pi^2} (\frac{W}{a_0})^2 \frac{1}{G} a$ (5.13b)

adaptation length of concentration: $\lambda_c \approx \bar{a}u/w_s$ (5.13c)

in which: G = coefficient of the gravitational term in the bed-load sediment direction model

The adaptation lengths for flow and bed level in the experiment are:

λ_w = 1.38 m, based on C

or, λ_w = 1.44 m, based on C_r

λ_s = 0.23 m, at $\theta \approx 1$; $G \approx 1.5$

The adaptation length of concentration depends mainly on the choice of boundary condition for the concentration at reference level (Talmon, 1988). The adaptation length depends further on the value of the Z parameter, the reference height and the Chézy value. The adaptation lengths are calculated based on the assumption of a logarithmic velocity profile and a Rouse distribution for the concentration. To this purpose software which is used in Talmon (1988) has been employed.

Curve fitting of the concentration profile yields: Z = 0.37

The Chézy value of the experiment is about: C = 20 $m^{0.5}/s$

The reference height should be chosen near the top of the dunes, consequently z_r will be in the range: $0.1 < z_r/a < 0.2$, (fig. 8)

Taking into account these ranges, the adaptation length of the concentration becomes:

In case of the concentration condition: $0.4 < \lambda_c < 0.5$ m

In case of the gradient condition: $1.1 < \lambda_c < 1.3$ m

5.6 Bed topography

The stationary bed topography in the 180 degree bend is depicted in fig. 5. A maximum of the transversal bed slope occurs at cross sections 15 to 17. A minimum of the transversal bed slope occurs at cross sections 24 and 25. From cross sections 30 to 45 the transversal bed slope is nearly constant. In this region a small difference between the bed topography of the inner and the outer part of the bend is noticed. In the inner part of the bend the water depth is constant with streamwise direction.

In the outer part of the bend the water depth is nearly constant, in cross section 31 to 36 the water depth is slightly greater than further downstream.

The bed topography displays a damped oscillation of the transversal slope. The main contribution of the harmonic oscillation is within the region of cross section 10...25. In the region of cross section 31...36 a small contribution of the harmonic oscillation is noticed in the outer part of the bend. The damping is strong enough to yield a region of axi-symmetrical bed topography within the 180 degree bend: cross section 35...45.

An analytical approximation the bed topography can be formulated by:

$$\frac{a'}{a_0} = (\hat{a}e^{iks} - i|\hat{a}|)e^{ik_b n} \qquad (5.14)$$

with: $\hat{a}$ complex amplitude (including a phase shift of the harmonic oscillation with regard to the bend entrance)

s coordinate in streamwise direction

n coordinate in transversal direction

$k_b = \pi/W$ wave number in transversal direction

k complex wave number

The $-i|\hat{a}|e^{ik_b n}$ term yields the axi-symmetrical bed topography (sinusioidal). Fitting equation (5.14) to the measured bed topography (cross section 10...45) yields:

$$re(k) = \frac{2\pi}{6.6} = 0.95 \qquad im(k) \approx 0.18 \qquad |\hat{a}| = 0.6$$

$im(k)$ and $\hat{a}$ are difficult to compute, consequently the accuracy is limited. These results indicate a wave length of oscillation of 6.6 m, and 63% damping (e^{-1}) at s = 5.6 m.

5.7 Concentrations in the axi-symmetrical region

The concentration field in the axi-symmetrical region is given in fig. 11. The iso-concentration contour line representation, fig. 11e. will be used to discuss the relevant physics.

In a straight reach the balance is between vertical turbulent diffusion and the fall velocity, while boundary conditions determine the concentration levels. In the axi-symmetrical region the secondary flow is also a factor to be included in the balance.
In the inner part of the bend the concentrations are expected to be low because of smaller bed shear stresses. The results depicted in fig. 11e confirm this. In the outermost part of the bend, beyond Y/W=0.8, the concentrations decrease as well in the upper as the lower part of the flow. The decrease of concentrations could be caused by an additional secondary flow (Taylor-Görtler type) cel due to the presence of the concave wall. Due to side wall friction the fluid velocity close to the wall is less than further remote from the wall. The centrifugal force acting on fluidum close to the wall is also less. This is an unstable situation favourable of yielding Taylor-Görtler types of secondary flow cels. Near the side wall sediment present in the upper part of the flow could be conveyed in downward direction by the combined action of the central region secondary flow cel (which is due to $\partial u/\partial z$) and a Taylor-Görtler type cel. Unfortunate in this type of experiments it is very difficult to measure the velocity accurately, consequently no data is available to confirm this effect.
In the region $Y/W > 0.8$ the near bed concentration and the vertical concentration gradient are less than in the region $0.5 < Y/W < 0.8$. This indicates that the bed shear stress available for sediment transport is less in this region. In case the efficiency factor for sediment transport is assumed constant the total bed shear stress will decrease in the outermost part of the bend. Only very close to the side wall a decrease of the shear stress was expected because in the remaining part the rough sediment bed is assumed to govern the physics. Whether a decrease of the total bed shear stress in the region $Y/W > 0.8$ does exist in unknown, if so it comes as a surprise.

5.8 The depth averaged concentration field

The depth averaged concentration field is given in fig. 12. The depth-averaged concentration field displays large variations.
In fig. 13a the depth averaged suspended sediment transport (=flux) in streamwise direction, $\bar{c}\,\bar{u}$ is shown. In fig 13b the depth integrated

suspended sediment transport (=suspended transport per unit width) in streamwise direction $\bar{c}\ u\ (a-z_r)$, is given.
The suspended sediment concentration $\bar{c}_{trs}$ in fig.12 and 13 is based on an estimate of 65% of suspended sediment transport: $\bar{c}_{trs} = 0.65\ \bar{c}_{tr}$.
The depth averaged velocity field which is used in these figures is obtained by using the Olesen depth averaged flow model. Input to the model is a smoothed version of the ensemble averaged bed topography. The flow model has been run with the following parameters: C=20 $m^{0.5}/s$, β=6.0, k_{sn}=0.5, λ_{sf}=1.3aC/$\sqrt{g}$.
in which: β = coefficient in the model for the direction of bed shear-stress
k_{sn} = secondary flow convection factor
λ_{sf} = adaptation length of bed shear-stress

The depth averaged concentration field displays the following features, fig. 12:

- In the inner part of the bend, upstream of the point bar, the concentration increases: $\approx 1.6\ \bar{c}_{trs}$.
- In the inner part of the bend, downstream of the point bar until bend exit, concentrations are low: $\approx 0.5\ \bar{c}_{trs}$.
- Concentrations downstream of the pool and point bar in the outer part of the bend and at centerline are of equal magnitude: $\approx 1.3\ \bar{c}_{trs}$
- Immediately downstream of the pool and point bar the concentration at centerline and in the outer part of the bend increases locally: $\approx 1.8\ \bar{c}_{trs}$.

The depth averaged transport and the depth integrated transport are characterized by, fig. 13a,b:

- Upstream of the pool and point bar the transport in the inner and outer part of the bend rapidly adjusts to the conditions imposed by flume curvature.
- Downstream of the pool and point bar the transport is, by crude approximation axi-symmetrical.
  - The transport in the outer part of the bend is about 10 times greater than in the inner part of the bend.
  - The transport is by crude approximation proportional with the transversal coordinate.

Because the depth averaged suspended sediment transport in streamwise direction is approximately symmetrical to the channel centerline, analytical modelling of the suspended transport by an equation of the type of eq.(5.14) could in this case be a useful approximation. (In the preceding experiment, run. no 1, the transport was non-symmetrical to channel centerline !)

6 CONCLUSIONS

The main features of the experiment are:

- The stationary bed topography displays over- and undershoot effects due to the abrupt change of curvature at the bend entrance. The bed topography is characterized by a damped oscillation of the radial bed slope.
- Due to sufficient damping an axi-symmetric part is included in the 180^0 bend. This is reflected in both the bed topography and the concentration field. The concentration field in the axi-symmetric part is characterized by a general increase of concentration towards the outer part of the bend.

The main parameters which characterize the experiment are:

- The Chézy value of the experiment is about: $C = 20\ m^{0.5}/s$
- The width/depth ratio of the channel is: 6.9 .
- The percentage suspended sediment transport is about: 65%.
- The Z parameter of the equilibrium concentration profile is estimated to be: $Z = 0.37 \pm 0.03$

In view of analytical and numerical simulations of the experiment the following has been investigated:

- The performance of several transport formulae is investigated. They fail to predict the total transport rate. This could be due to an erroneous estimate of the ratio of friction drag and total drag.
- Adaptation lengths of flow velocity, bed level and concentration have been calculated.
- The wavelength of harmonic oscillation of the bed topography and its damping have been estimated.
- In a relatively large region near the outer wall concentrations decrease somewhat. This is probably due to a Taylor-Görtler type of flow instability caused by the concave side wall.
- The depth-integrated suspended transport in the outer part of the bend is estimated to be about 10 times the transport in the inner part of the bend.
- Due relatively large dune dimensions the reference height of a suspended sediment model should be chosen within: $0.1 < z_r/a < 0.2$

REFERENCES

Ackers, P. and W.R. White, 1973, Sediment transport: a new approach and analysis, Journal of the Hydraulics Division, ASCE, vol. 99, no. HY11, pp. 2041-2060

Brownlie, W.R., 1981, Prediction of flow depth and sediment discharge in open channels, W.M. Keck Laboratory of Hydraulics and Water Resources, California Institute Of Technology, Pasadena California, rep. no. KH-R-43A

Engelund, F. and E. Hansen, 1967, A monograph on sediment transport in alluvial streams, Teknisk Forlag, Copenhagen, Denmark

Coleman, N.L., 1970, Flume studies of the sediment transfer coefficient Water Resources, Vol 6, no 3.

Csanady, G.T., 1973, Turbulent diffusion in the environment, D. Reidel Publishing Co., Dordrecht, the Netherlands

Delft Hydraulics, 1986, Optical concentration meter, model OPCON, Technical manual

Guy, H.P.; D.B. Simons and E.V. Richardson, 1966, Summary of alluvial channel data from flume experiments, 1956-1961, Geological Survey Professional Paper 462-I,Washington, D.C.

Hinze, J.O., 1959, Turbulence, McGraw-Hill, New York

Mantz, P.A., 1977, Incipicient transport of fine grains and flakes by fluids - extended Shields diagram, Journal Hydraulics Div. ASCE, Vol. 103, no. HY6, pp. 601-615

Olesen, K.W., Bed topography in shallow river bends
Doctoral thesis Delft University of Technology, 1987
(also: ISSN 0169-6548 Communications on Hydraulic and Geotechnical Engineering, Delft University of Technology, Faculty of Civil Engineering)

Rijn, L.C. van, 1984a, Sediment transport, part I: bed load transport, Journal of Hydraulic Engineering, Vol 110, no. 10, pp. 1431-1456

Rijn, L.C. van, 1984b, Sediment transport, part II: suspended load transport, Journal of Hydraulic Engineering, Vol 110, no. 11, pp. 1613-1641

Rijn, L.C. van, 1984c, Sediment transport, part III: bed form and alluvial roughness, Journal of Hydraulic Engineering, Vol 110, no. 12, pp. 1733-1754

Rijn, L.C. van, 1987, Mathematical modelling of morphological processes in the case of suspended sediment transport
Doctoral thesis Delft University of Technology, 1987
(also: Delft Hydraulics Communication no. 382)

Slot, R.E., 1983, Terminal velocity formula for spheres in a viscous fluid. Delft Univ. of Techn., Dept. Civil Engrg., Laboratory of Fluid Mechanics, rep. no. 4-83,

Slot, R.E. and H.J.Geldof, 1986, An improved settling tube system for sand. Communications on Hydraulics and Geotechnical Engineering, Delft Univ. of Techn., Dept. Civil Engrg., rep. no. 86-12,

Struiksma, N.; K.W. Olesen, C. Flokstra and H.J. de Vriend, 1985, Bed deformation in alluvial channel bends. IAHR, Journal of Hydraulic Research, vol. 23, no. 1, pp. 57-79

Talmon, A.M., 1988, A theoretical model for suspended sediment transport Delft Univ. of Techn., Dept. Civil Eng., rep. no. 7-88

Talmon, A.M. and E.R.A. Marsman, 1988, Suspended-load experiments in a curved flume, run no.1, Delft Univ. of Techn., Dept. Civil Eng., rep. no. 8-88

Vanoni, V.A. and N.H. Brooks, 1957, Laboratory studies of the roughness and suspended load of alluvial streams, M.R.D. Sediment series no. 11, California Institute of Technology Sedimentation Laboratory, pp. 121

White, W.R., 1972, Sediment transport in channels: a general function, rep. INT 104, Hydraulics Research Station, England

Appendix A: Ensemble averaged water depths.

In this appendix the ensemble averaged relative water depths of the 11 measurements are tabulated.

Discharge 0.0077 m^3/s. Sediment transport 3.9 kg/h dry sand.

Relative mean water depth a/a_0. (a_0 = 0.072 m.)

from inner side of bend	CS01	CS02	CS03	CS04	CS05	CS06	CS07
0.05	1.00	1.00	0.99	1.01	0.98	0.95	0.94
0.10	0.97	0.97	0.97	1.01	1.01	0.99	1.00
0.15	1.00	0.96	0.99	1.07	1.04	0.94	1.01
0.20	0.99	0.95	0.99	0.99	0.99	0.94	1.05
0.25	1.03	1.05	0.94	0.92	0.92	0.98	1.04
0.30	1.01	1.00	0.99	0.96	0.96	1.03	0.99
0.35	0.99	0.96	0.96	0.97	0.95	1.00	1.00
0.40	1.00	0.94	0.95	1.00	1.03	1.00	1.06
0.45	1.01	0.99	0.99	0.96	1.01	0.95	1.12

from inner side of bend	CS08	CS09	CS10	CS11	CS12	CS13	CS14
0.05	0.85	0.71	0.59	0.54	0.42	0.32	0.28
0.10	0.88	0.82	0.73	0.62	0.49	0.44	0.31
0.15	0.93	0.90	0.80	0.71	0.62	0.55	0.43
0.20	0.96	0.91	0.86	0.77	0.78	0.67	0.63
0.25	0.99	0.90	1.00	0.93	0.93	0.85	0.85
0.30	1.03	1.04	1.08	1.08	1.14	1.12	1.17
0.35	1.08	1.17	1.18	1.22	1.33	1.25	1.37
0.40	1.11	1.23	1.30	1.34	1.48	1.40	1.57
0.45	1.15	1.32	1.35	1.45	1.54	1.57	1.69

from inner side of bend	CS15	CS16	CS17	CS18	CS19	CS20	CS21
0.05	0.20	0.12	0.17	0.29	0.37	0.47	0.48
0.10	0.26	0.30	0.24	0.33	0.42	0.49	0.52
0.15	0.41	0.47	0.38	0.48	0.48	0.50	0.64
0.20	0.64	0.62	0.62	0.65	0.67	0.66	0.73
0.25	0.85	0.87	0.91	0.87	0.90	0.84	0.84
0.30	1.13	1.16	1.21	1.21	1.13	1.10	1.05
0.35	1.40	1.41	1.46	1.40	1.38	1.34	1.32
0.40	1.60	1.64	1.63	1.58	1.60	1.54	1.49
0.45	1.68	1.86	1.80	1.74	1.71	1.69	1.58

Discharge 0.0077 m^3/s. Sediment transport 3.9 kg/h dry sand.

Relative mean water depth a/a_0. (a_0 = 0.072 m.)

from inner side of bend	CS22	CS23	CS24	CS25	CS26	CS27	CS28
0.05	0.61	0.58	0.68	0.67	0.65	0.69	0.63
0.10	0.61	0.63	0.71	0.70	0.68	0.68	0.63
0.15	0.61	0.67	0.69	0.69	0.69	0.68	0.71
0.20	0.69	0.78	0.72	0.73	0.74	0.77	0.75
0.25	0.80	0.89	0.84	0.85	0.84	0.85	0.87
0.30	1.03	1.09	1.03	1.02	0.97	0.98	1.03
0.35	1.20	1.27	1.18	1.23	1.12	1.19	1.22
0.40	1.41	1.37	1.40	1.37	1.32	1.29	1.37
0.45	1.55	1.53	1.49	1.46	1.44	1.44	1.46

from inner side of bend	CS29	CS30	CS31	CS32	CS33	CS34	CS35
0.05	0.62	0.58	0.54	0.53	0.53	0.54	0.55
0.10	0.69	0.62	0.63	0.65	0.60	0.60	0.62
0.15	0.69	0.70	0.70	0.65	0.65	0.70	0.67
0.20	0.77	0.78	0.80	0.76	0.72	0.75	0.75
0.25	0.84	0.86	0.88	0.88	0.85	0.91	0.87
0.30	0.99	1.02	1.02	1.04	1.06	1.07	1.10
0.35	1.23	1.14	1.18	1.28	1.26	1.25	1.25
0.40	1.32	1.32	1.29	1.38	1.39	1.45	1.40
0.45	1.48	1.44	1.41	1.50	1.60	1.52	1.60

from inner side of bend	CS36	CS37	CS38	CS39	CS40	CS41	CS42
0.05	0.58	0.54	0.62	0.59	0.61	0.54	0.57
0.10	0.61	0.61	0.61	0.65	0.63	0.60	0.64
0.15	0.63	0.68	0.68	0.65	0.64	0.68	0.69
0.20	0.76	0.75	0.78	0.79	0.79	0.76	0.76
0.25	0.85	0.91	0.91	0.87	0.89	0.92	0.88
0.30	1.11	1.12	1.12	1.12	1.10	1.08	1.03
0.35	1.27	1.29	1.29	1.26	1.22	1.23	1.17
0.40	1.45	1.46	1.38	1.38	1.33	1.38	1.39
0.45	1.54	1.53	1.50	1.51	1.47	1.46	1.47

Discharge 0.0077 m^3/s. Sediment transport 3.9 kg/h dry sand.

Relative mean water depth a/a_0. (a_0 = 0.072 m.)

from inner side of bend	CS43	CS44	CS45	CS46	CS47	CS48
0.05	0.58	0.62	0.58	0.60	0.72	0.75
0.10	0.61	0.63	0.65	0.63	0.69	0.84
0.15	0.74	0.68	0.71	0.73	0.72	0.78
0.20	0.80	0.81	0.77	0.80	0.79	0.85
0.25	0.87	0.92	0.89	0.88	0.91	0.95
0.30	1.01	1.11	1.07	1.10	1.13	1.12
0.35	1.19	1.19	1.18	1.19	1.18	1.19
0.40	1.37	1.28	1.37	1.32	1.29	1.19
0.45	1.53	1.42	1.43	1.49	1.38	1.20

Appendix B: Concentration measurements.

Cross section 1.

location in cross-direction [y/W]	Mean water depth [mm]	Distance beneath water surface [mm]	Concentration [g/l]						
4/8	72	10	0.04	0.1	0.07	0.08	0.07	0.03	
		15	0.07	0.06	0.06	0.08			
		20	0.05	0.12	0.08	0.1	0.1	0.08	0.1
			0.07	0.09	0.11				
		25	0.1	0.12	0.07	0.08	0.07	0.11	
		30	0.12	0.12	0.09	0.11	0.12	0.09	
			0.11	0.15	0.14	0.12	0.13	0.06	
		35	0.1	0.13	0.13	0.12	0.09	0.11	
		40	0.08	0.15	0.13	0.13	0.15	0.14	
			0.1	0.14	0.13	0.17	0.13	0.15	
		45	0.17	0.14	0.11	0.14	0.12		
		50	0.18	0.17	0.16	0.15	0.19	0.2	
		55	0.19	0.39					

Cross section 5.

Location in cross-direction [y/W]	Mean water depth [mm]	Distance beneath water surface [mm]	Concentration [g/l]		
4/8	72	5	0.07		
		10	0.07		
		15	0.09	0.1	
		20	0.09	0.09	0.1
		25	0.09	0.13	0.12
		30	0.13	0.11	0.1
		35	0.12	0.14	0.16
		40	0.14	0.13	0.17
		45	0.12	0.12	0.23
		50	0.22		

Cross section 10.

Location in cross-direction [y/W]	Mean water depth [mm]	Distance beneath water surface [mm]	Concentration [g/l]	
2/8	55	5	0.09	
		15	0.12	0.15
		25	0.15	0.19
		35	0.24	0.19
		45	0.27	

4/8	72	5	0.04			
		10	0.08			
		15	0.06			
		20	0.1	0.1	0.09	
		25	0.08			
		30	0.14	0.13	0.13	
		35	0.09			
		40	0.17	0.16	0.15	
		50	0.24	0.21		
6/8	89	5	0.02			
		10	0.06			
		15	0.04			
		20	0.11	0.09		
		25	0.05	0.05		
		30	0.11	0.1	0.1	
		35	0.06	0.06	0.11	
		40	0.13	0.13	0.11	0.11
		45	0.06	0.12	0.11	
		50	0.14	0.15	0.12	0.15
		55	0.07	0.12	0.12	
		60	0.18	0.12	0.15	
		65	0.12	0.13		
		70	0.14	0.22		
		75	0.15			
		80	0.2			

Cross section 15.

Location in cross-direction [y/W]	Mean water depth [mm]	Distance beneath water surface [mm]	Concentration [g/l]			
2/8	28	5	0.05	0.03		
		15	0.03	0.09		
		25	0.03			
4/8	61	5	0.04			
		10	0.09			
		15	0.06			
		20	0.14	0.1	0.12	
		25	0.09			
		30	0.16	0.13	0.12	
		35	0.12			
		40	0.15	0.18	0.13	
		50	0.17	0.17		
6/8	108	5	0.03			
		10	0.05			
		15	0.05			
		20	0.12	0.07		
		25	0.07	0.07		
		30	0.14	0.08		
		35	0.15	0.08	0.08	
		40	0.14	0.16	0.08	0.16
		45	0.11	0.1	0.17	
		50	0.16	0.13	0.17	0.17
		55	0.16	0.14	0.19	0.12
		60	0.18	0.18	0.14	0.16

65	0.15	0.13	0.18	0.16
70	0.2	0.17	0.16	
75	0.15	0.17	0.12	
80	0.2	0.17		
85	0.15	0.18		
90	0.29			
95	0.14			

Cross section 20.

Location in cross-direction [y/W]	Mean water depth [mm]	Distance beneath water surface [mm]	Concentration [g/l]			
2/8	36	5	0.03			
		10	0.06			
		15	0.04			
		20	0.09			
		25	0.05			
		30	0.33			
4/8	60	5	0.06			
		10	0.12			
		15	0.1	0.12		
		20	0.19			
		25	0.16	0.14	0.16	
		30	0.25			
		35	0.26	0.22	0.18	
		40	0.34			
		45	0.32	0.26		
		55	0.38			
6/8	104	5	0.04			
		10	0.06			
		15	0.07	0.06		
		20	0.07	0.11		
		25	0.09	0.09	0.06	
		30	0.08	0.13	0.07	
		35	0.09	0.09	0.09	0.15
		40	0.16	0.1	0.2	0.09
		45	0.13	0.09	0.1	0.19
		50	0.15	0.1	0.19	0.15
		55	0.22	0.11	0.14	0.16
		60	0.19	0.18	0.12	
		65	0.14	0.2	0.22	
		70	0.2	0.2		
		75	0.15	0.25		
		80	0.27			
		85	0.36			

Cross section 25.

Location in cross-direction [y/W]	Mean water depth [mm]	Distance beneath water surface [mm]	Concentration [g/l]			
2/8	50	5	0.02			
		10	0.03			
		15	0.03			
		20	0.05			
		25	0.05			
		30	0.06			
		35	0.08			
		40	0.09			
4/8	61	5	0.08			
		10	0.09			
		15	0.14			
		20	0.17			
		25	0.09	0.14	0.2	
		30	0.21			
		35	0.15	0.22	0.19	
		40	0.25			
		45	0.19	0.26		
		55	0.29			
6/8	94	5	0.05			
		10	0.07			
		15	0.05	0.09		
		20	0.1	0.14		
		25	0.15	0.1		
		30	0.12	0.16	0.13	
		35	0.2	0.15	0.12	0.11
		40	0.16	0.13	0.19	0.14
		45	0.18	0.13	0.22	0.16
		50	0.23	0.16	0.18	
		55	0.19	0.18	0.25	0.16
		60	0.15	0.21		
		65	0.26	0.22	0.22	
		70	0.23			
		75	0.24	0.28		

Cross section 30.

Location in cross-direction [y/W]	Mean water depth [mm]	Distance beneath water surface [mm]	Concentration [g/l]	
2/8	48	5	0.01	0.03
		10	0.02	0.04
		15	0.01	0.04
		20	0.06	0.04
		25	0.03	0.06
		30	0.05	0.07
		35	0.06	0.08
		40	0.05	0.26

4/8	62	5	0.04	0.05				
		10	0.07	0.07				
		15	0.08	0.06	0.09	0.07		
		20	0.08	0.11	0.12	0.12		
		25	0.1	0.09	0.14	0.15	0.13	0.1
		30	0.13	0.16	0.16	0.16	0.12	
		35	0.13	0.2	0.13	0.16	0.2	0.12
		40	0.19	0.21	0.29	0.21	0.15	
		45	0.26	0.15	0.21	0.17		
		50	0.22	0.29	0.2			
		55	0.22	0.36				
		60	0.27					
6/8	89	5	0.04	0.03				
		10	0.06					
		15	0.07	0.04				
		20	0.08	0.09				
		25	0.07	0.08	0.09	0.09		
		30	0.09	0.1	0.1			
		35	0.1	0.11	0.11	0.08	0.1	
		40	0.13	0.11	0.12	0.1		
		45	0.1	0.13	0.12			
		50	0.13	0.14	0.15			
		55	0.16	0.12	0.15			
		60	0.19	0.18				
		65	0.23					
		70	0.28					

Cross section 35.

Location in cross-direction [y/W]	Mean water depth [mm]	Distance beneath water surface [mm]	Concentration [g/l]					
2/8	46	5	0.01	0.03				
		10	0.03	0.02				
		15	0.05	0.01				
		20	0.04	0.04				
		25	0.07	0.03				
		30	0.05	0.06				
		35	0.1	0.06				
		40	0.07					
4/8	63	5	0.03	0.03				
		10	0.07	0.07				
		15	0.07	0.06	0.07			
		20	0.1	0.1	0.1	0.07		
		25	0.1	0.1	0.08	0.08	0.09	0.09
		30	0.15	0.14	0.13	0.1		
		35	0.12	0.1	0.12	0.12	0.13	0.13
		40	0.19	0.16	0.2	0.12		
		45	0.17	0.15	0.15	0.16		
		50	0.29	0.18				
		55	0.21	0.23				
6/8	95	5	0.07	0.05				
		10	0.06					
		15	0.07	0.11	0.1			
		20	0.11	0.07				

25	0.11	0.12	0.13	0.1	
30	0.12	0.09	0.09		
35	0.13	0.13	0.11	0.1	0.15
40	0.13	0.09	0.11	0.11	
45	0.14	0.12	0.21	0.17	
50	0.16	0.1	0.2	0.13	
55	0.22	0.16	0.27	0.12	
60	0.12	0.15	0.14	0.24	
65	0.3	0.14	0.14		
70	0.22	0.15	0.26		
75	0.22	0.32			
80	0.32	0.31			

Cross section 40.

Location in cross-direction [y/W]	Mean water depth [mm]	Distance beneath water surface [mm]	Concentration [g/l]				
1/8	44	5	0.02				
		10	0.05				
		15	0.03	0.04			
		20	0.06				
		25	0.04	0.04			
		30	0.06				
		35	0.04	0.06			
		40	0.1				
		45	0.07				
2/8	46	5	0.03	0.05			
		10	0.06				
		15	0.05	0.05			
		20	0.07				
		25	0.06	0.07			
		30	0.09				
		35	0.08	0.1			
3/8	54	5	0.02	0.03			
		10	0.03	0.03	0.06		
		15	0.11	0.05	0.04	0.03	
		20	0.07	0.04	0.08	0.06	0.04
		25	0.13	0.04	0.06	0.08	
		30	0.08	0.06	0.13	0.05	0.12
		35	0.08	0.11	0.05	0.17	
		40	0.07	0.16	0.09	0.17	0.15
		45	0.07	0.22			
		50	0.14				
4/8	64	5	0.06				
		10	0.07				
		15	0.08	0.08	0.09		
		20	0.1	0.13			
		25	0.14	0.15	0.11	0.13	
		30	0.16	0.13			
		35	0.18	0.2	0.16	0.15	
		40	0.21	0.15			
		45	0.27	0.25	0.2		
		50	0.38				
		55	0.34				

5/8	81	5	0.07		
		10	0.09		
		15	0.1	0.1	
		20	0.11	0.14	
		25	0.16	0.15	
		30	0.16	0.18	
		35	0.19	0.19	0.2
		40	0.25	0.21	0.21
		45	0.18	0.25	
		50	0.26	0.23	
		55	0.26		
		60	0.28		
		65	0.23		
		70	0.73		
6/8	92	5	0.05		
		10	0.09		
		15	0.08	0.09	
		20	0.13	0.13	
		25	0.1	0.1	0.13
		30	0.05	0.14	0.14
		35	0.13	0.14	0.11
		40	0.12	0.15	0.14
		45	0.17	0.13	0.12
		50	0.13	0.12	0.15
		55	0.16	0.14	0.2
		60	0.18	0.13	0.15
		65	0.15	0.18	
		70	0.17	0.2	
		75	0.23	0.16	
		80	0.22	0.2	
		85	0.27		
		90	0.34		
7/8	104	5	0.05		
		10	0.05		
		15	0.03	0.04	
		20	0.05	0.04	
		25	0.03	0.04	
		30	0.05	0.04	
		35	0.04	0.1	
		40	0.09	0.05	0.1
		45	0.05	0.09	0.11
		50	0.07	0.1	
		55	0.1		
		60	0.11	0.14	
		65	0.13		
		70	0.15	0.15	
		75	0.22		
		80	0.19		

Cross section 45.

Location in cross-direction [y/W]	Mean water depth [mm]	Distance beneath water surface [mm]	Concentration [g/l]				
1/8	43	5	0.02	0.03			
		10	0.03				
		15	0.04	0.03			
		20	0.05				
		25	0.04	0.04			
2/8	49	5	0.02	0.02			
		10	0.03				
		15	0.03	0.05			
		20	0.03				
		25	0.05	0.05			
		30	0.04				
		35	0.06	0.05			
3/8	54	5	0.01	0.01	0.07		
		10	0.03	0.01	0.07	0.07	
		15	0.09	0.02	0.04	0.02	
		20	0.03	0.04	0.02	0.09	0.12
		25	0.05	0.04	0.04	0.13	
		30	0.05	0.11	0.05	0.03	0.12
		35	0.07	0.06	0.19	0.05	
		40	0.05	0.15	0.08	0.13	0.09
		45	0.06				
		50	0.08				
4/8	64	5	0.03				
		10	0.05				
		15	0.1	0.05	0.07		
		20	0.1	0.09			
		25	0.15	0.08	0.11	0.1	
		30	0.14				
		35	0.12	0.18	0.15	0.15	
		40	0.18	0.15			
		45	0.19	0.2	0.15		
		50	0.19				
		55	0.23	0.23			
5/8	79	5	0.06				
		10	0.07				
		15	0.08	0.1			
		20	0.1	0.12			
		25	0.12	0.13			
		30	0.15	0.14			
		35	0.16	0.18	0.15		
		40	0.19	0.18	0.19		
		45	0.2	0.18			
		50	0.27	0.24			
		55	0.27				
		60	0.29				
		65	0.35				
		70	0.38				

6/8	93	5	0.05			
		10	0.09			
		15	0.12	0.08		
		20	0.11	0.09		
		25	0.17	0.13	0.1	
		30	0.13	0.14	0.11	
		35	0.19	0.16	0.14	
		40	0.15	0.17	0.14	
		45	0.13	0.12	0.2	0.2
		50	0.17	0.18	0.17	0.15
		55	0.23	0.15	0.16	
		60	0.2	0.2	0.22	
		65	0.19	0.19		
		70	0.25	0.22		
		75	0.24	0.2		
		80	0.41	0.26		
7/8	100	5	0.02			
		10	0.03			
		15	0.03	0.04		
		20	0.04	0.04		
		25	0.03	0.05		
		30	0.04	0.05		
		35	0.03	0.1		
		40	0.04	0.06	0.08	
		45	0.11	0.04		
		50	0.08	0.06	0.14	
		55	0.12			
		60	0.09	0.17		
		65	0.14			
		70	0.1	0.2		
		75	0.15			
		80	0.2			

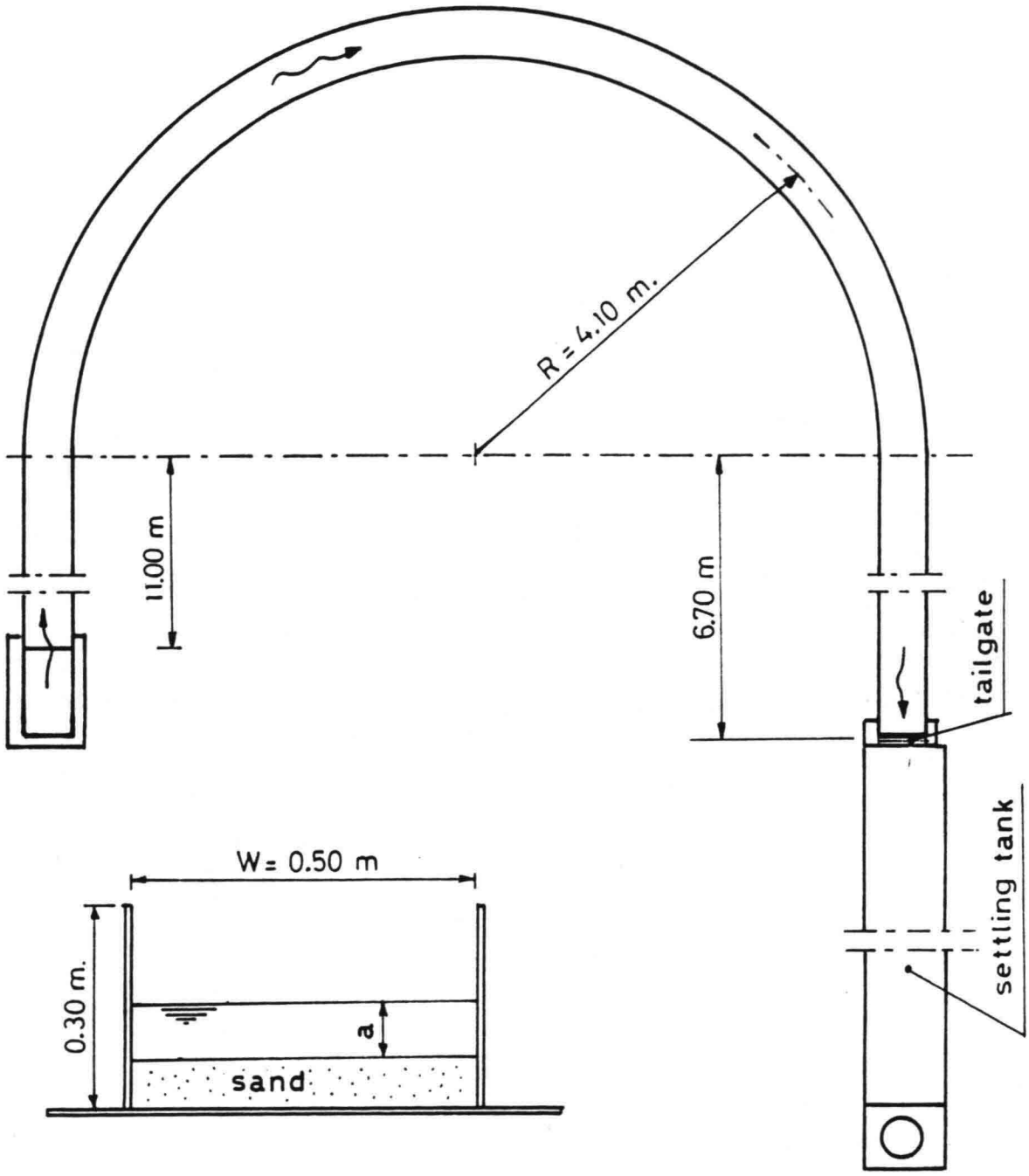

LAYOUT, LABORATORY OF FLUID MECHANICS CURVED FLUME

FIG. 1

DELFT UNIVERSITY OF TECHNOLOGY

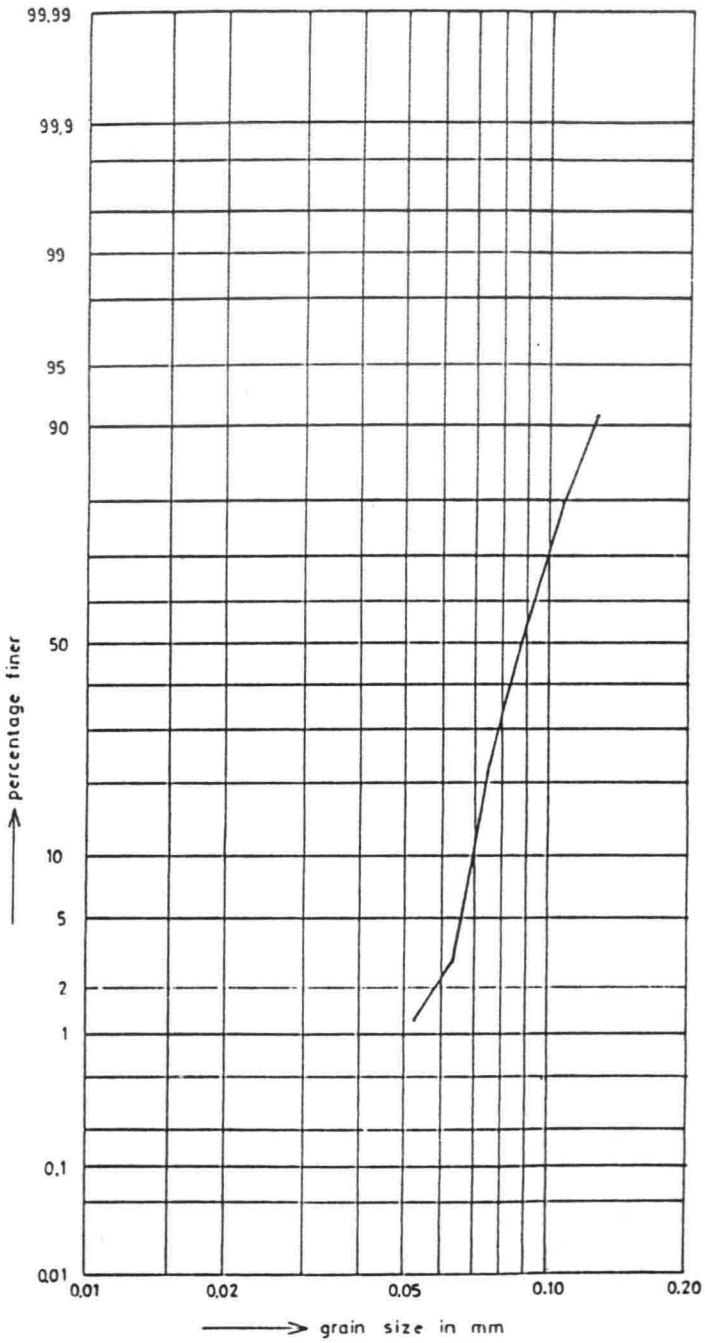

$D_{10} = 69\,\mu m.$ $D_{50} = 88\,\mu m.$ $D_{90} = 122\,\mu m.$

SIEVE CURVE OF BED MATERIAL

FIG. 2

DELFT UNIVERSITY OF TECHNOLOGY

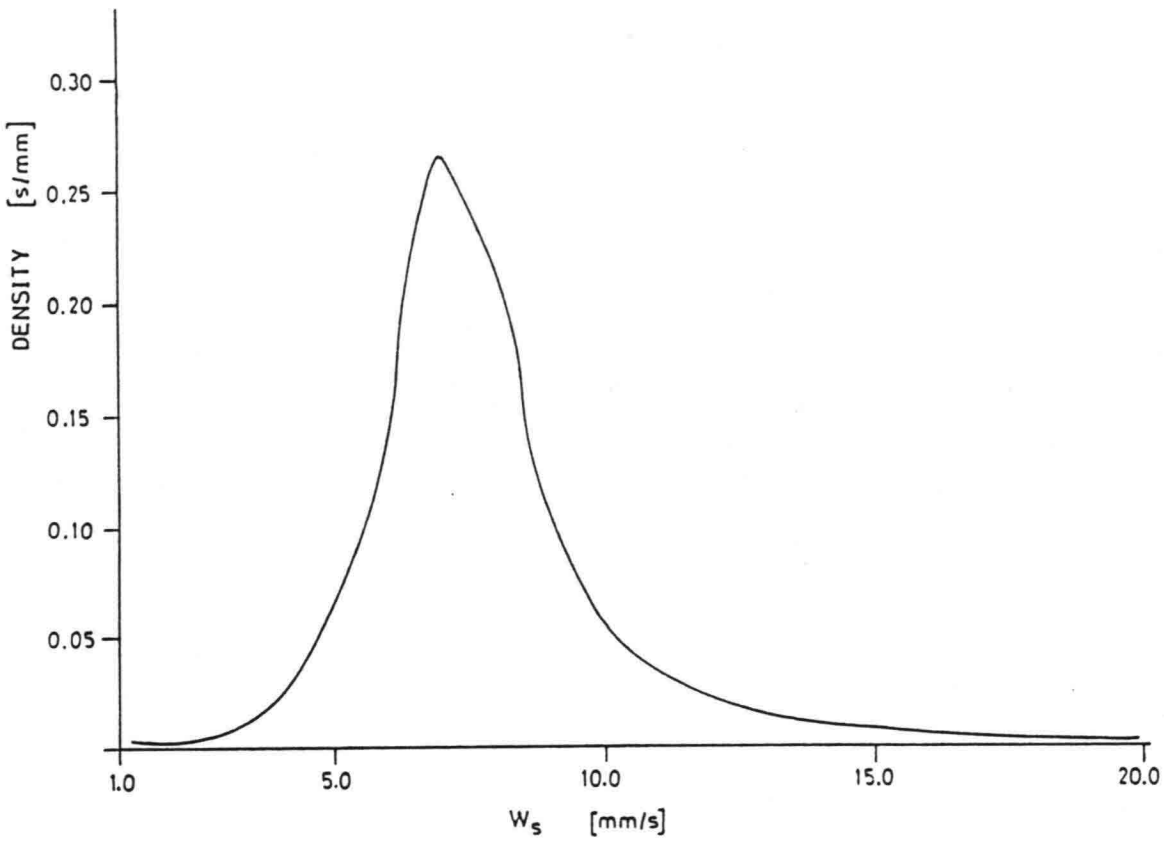

PROBABILITY DENSITY DISTRIBUTION OF FALL VELOCITY

FIG. 3

DELFT UNIVERSITY OF TECHNOLOGY

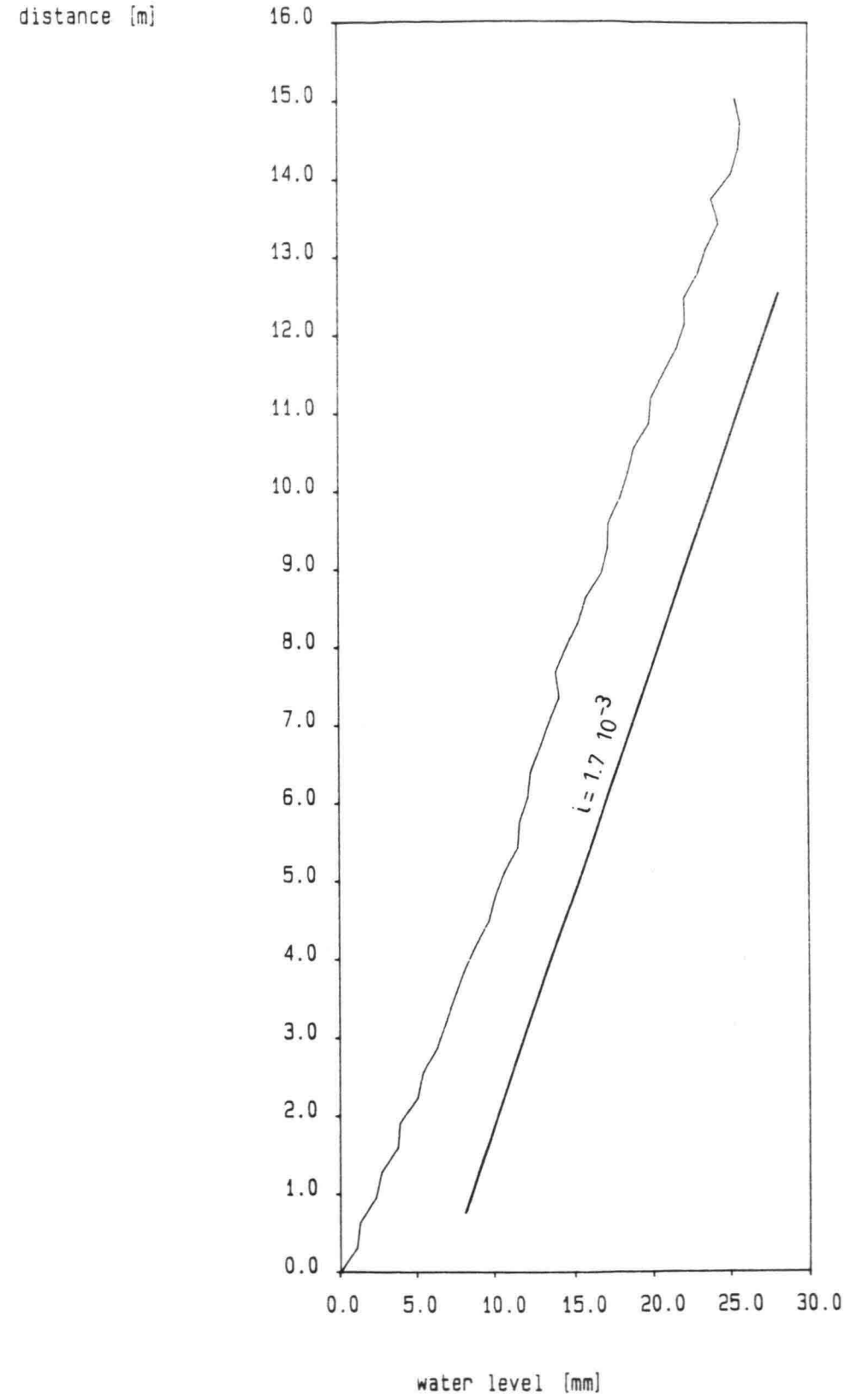

LONGITUDINAL WATER LEVEL SLOPE

FIG. 4

DELFT UNIVERSITY OF TECHNOLOGY

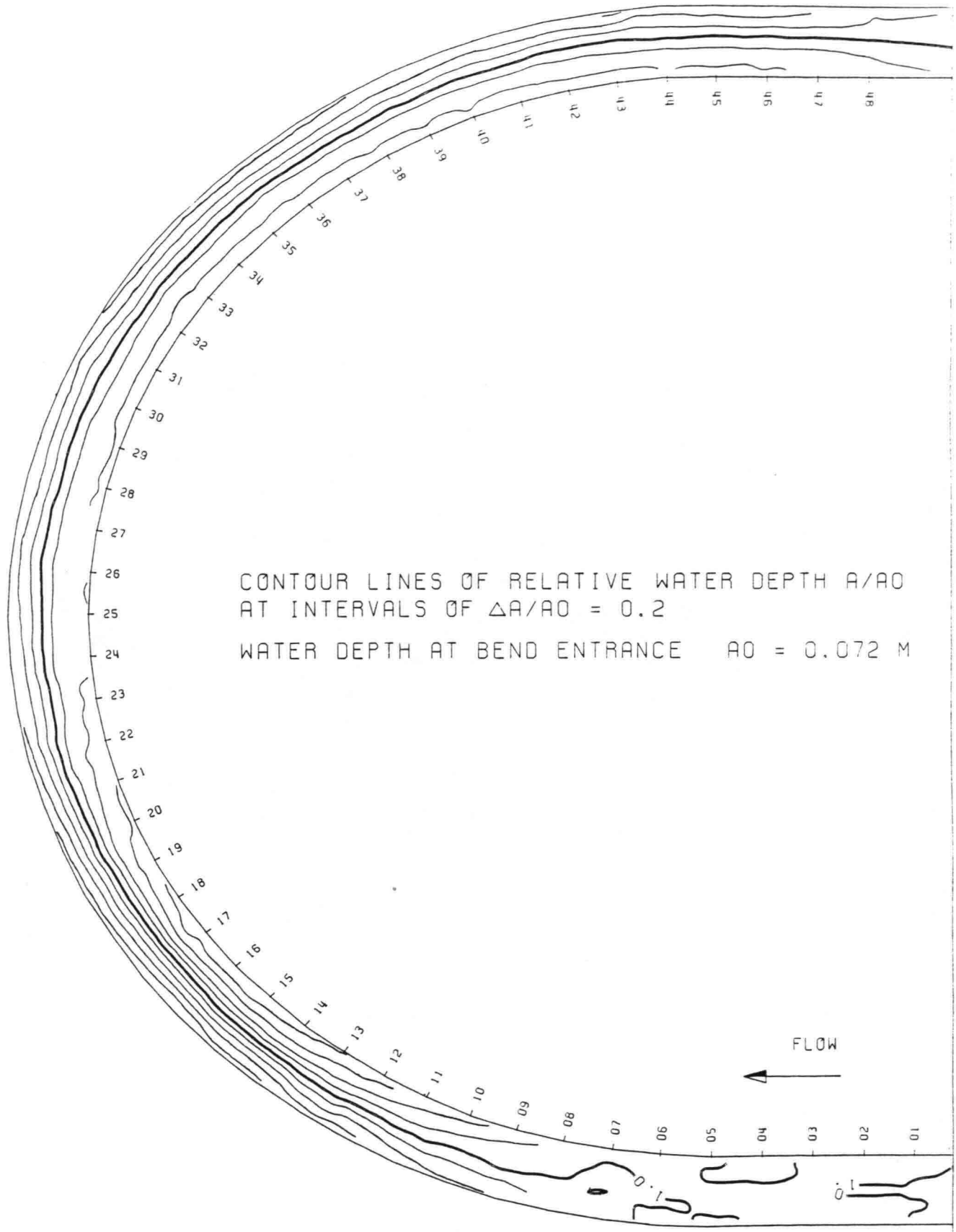

MODEL OF RIVER BEND, SUSPENDED-LOAD EXPERIMENT
ENSEMBLE MEAN OF 11 LONGITUDINAL TRAVERSES

DELFT UNIVERSITY OF TECHNOLOGY

FIG.5

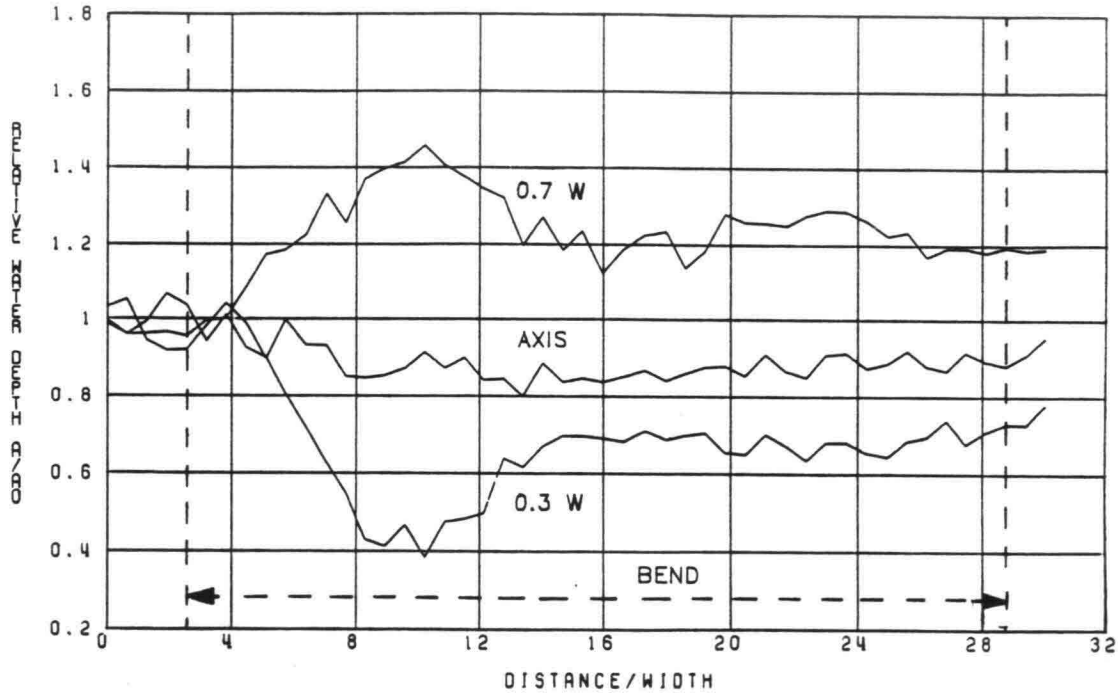

W = 0.5 M A0 = 0.072 M

LONGITUDINAL PROFILE OF THE WATER DEPTH

FIG. 6

DELFT UNIVERSITY OF TECHNOLOGY

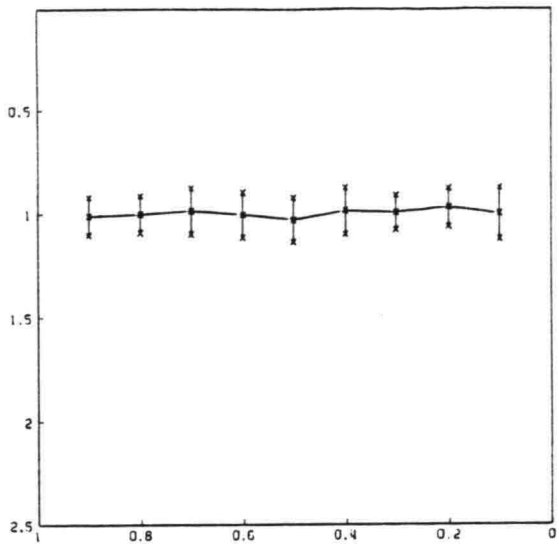

CROSS-SECTION 1

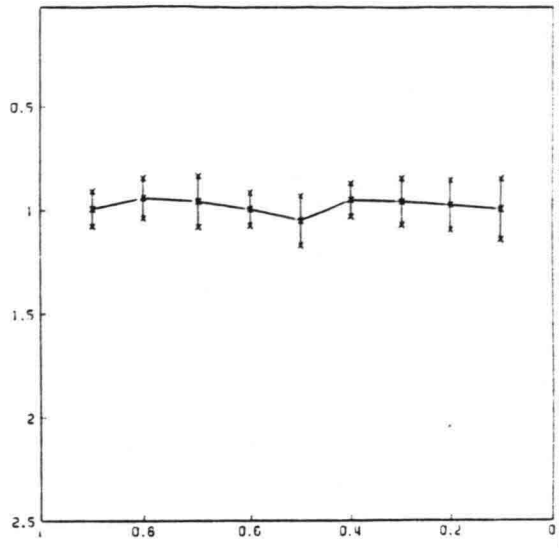

CROSS-SECTION 2

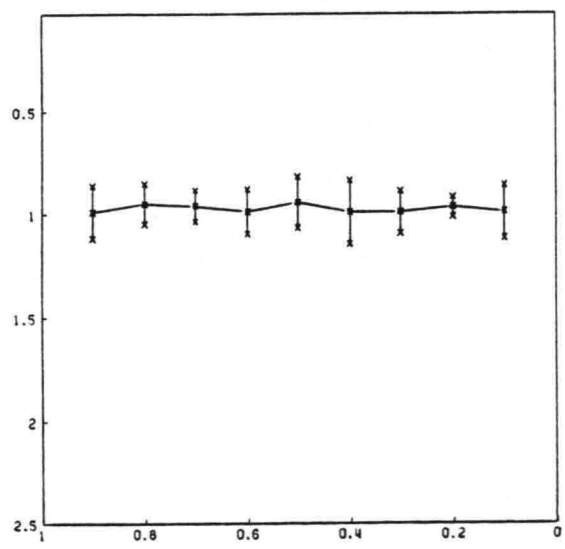

CROSS-SECTION 3

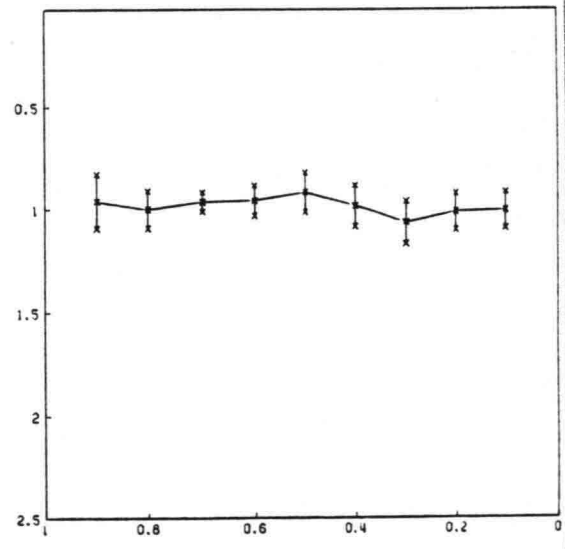

CROSS-SECTION 4

W = 0.5 M A0 = 0.072 M

± σ OF 11 MEASUREMENTS

WATER DEPTH IN CROSS-DIRECTION

FIG 7A

DELFT UNIVERSITY OF TECHNOLOGY

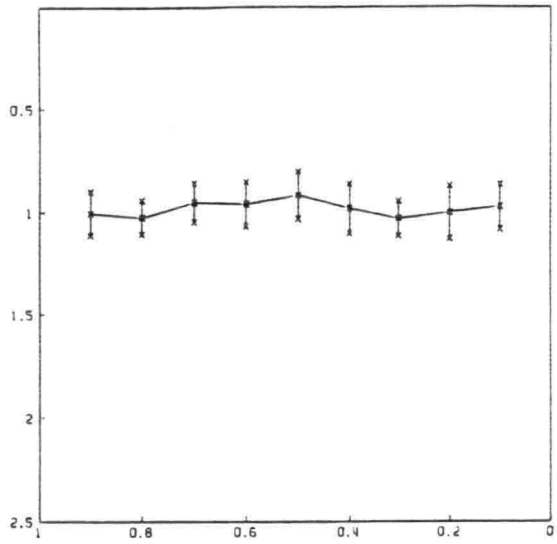

CROSS-SECTION 5

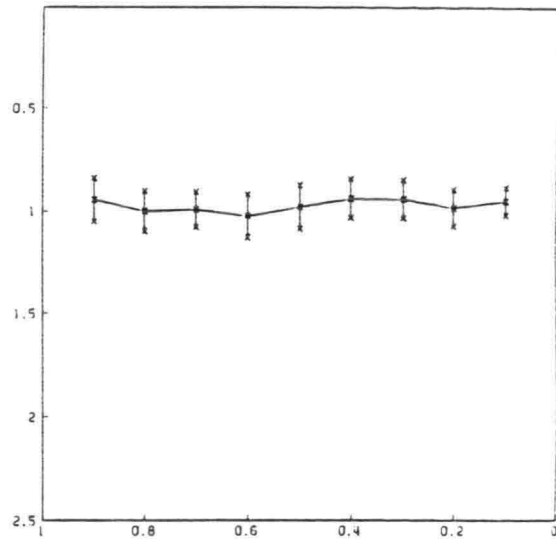

CROSS-SECTION 6

WATER DEPTH A/AO

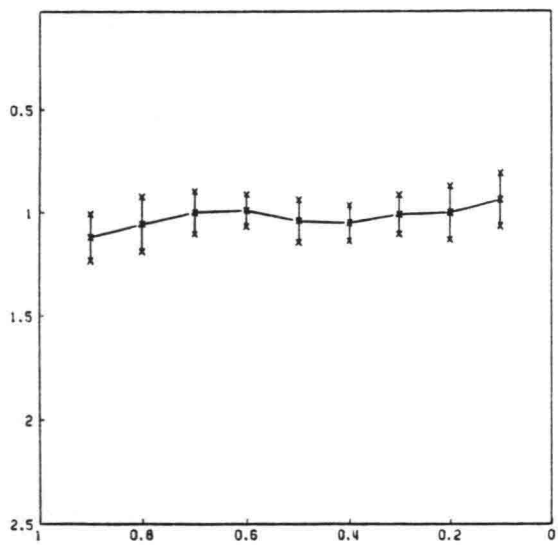

DISTANCE FROM INNERSIDE BEND Y/W

CROSS-SECTION 7

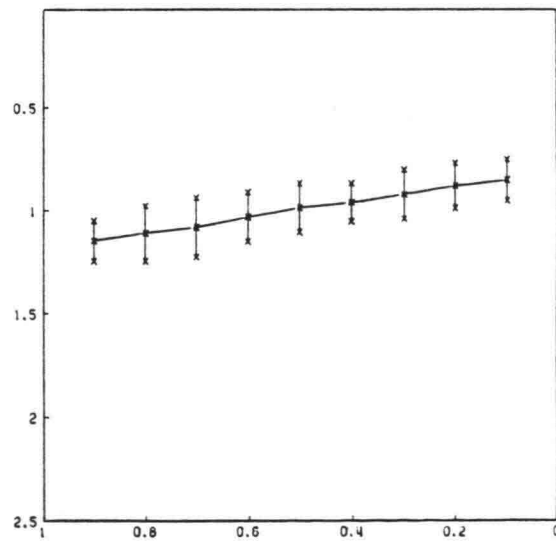

CROSS-SECTION 8

W = 0.5 M AO = 0.072 M

$\pm\sigma$ OF 11 MEASUREMENTS

WATER DEPTH IN CROSS-DIRECTION

FIG 7B

DELFT UNIVERSITY OF TECHNOLOGY

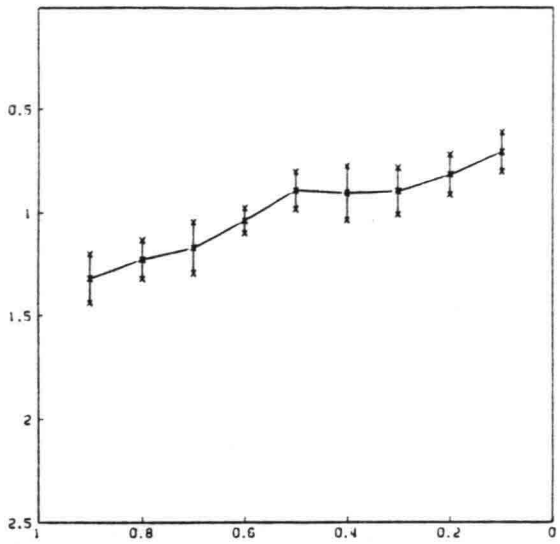

CROSS-SECTION 9

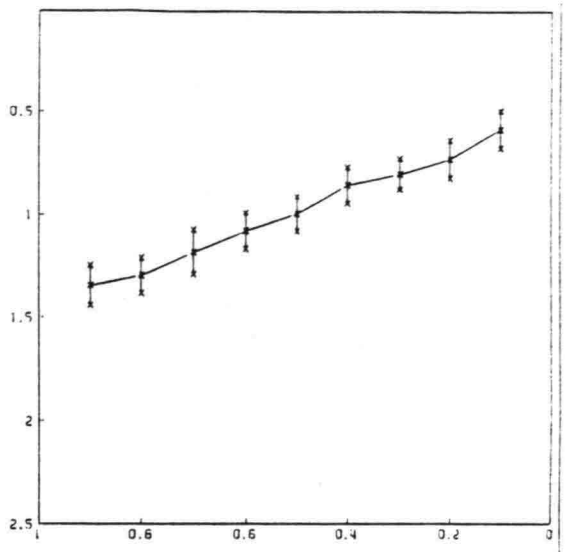

CROSS-SECTION 10

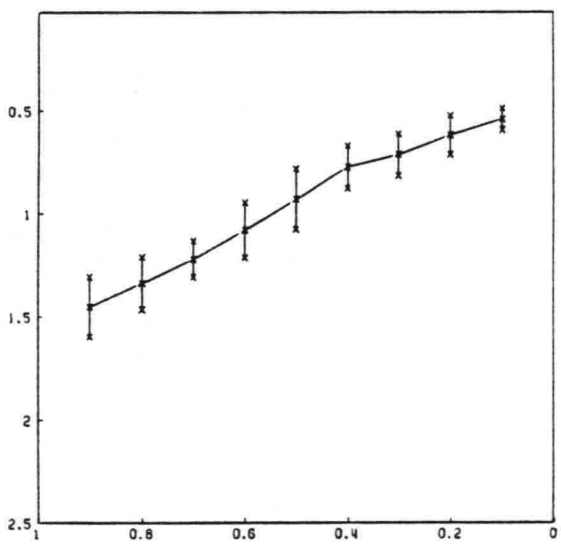

CROSS-SECTION 11

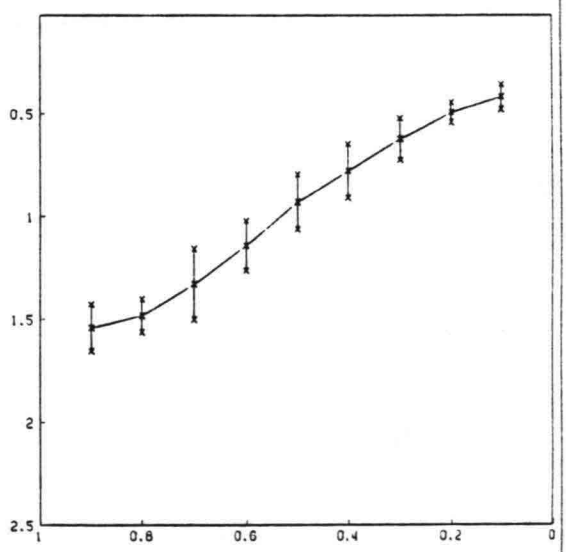

CROSS-SECTION 12

W = 0.5 M A0 = 0.072 M

± σ OF 11 MEASUREMENTS

WATER DEPTH IN CROSS-DIRECTION

FIG 7C

DELFT UNIVERSITY OF TECHNOLOGY

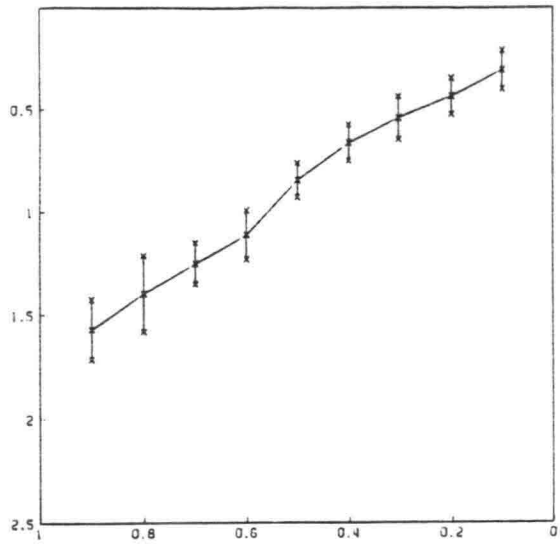

CROSS-SECTION 13

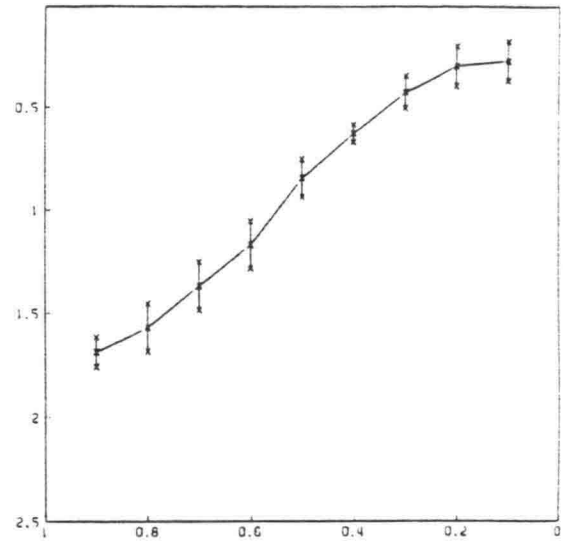

CROSS-SECTION 14

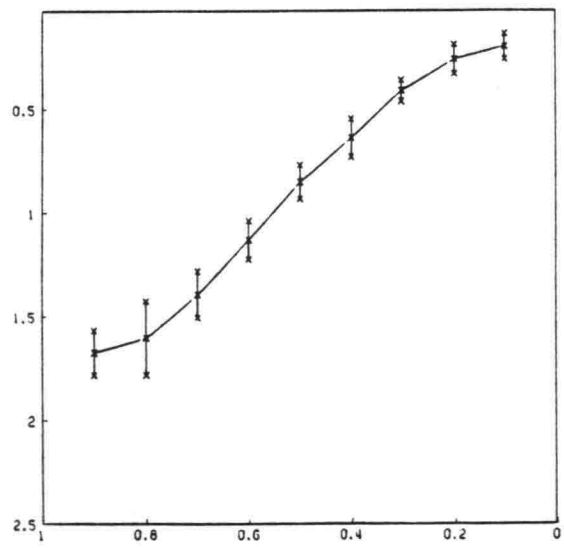

CROSS-SECTION 15

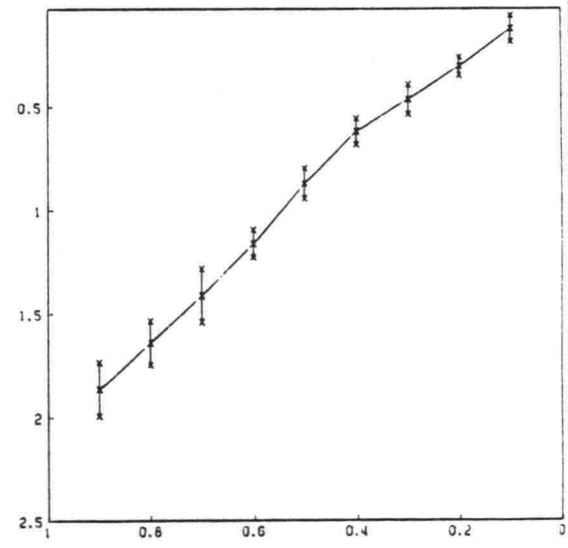

CROSS-SECTION 16

W = 0.5 M A0 = 0.072 M

$\pm\sigma$ OF 11 MEASUREMENTS

WATER DEPTH IN CROSS-DIRECTION

FIG 7D

DELFT UNIVERSITY OF TECHNOLOGY

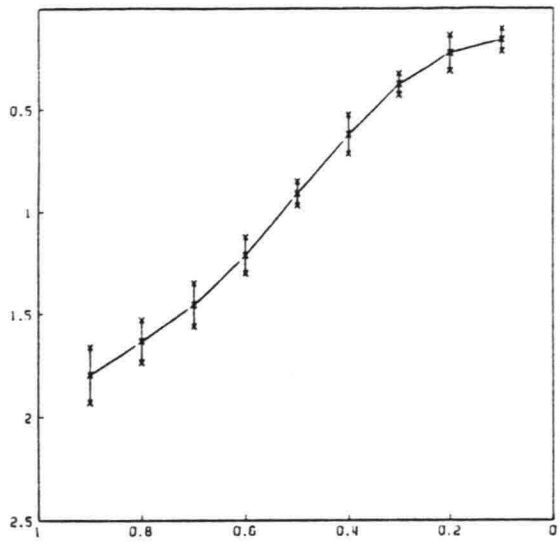

CROSS-SECTION 17

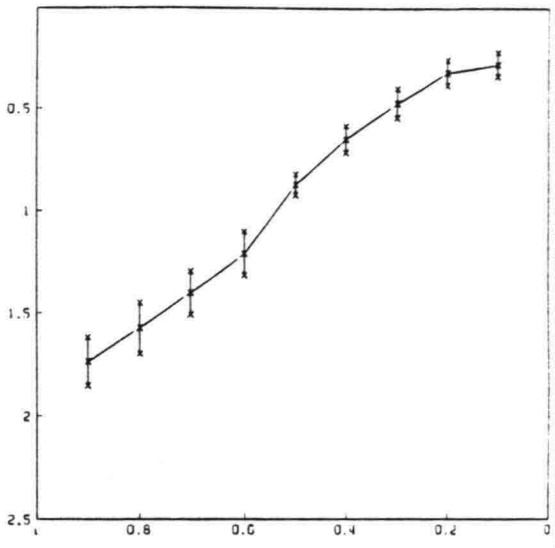

CROSS-SECTION 18

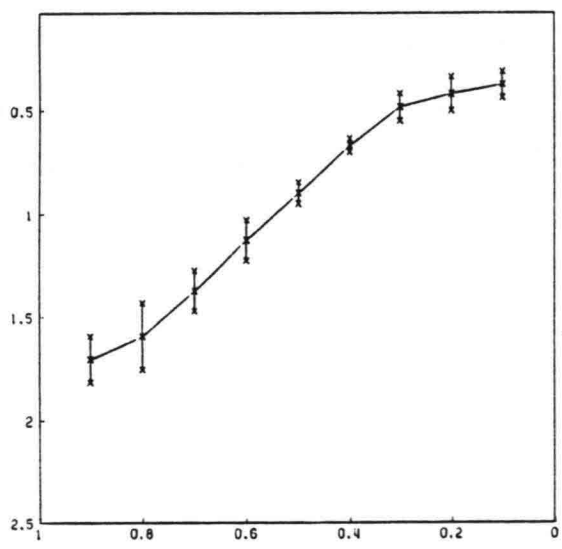

CROSS-SECTION 19

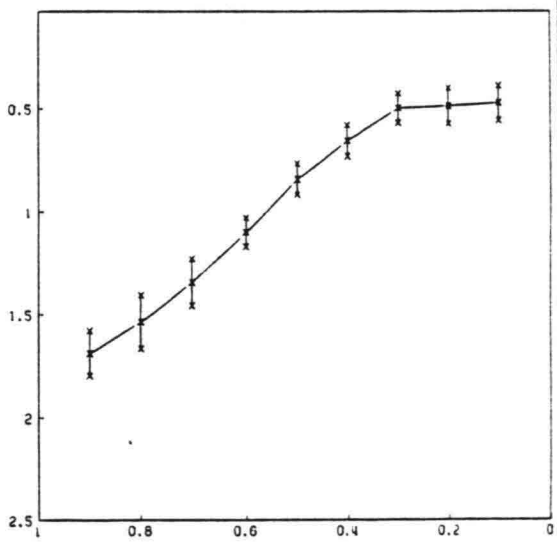

CROSS-SECTION 20

W = 0.5 M A0 = 0.072 M

± σ OF 11 MEASUREMENTS

WATER DEPTH IN CROSS-DIRECTION

FIG 7E

DELFT UNIVERSITY OF TECHNOLOGY

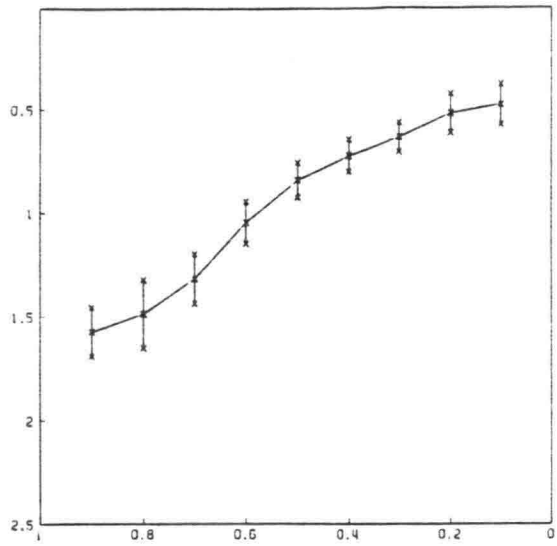

CROSS-SECTION 21

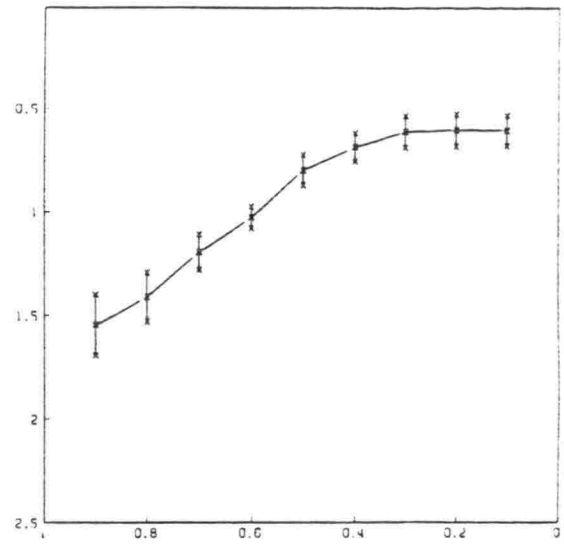

CROSS-SECTION 22

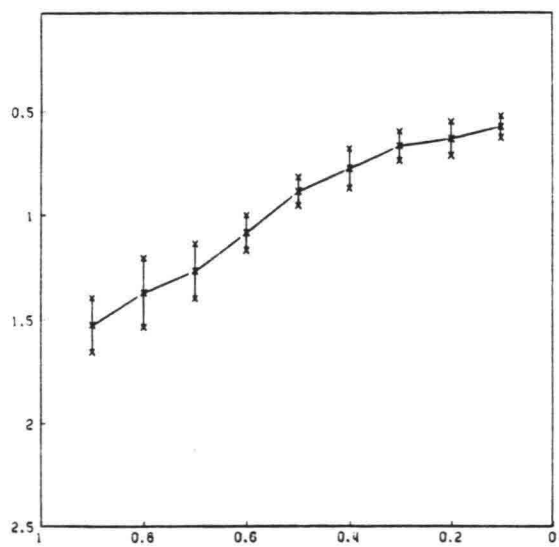

CROSS-SECTION 23

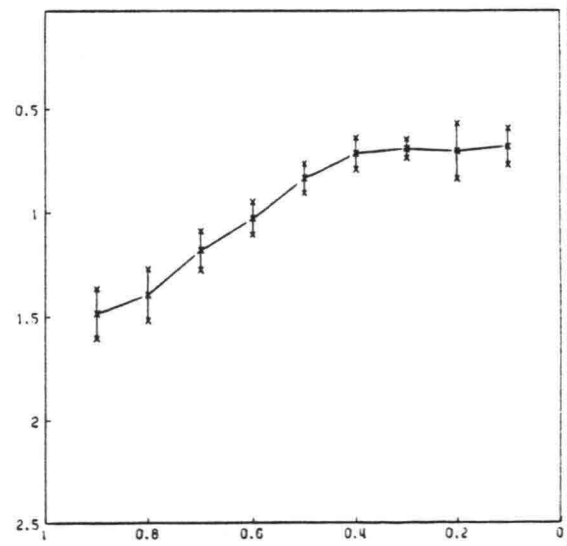

CROSS-SECTION 24

W = 0.5 M A0 = 0.072 M

± σ OF 11 MEASUREMENTS

WATER DEPTH IN CROSS-DIRECTION

FIG 7F

DELFT UNIVERSITY OF TECHNOLOGY

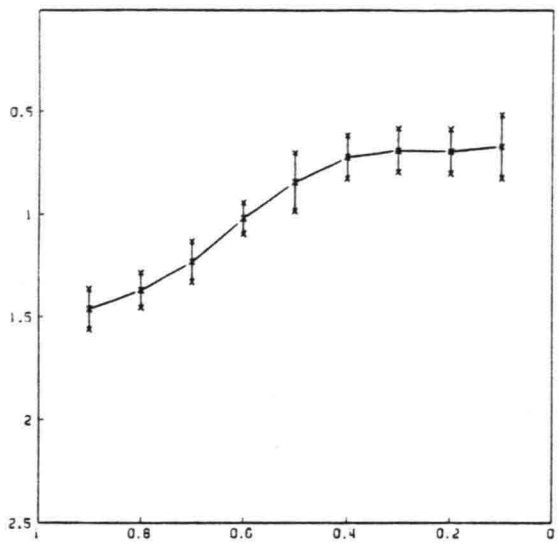

CROSS-SECTION 25

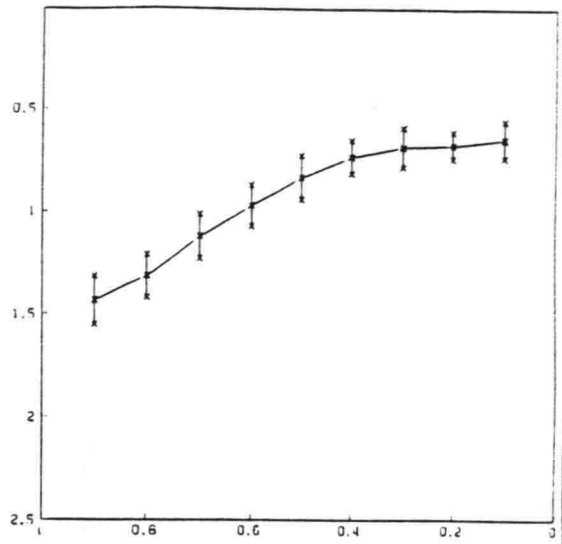

CROSS-SECTION 26

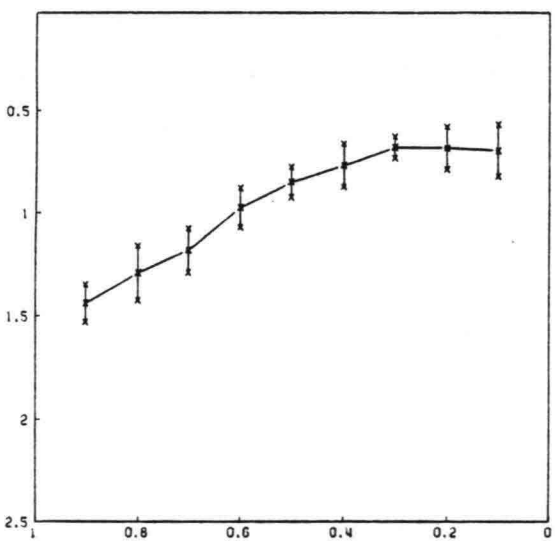

CROSS-SECTION 27

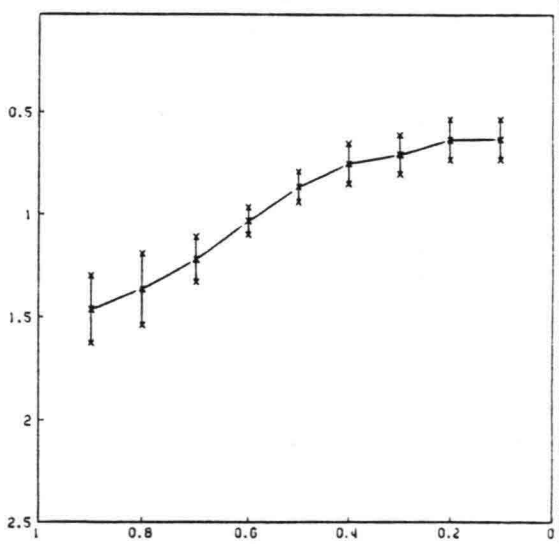

CROSS-SECTION 28

W = 0.5 M A0 = 0.072 M

$\pm\sigma$ OF 11 MEASUREMENTS

WATER DEPTH IN CROSS-DIRECTION

FIG 7G

DELFT UNIVERSITY OF TECHNOLOGY

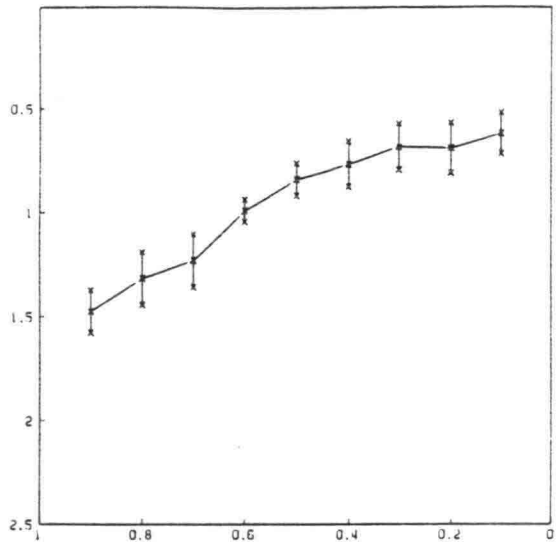

CROSS-SECTION 29

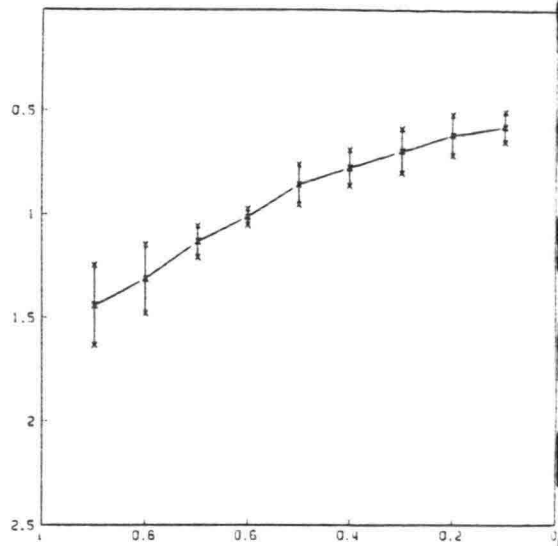

CROSS-SECTION 30

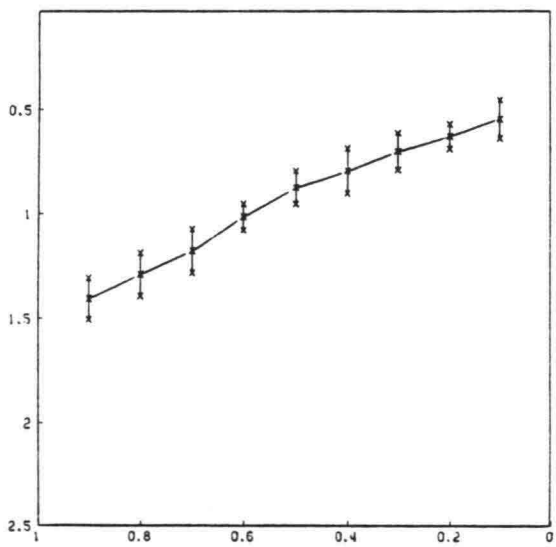

CROSS-SECTION 31

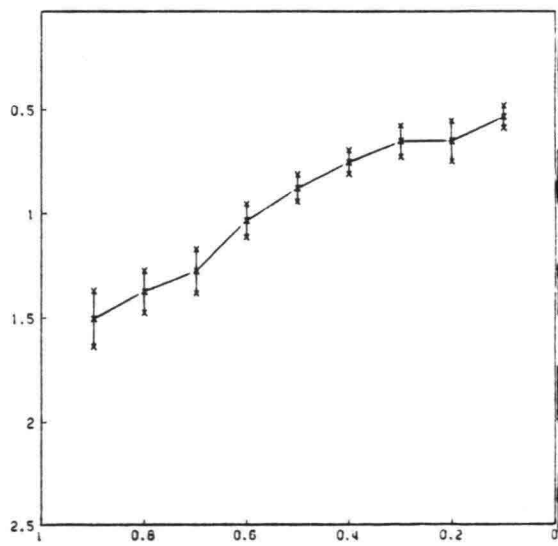

CROSS-SECTION 32

W = 0.5 M A0 = 0.072 M

± σ OF 11 MEASUREMENTS

WATER DEPTH IN CROSS-DIRECTION

FIG 7H

DELFT UNIVERSITY OF TECHNOLOGY

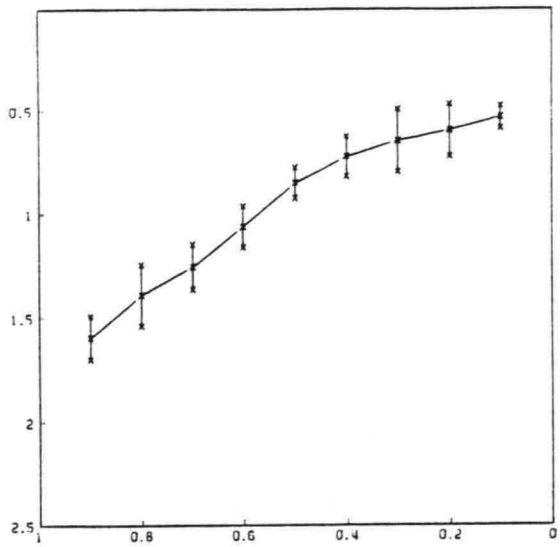

CROSS-SECTION 33

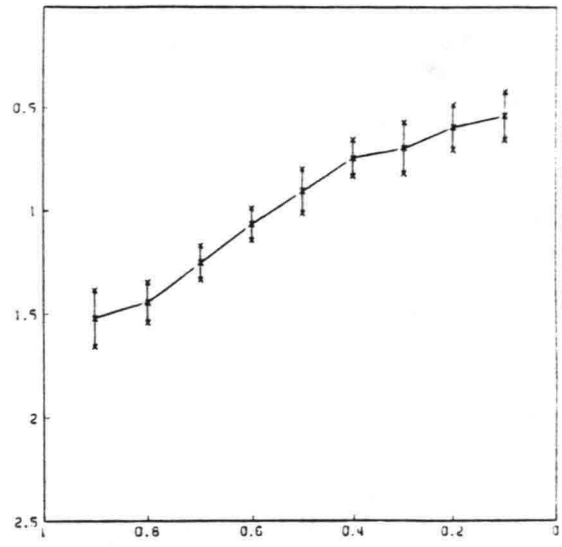

CROSS-SECTION 34

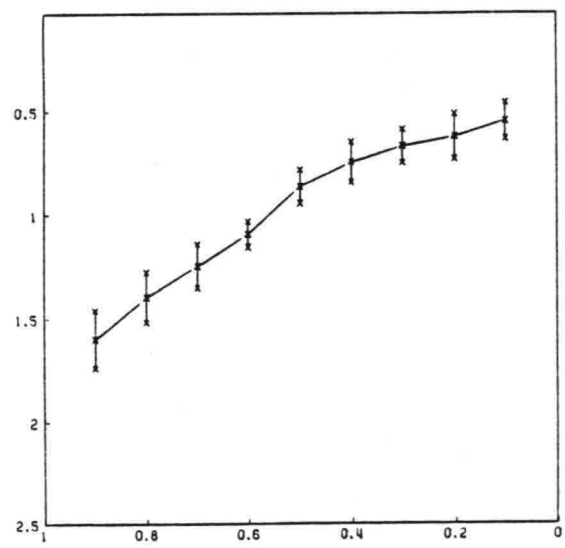

CROSS-SECTION 35

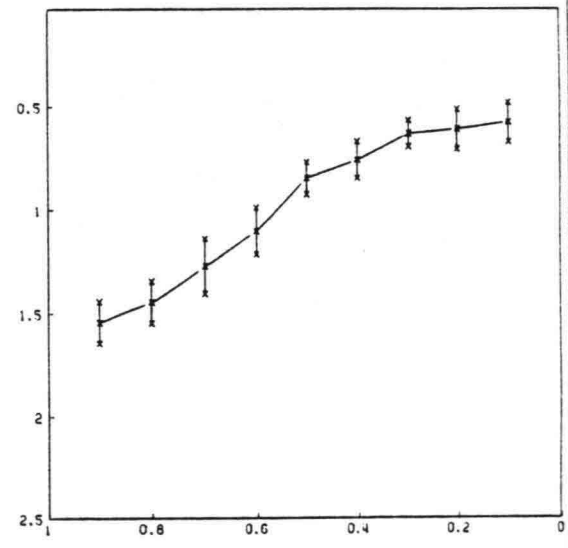

CROSS-SECTION 36

W = 0.5 M A0 = 0.072 M

± σ OF 11 MEASUREMENTS

WATER DEPTH IN CROSS-DIRECTION

FIG 7I

DELFT UNIVERSITY OF TECHNOLOGY

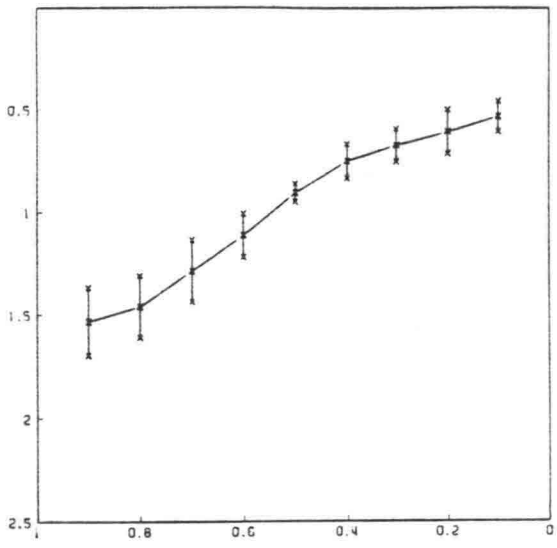

CROSS-SECTION 37

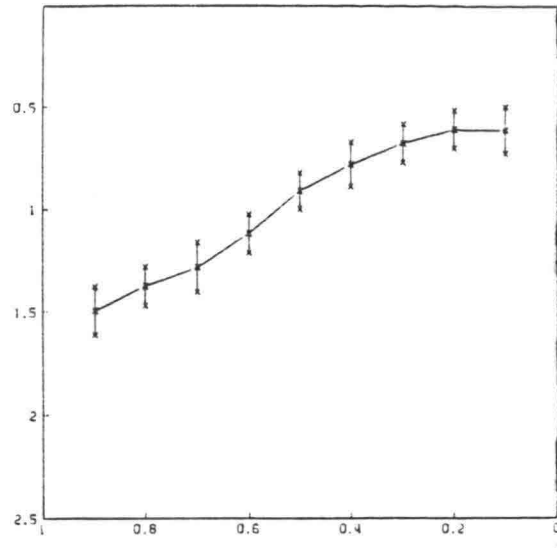

CROSS-SECTION 38

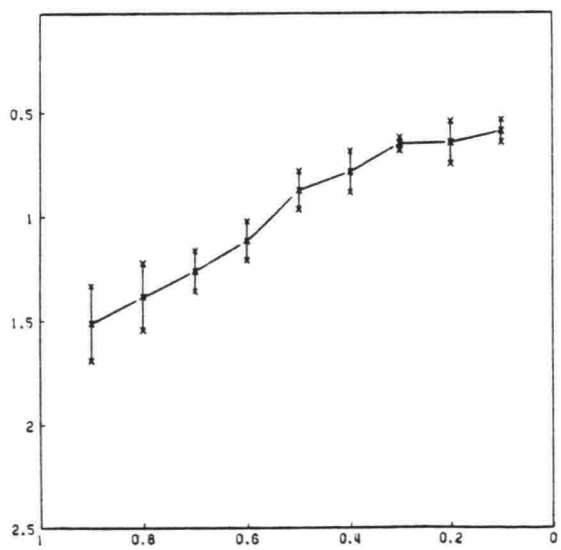

CROSS-SECTION 39

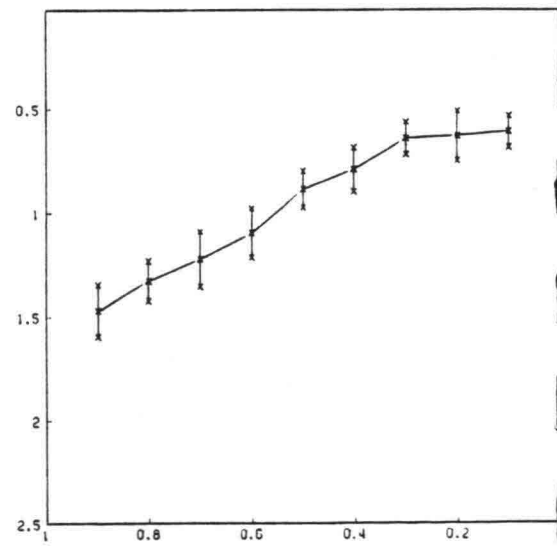

CROSS-SECTION 40

W = 0.5 M A0 = 0.072 M

± σ OF 11 MEASUREMENTS

WATER DEPTH IN CROSS-DIRECTION

FIG 7J

DELFT UNIVERSITY OF TECHNOLOGY

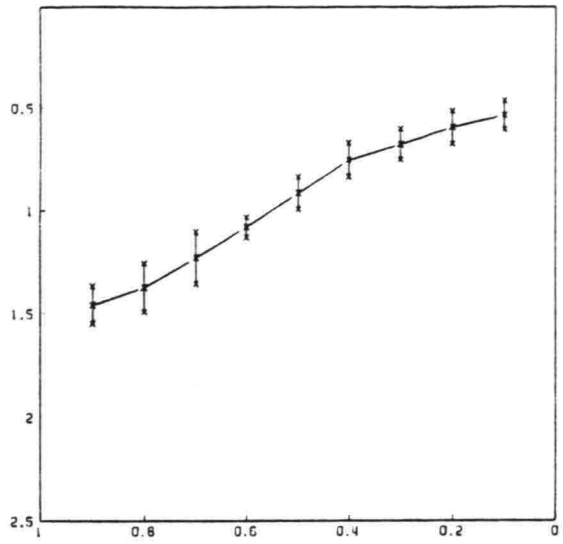

CROSS-SECTION 41

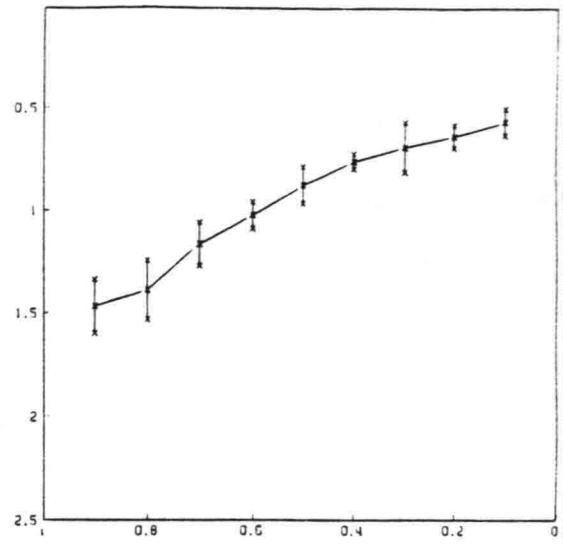

CROSS-SECTION 42

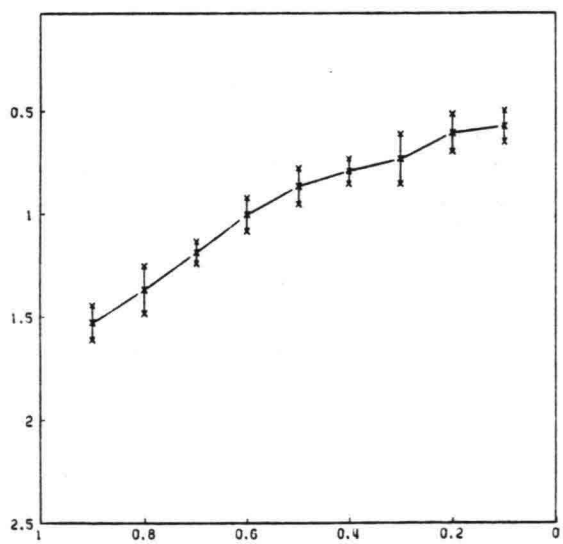

CROSS-SECTION 43

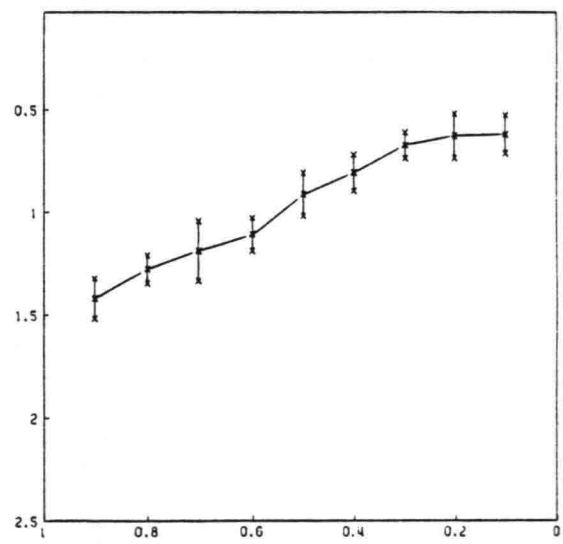

CROSS-SECTION 44

W = 0.5 M A0 = 0.072 M

$\pm \sigma$ OF 11 MEASUREMENTS

WATER DEPTH IN CROSS-DIRECTION

FIG 7K

DELFT UNIVERSITY OF TECHNOLOGY

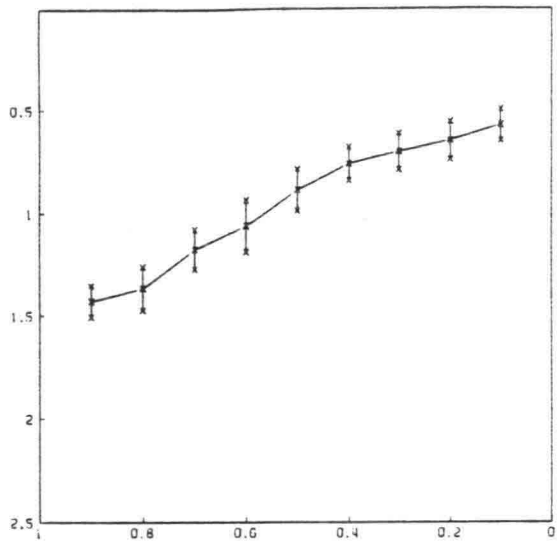

CROSS-SECTION 45

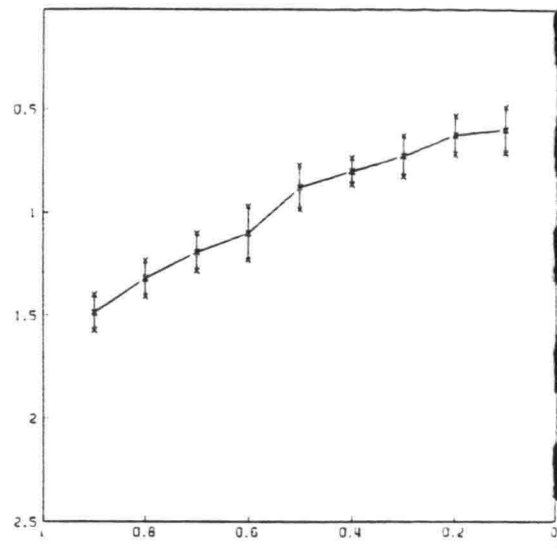

CROSS-SECTION 46

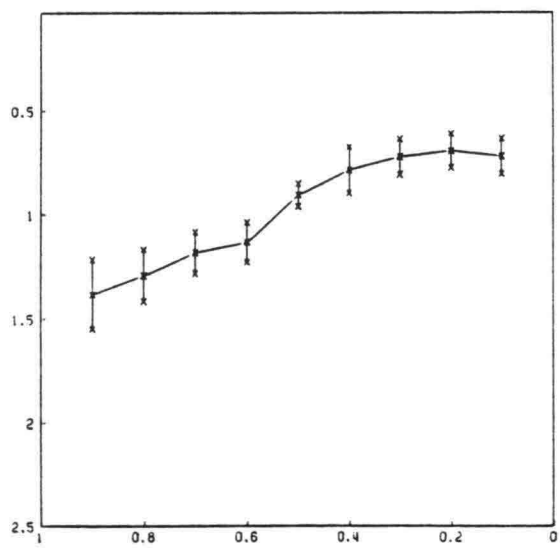

CROSS-SECTION 47

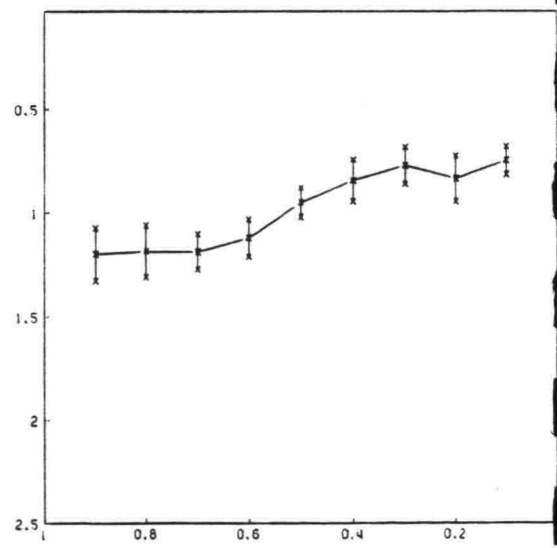

CROSS-SECTION 48

W = 0.5 M A0 = 0.072 M

± σ OF 11 MEASUREMENTS

WATER DEPTH IN CROSS-DIRECTION

FIG 7L

DELFT UNIVERSITY OF TECHNOLOGY

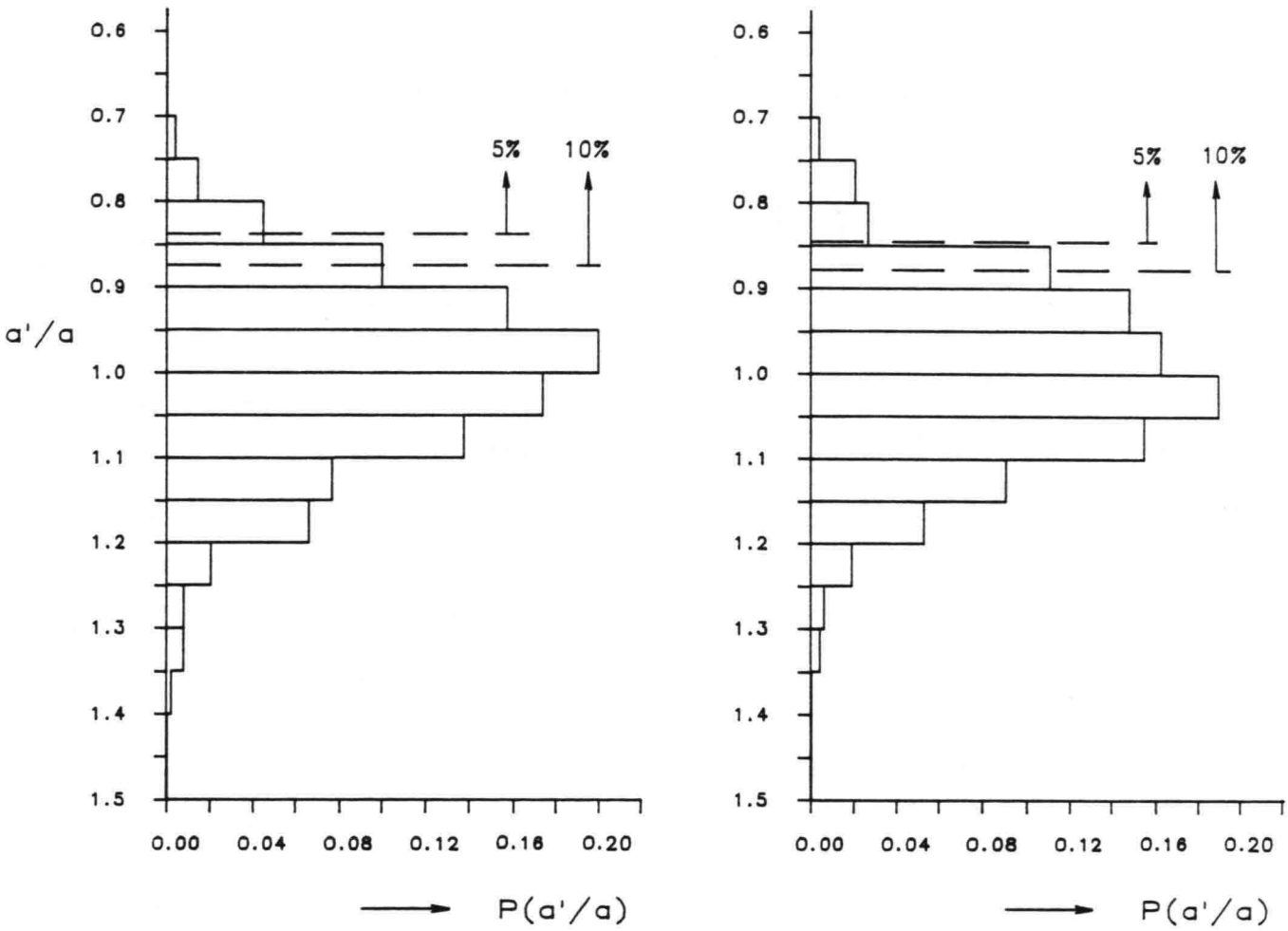

a' local water depth

a ensemble mean local water depth

PROBABILITY DISTRIBUTION OF BED LEVEL

FIG. 8

DELFT UNIVERSITY OF TECHNOLOGY

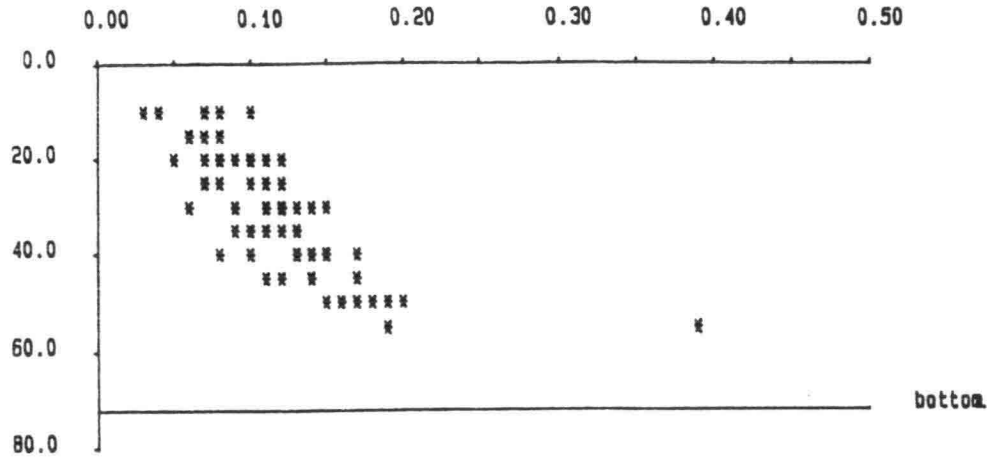

CROSS-SECTION 1

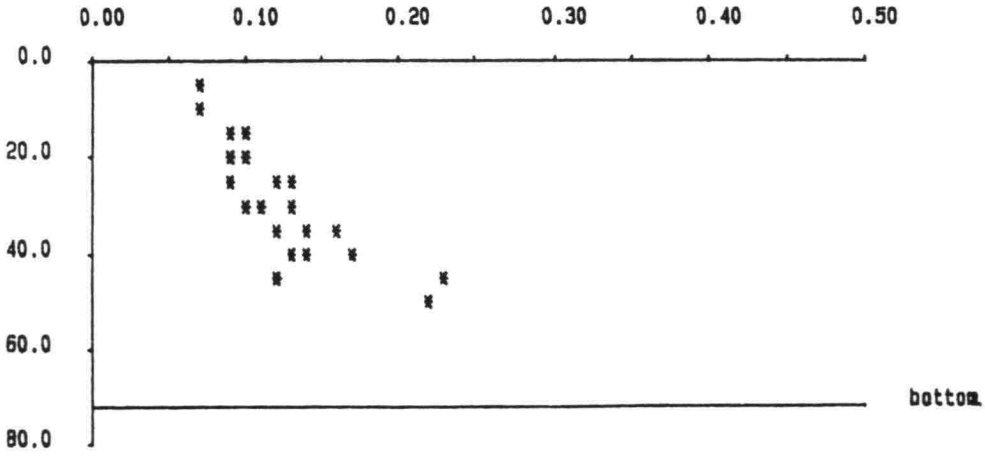

CROSS-SECTION 5

CONCENTRATION PROFILES
(mean water depth of 11 measurements)

FIG. 9 a

DELFT UNIVERSITY OF TECHNOLOGY

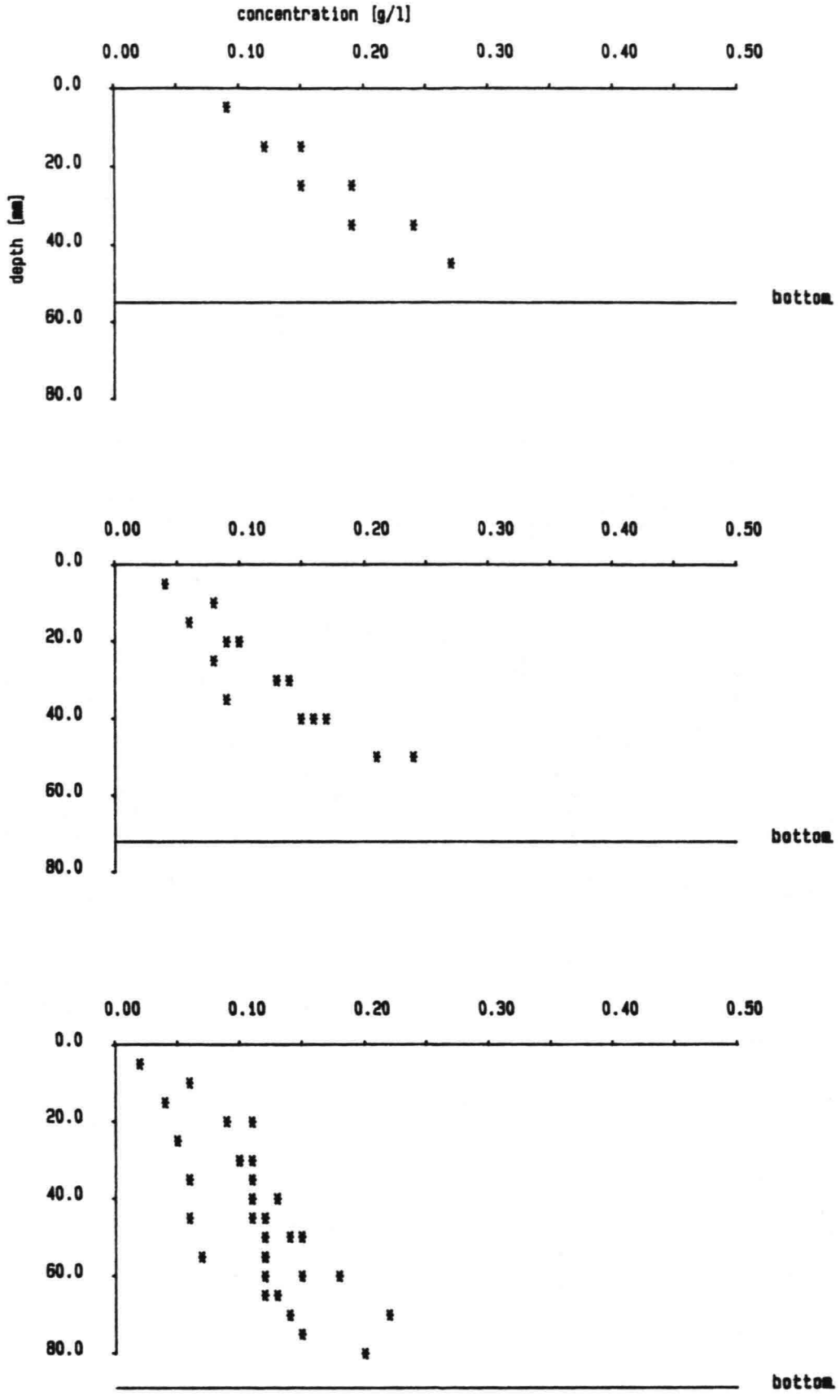

CROSS-SECTION 10

CONCENTRATION PROFILES
(mean water depth of 11 measurements)

FIG. 9 b

DELFT UNIVERSITY OF TECHNOLOGY

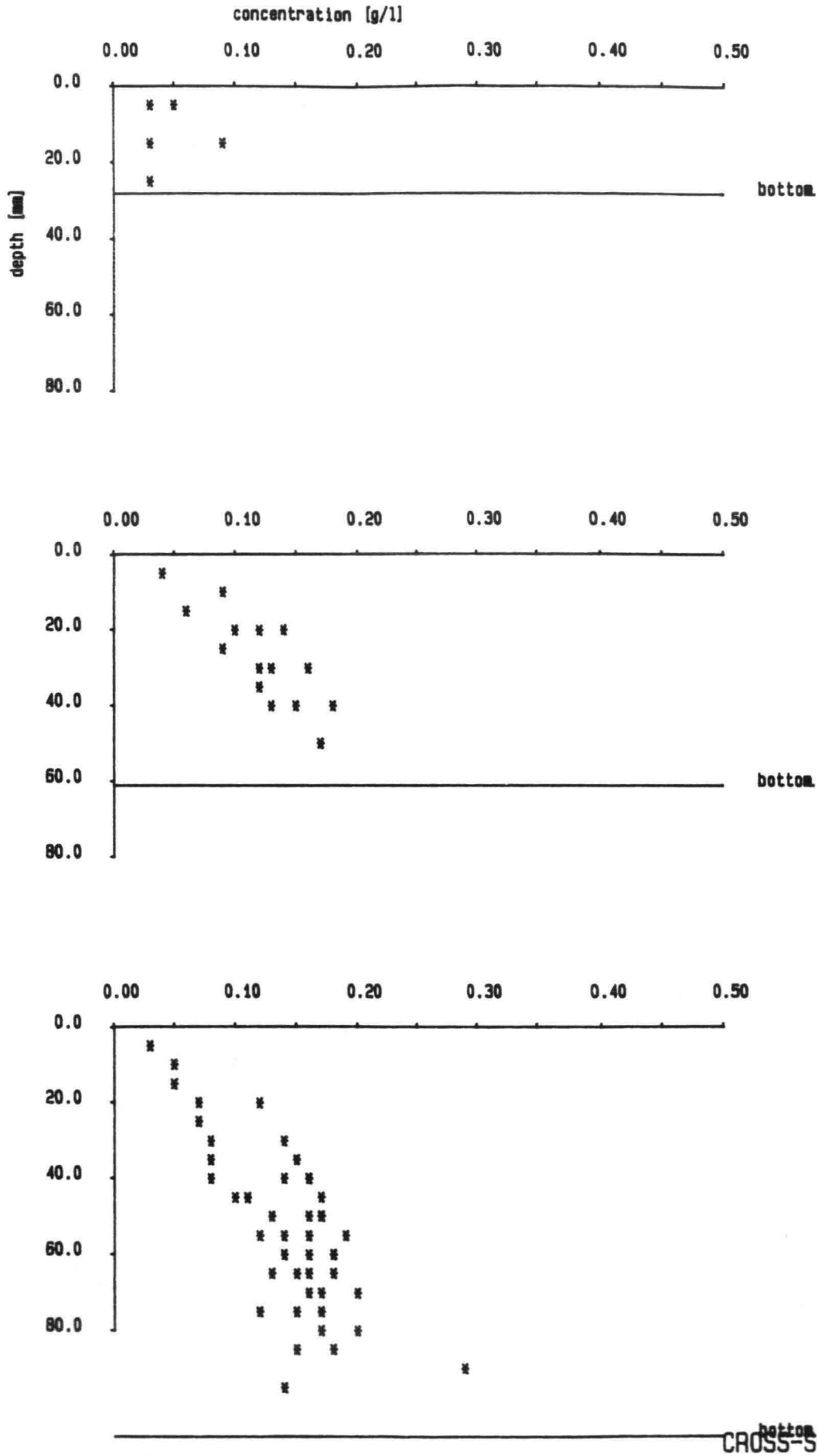

CROSS-SECTION 15

CONCENTRATION PROFILES
(mean water depth of 11 measurements)

FIG. 9 c

DELFT UNIVERSITY OF TECHNOLOGY

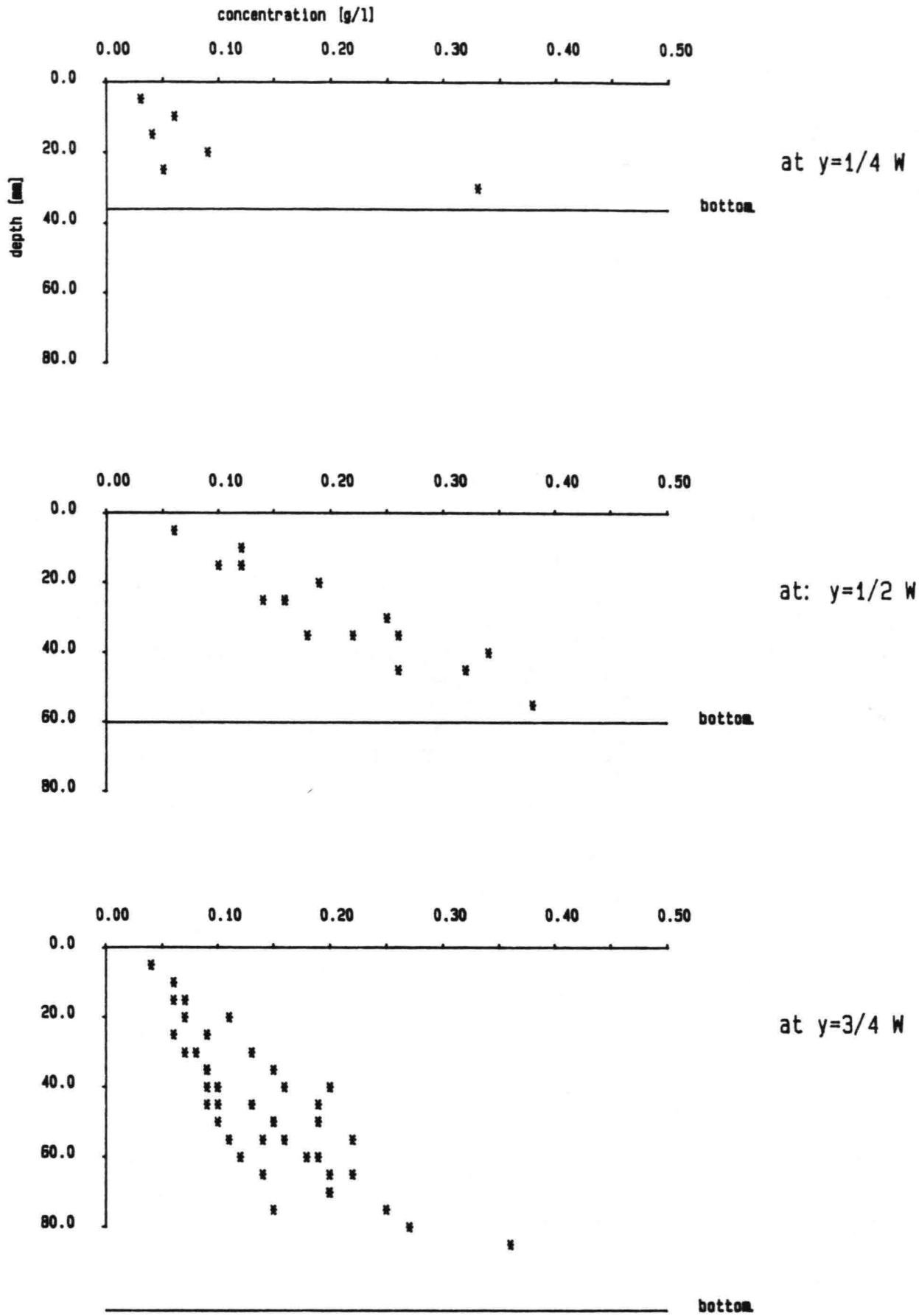

CROSS-SECTION 20

CONCENTRATION PROFILES
(mean water depth of 11 measurements)

FIG. 9 d

DELFT UNIVERSITY OF TECHNOLOGY

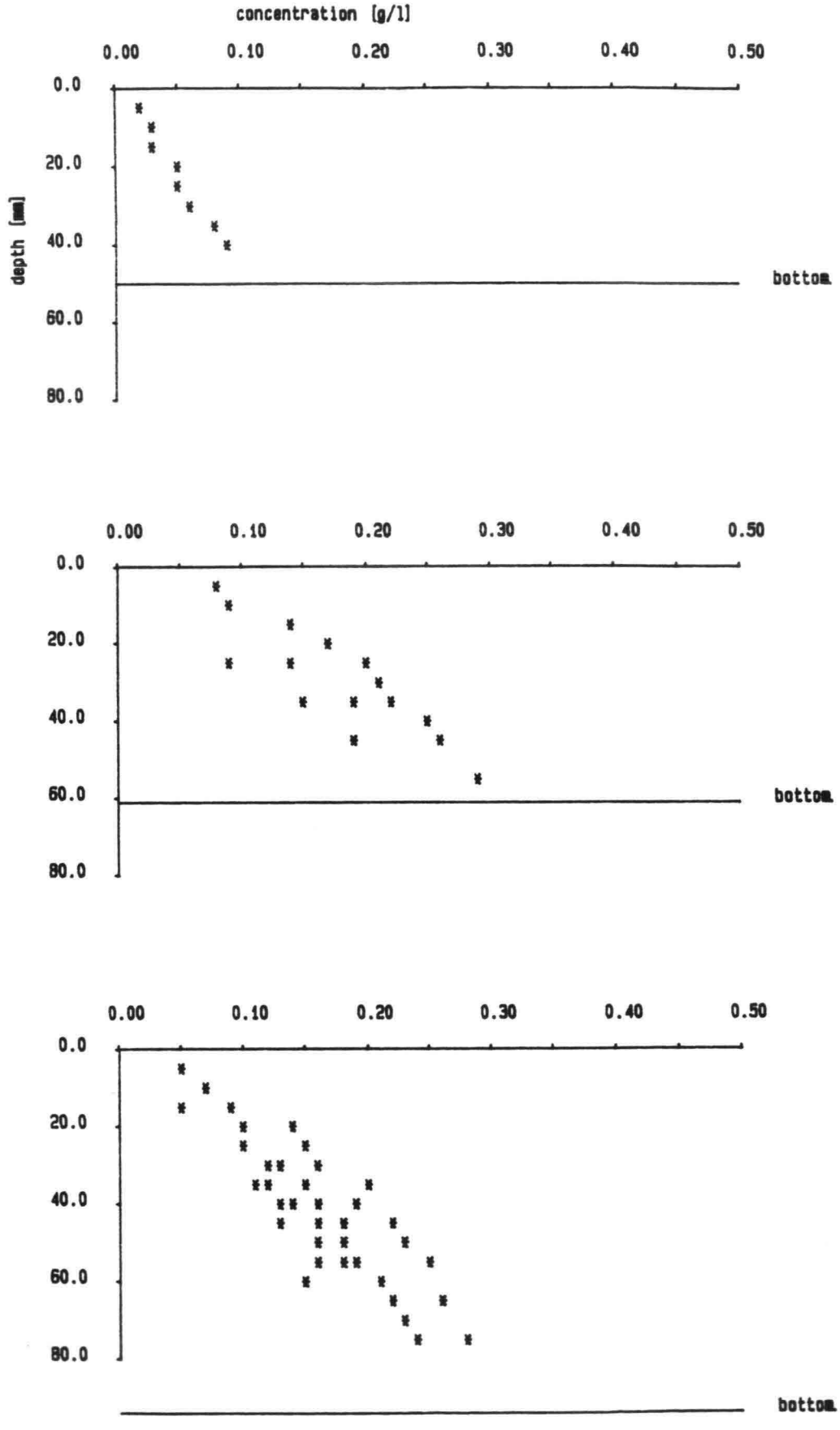

CROSS-SECTION 25

CONCENTRATION PROFILES
(mean water depth of 11 measurements)

FIG. 9 e

DELFT UNIVERSITY OF TECHNOLOGY

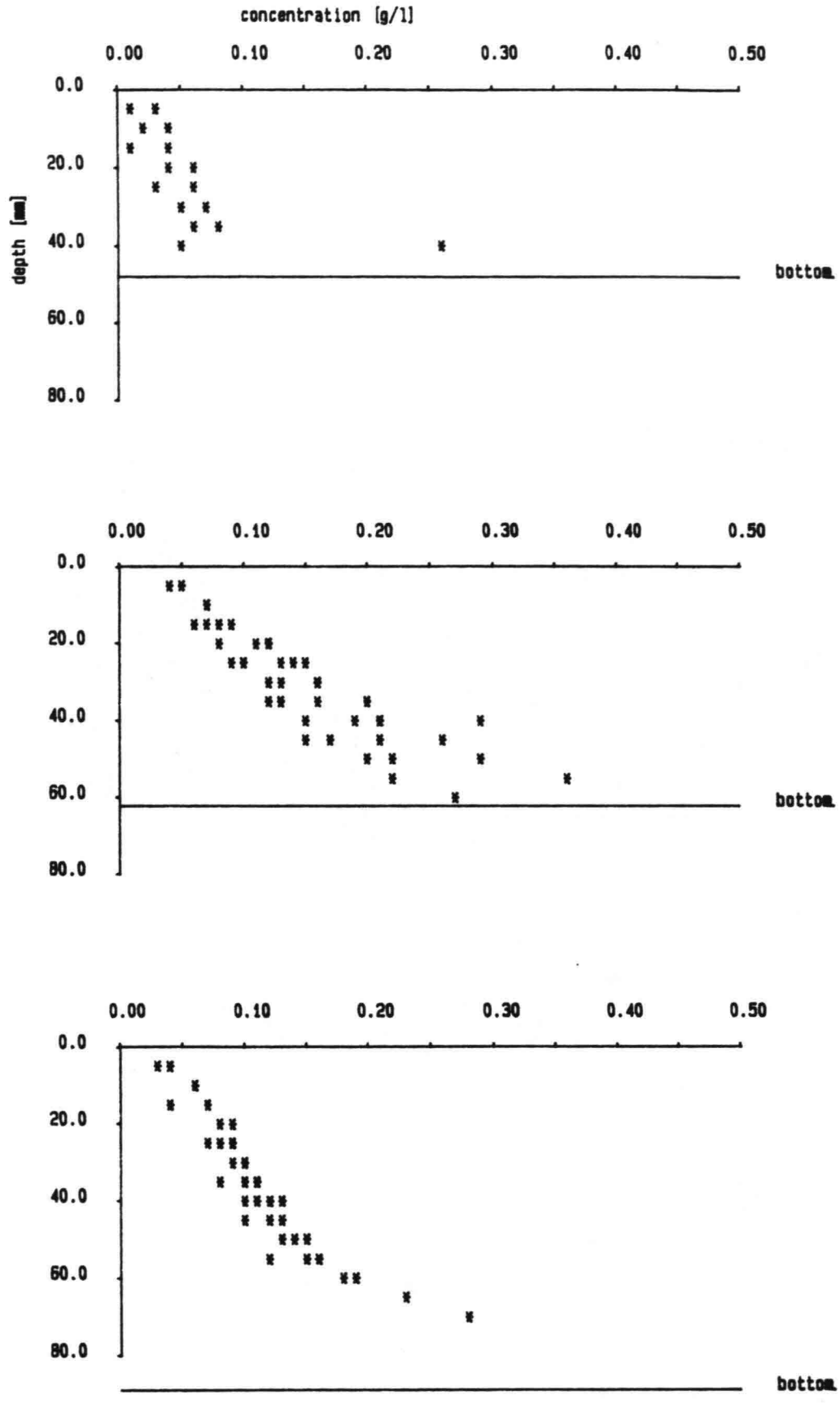

CROSS-SECTION 30

CONCENTRATION PROFILES
(mean water depth of 11 measurements)

FIG. 9 f

DELFT UNIVERSITY OF TECHNOLOGY

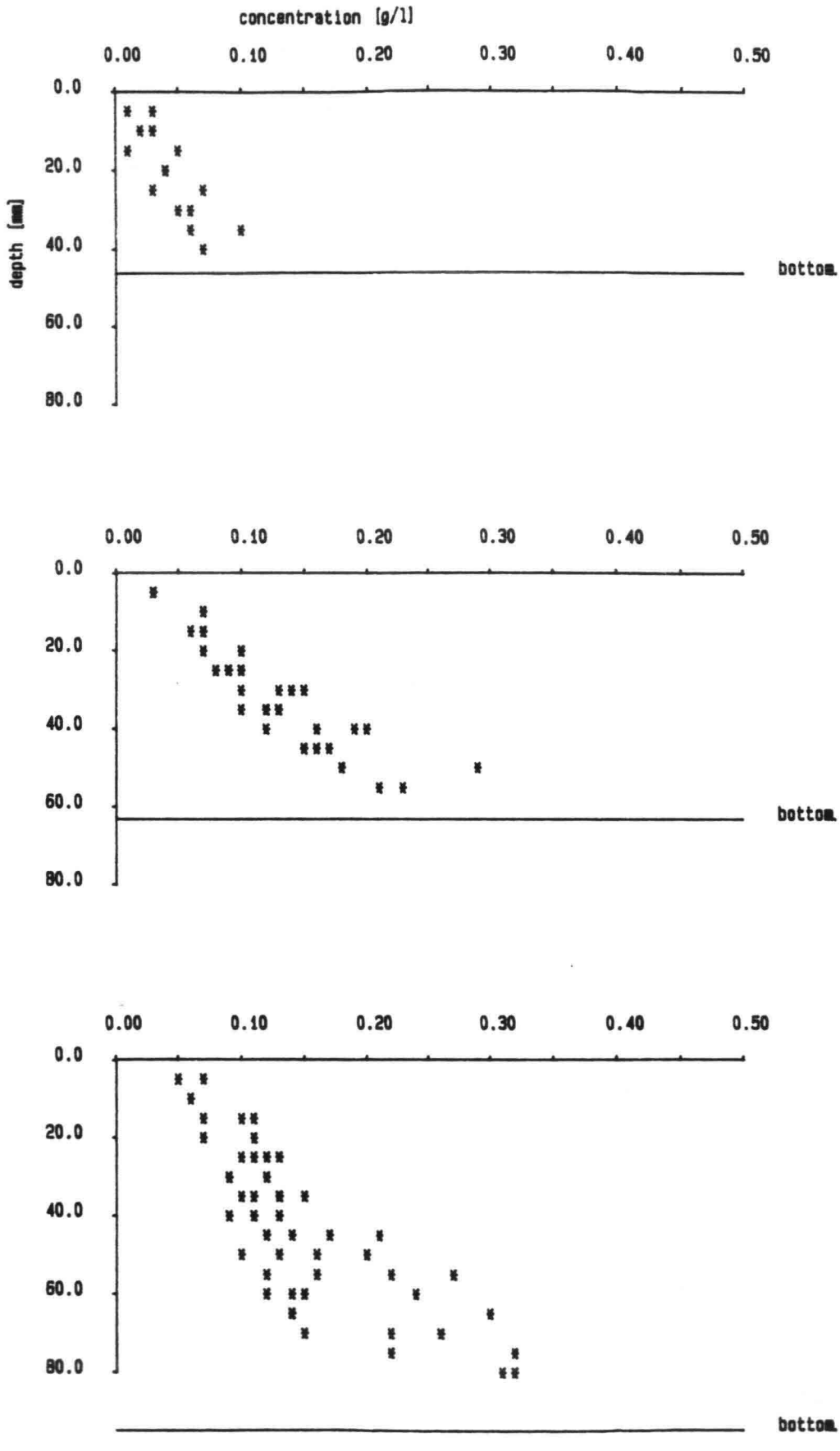

CROSS-SECTION 35

CONCENTRATION PROFILES
(mean water depth of 11 measurements)

FIG. 9 g

DELFT UNIVERSITY OF TECHNOLOGY

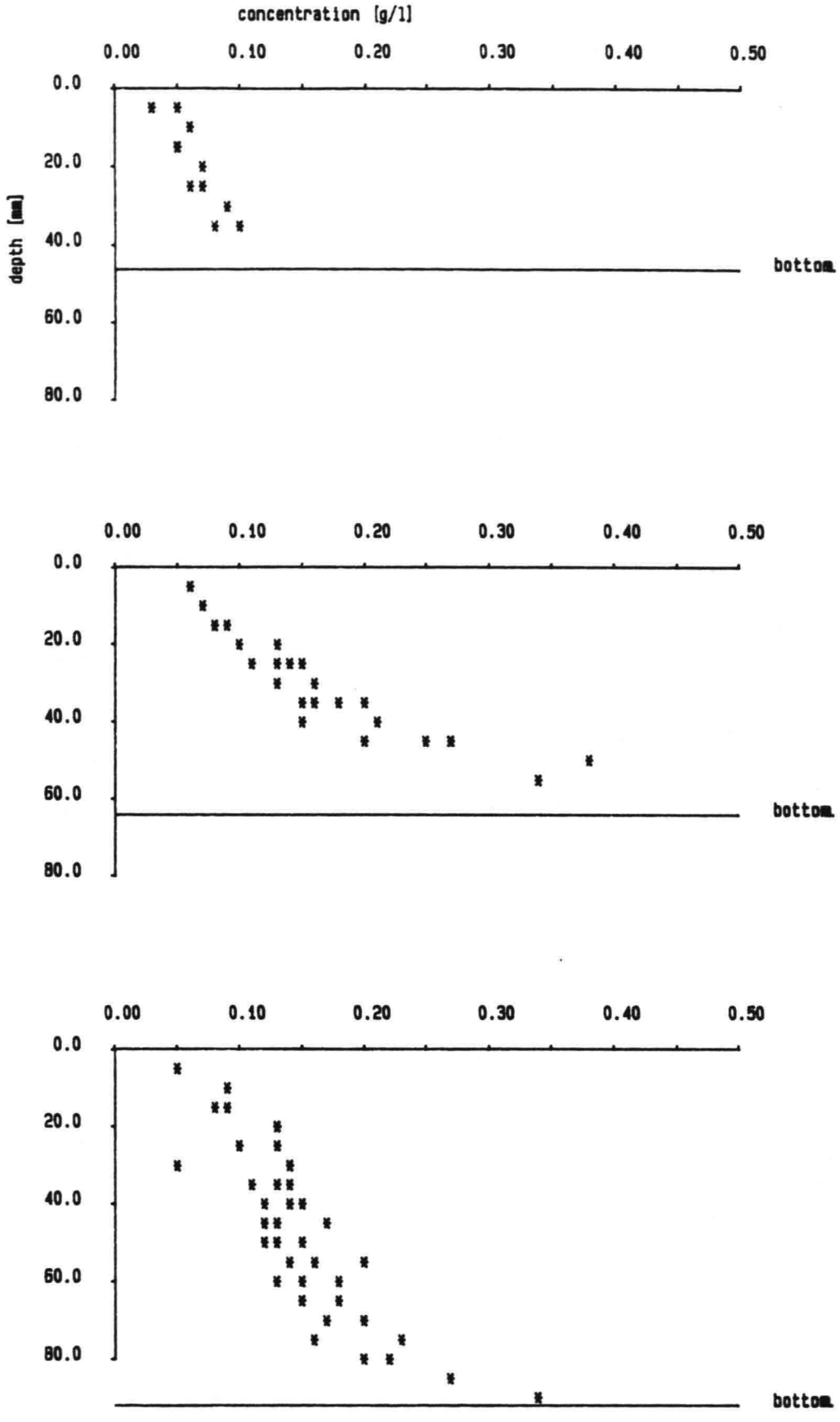

CROSS-SECTION 40

CONCENTRATION PROFILES
(mean water depth of 11 measurements)

FIG. 9 h

DELFT UNIVERSITY OF TECHNOLOGY

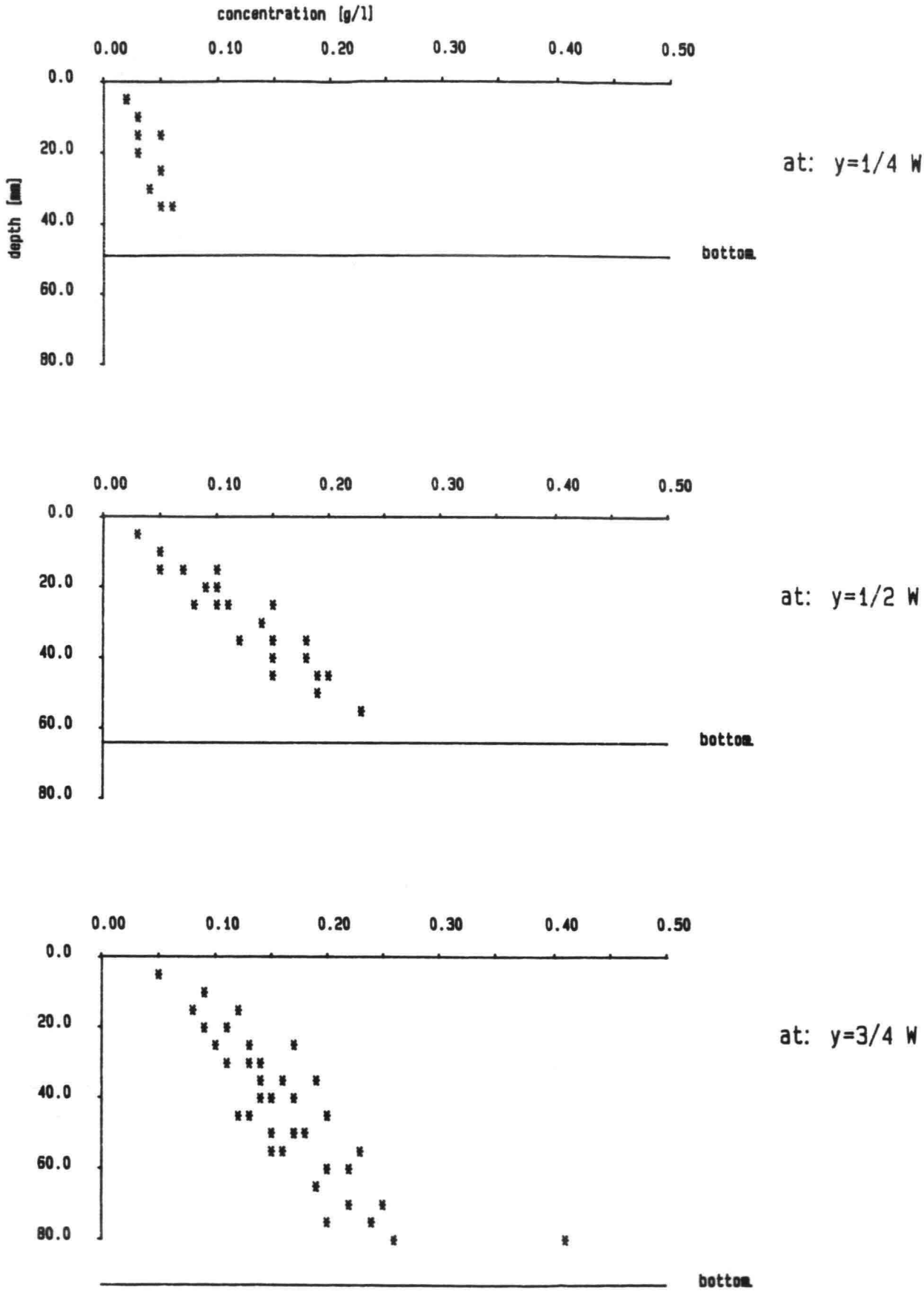

CROSS-SECTION 45

CONCENTRATION PROFILES
(mean water depth of 11 measurements)

FIG. 9 i

DELFT UNIVERSITY OF TECHNOLOGY

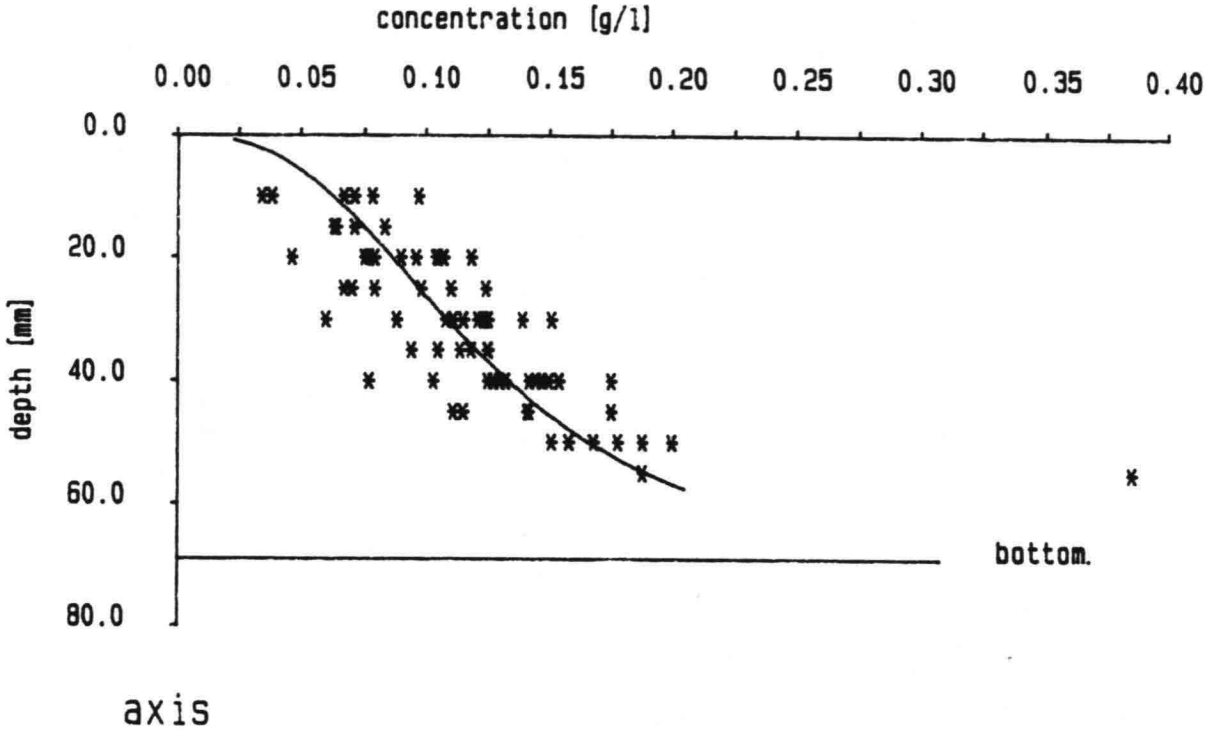

CROSS-SECTION 1

CURVE FIT OF EQUILIBRIUM PROFILE

FIG. 10

DELFT UNIVERSITY OF TECHNOLOGY

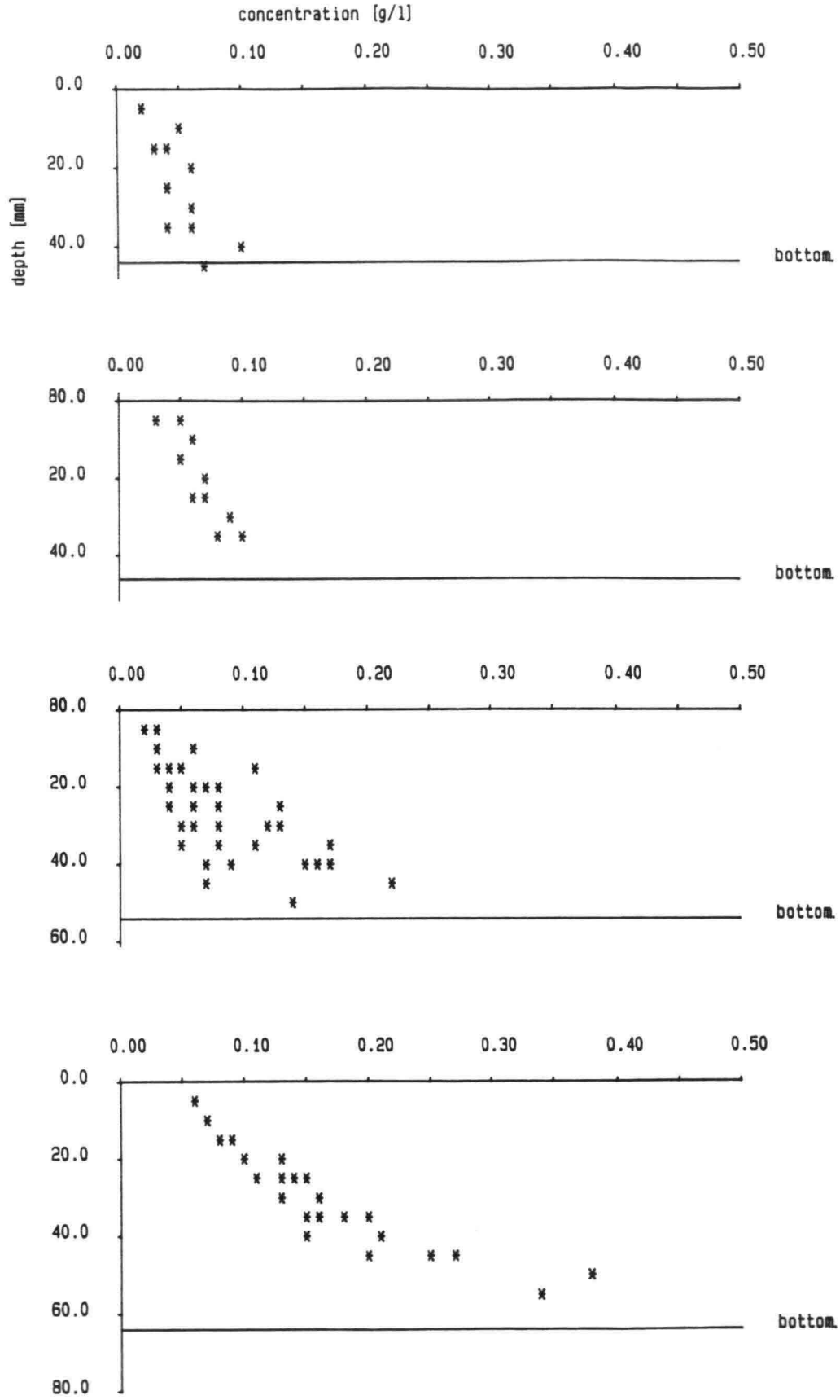

CROSS-SECTION 40

CONCENTRATION PROFILES IN AXI-SYMMETRICAL REGION
(mean water depth of 11 measurements)

FIG. 11 a

DELFT UNIVERSITY OF TECHNOLOGY

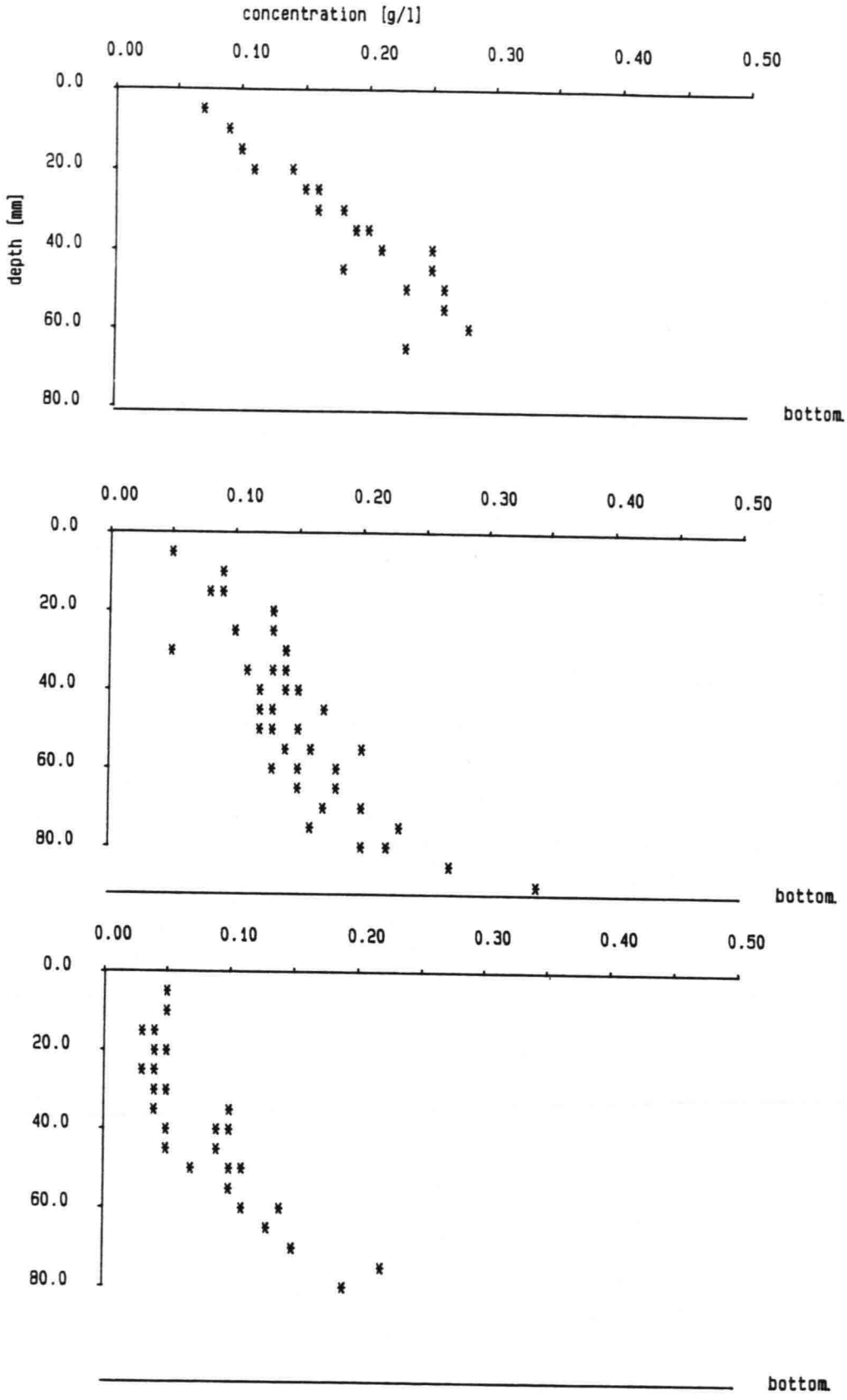

CROSS-SECTION 40

CONCENTRATION PROFILES IN AXI-SYMMETRICAL REGION
(mean water depth of 11 measurements)

DELFT UNIVERSITY OF TECHNOLOGY

FIG. 11 b

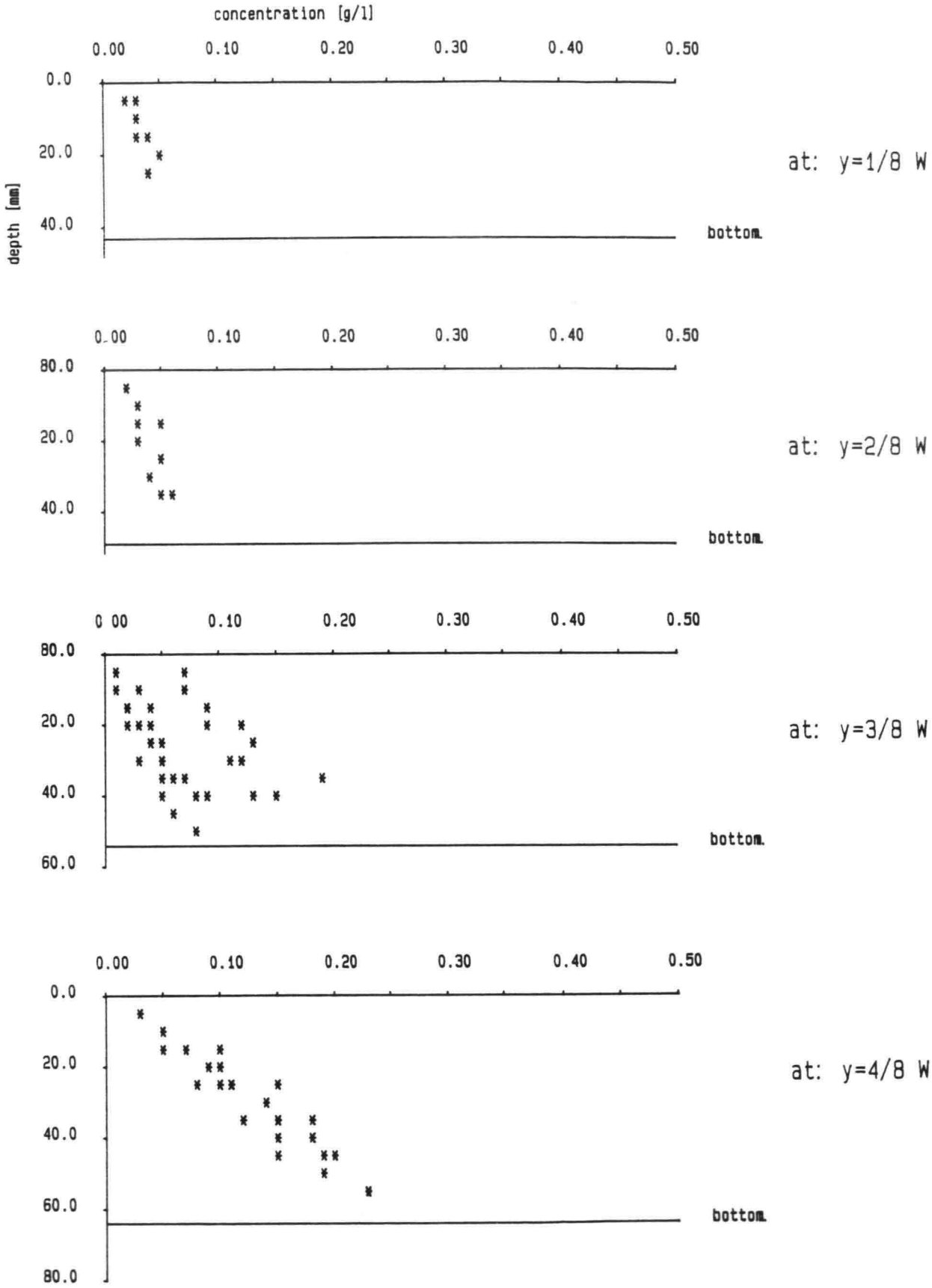

CROSS-SECTION 45

CONCENTRATION PROFILES IN AXI-SYMMETRICAL REGION
(mean water depth of 11 measurements)

FIG. 11 c

DELFT UNIVERSITY OF TECHNOLOGY

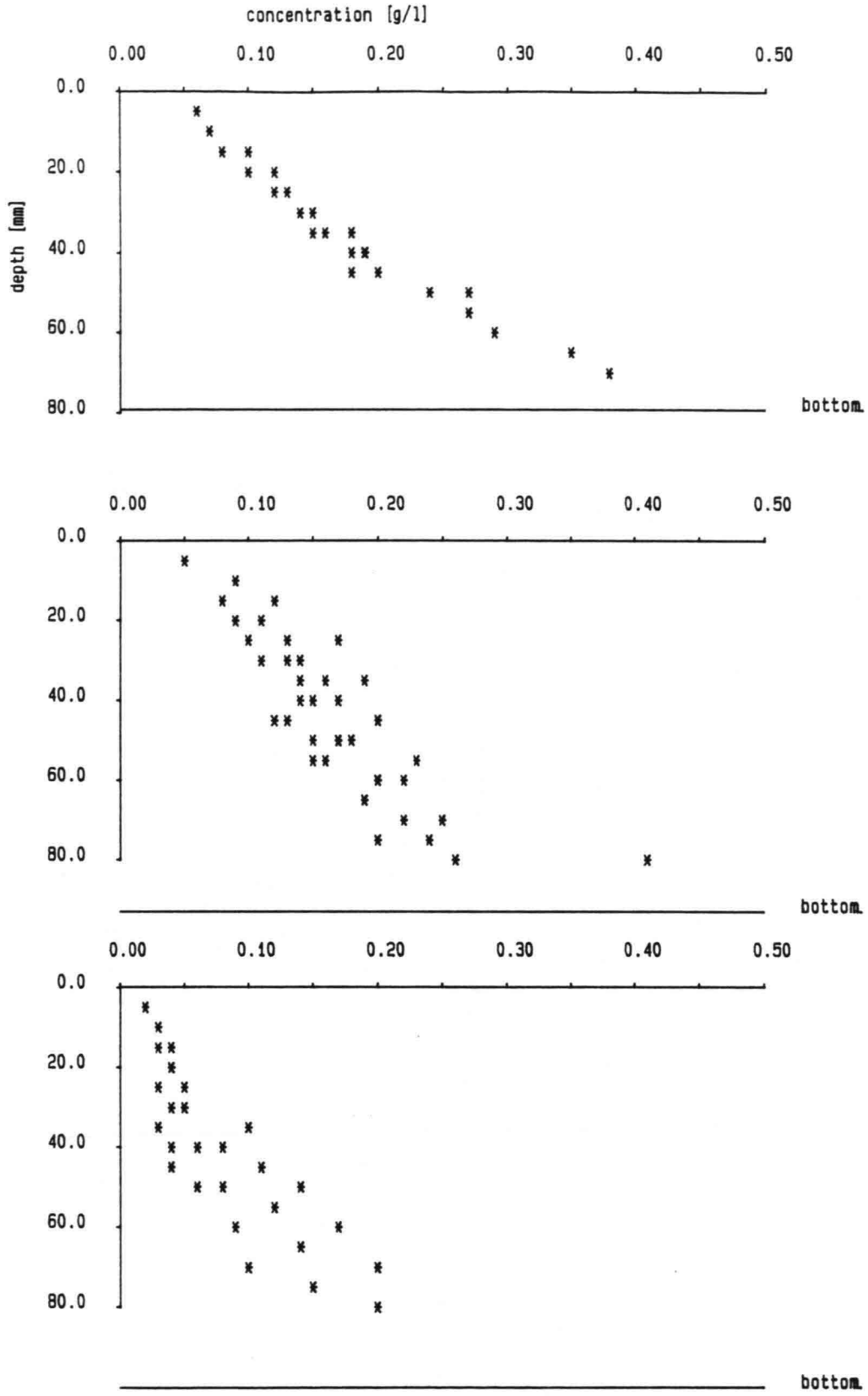

CROSS-SECTION 45

CONCENTRATION PROFILES IN AXI-SYMMETRICAL REGION
(mean water depth of 11 measurements)

FIG. 11 d

DELFT UNIVERSITY OF TECHNOLOGY

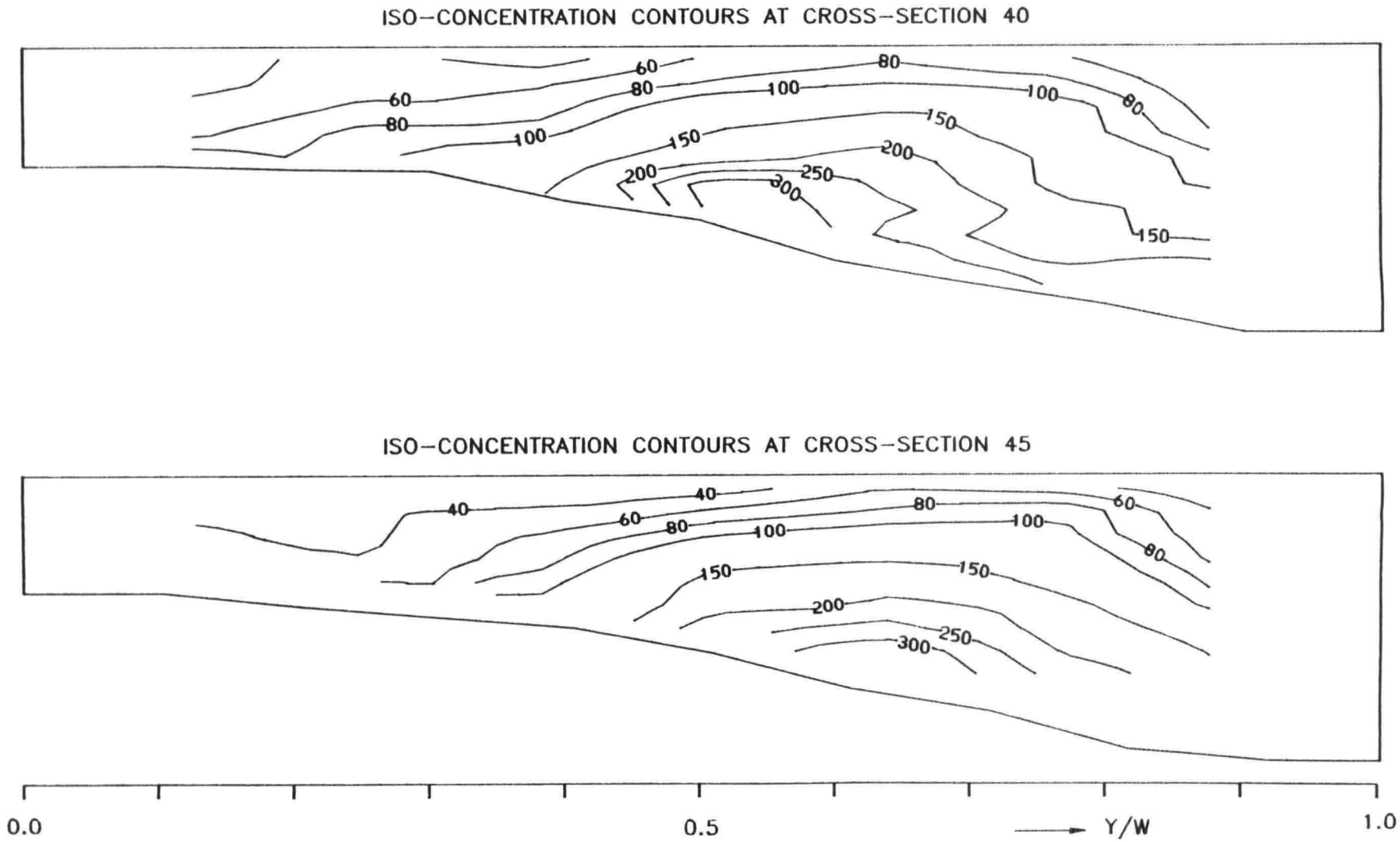

ISO-CONCENTRATION CONTOURS IN THE AXI-SYMMETRICAL REGION, CROSS-SECTIONS 40 AND 45

DELFT UNIVERSITY OF TECHNOLOGY

FIG. 11e

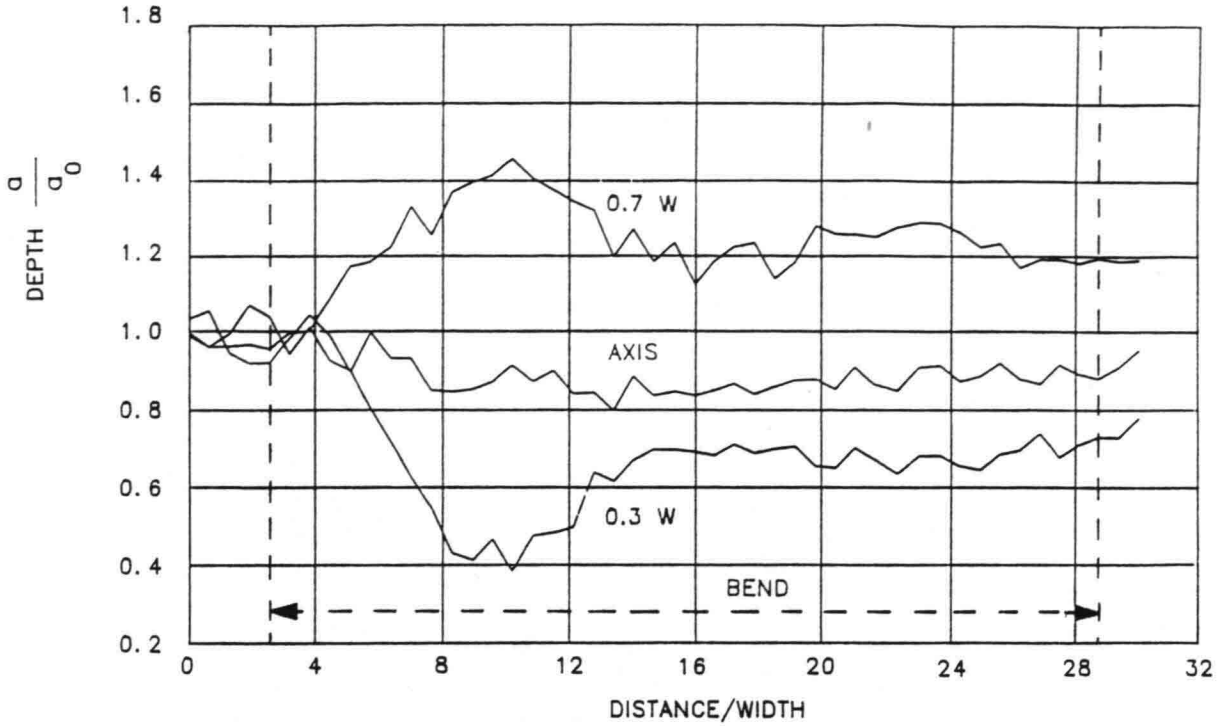

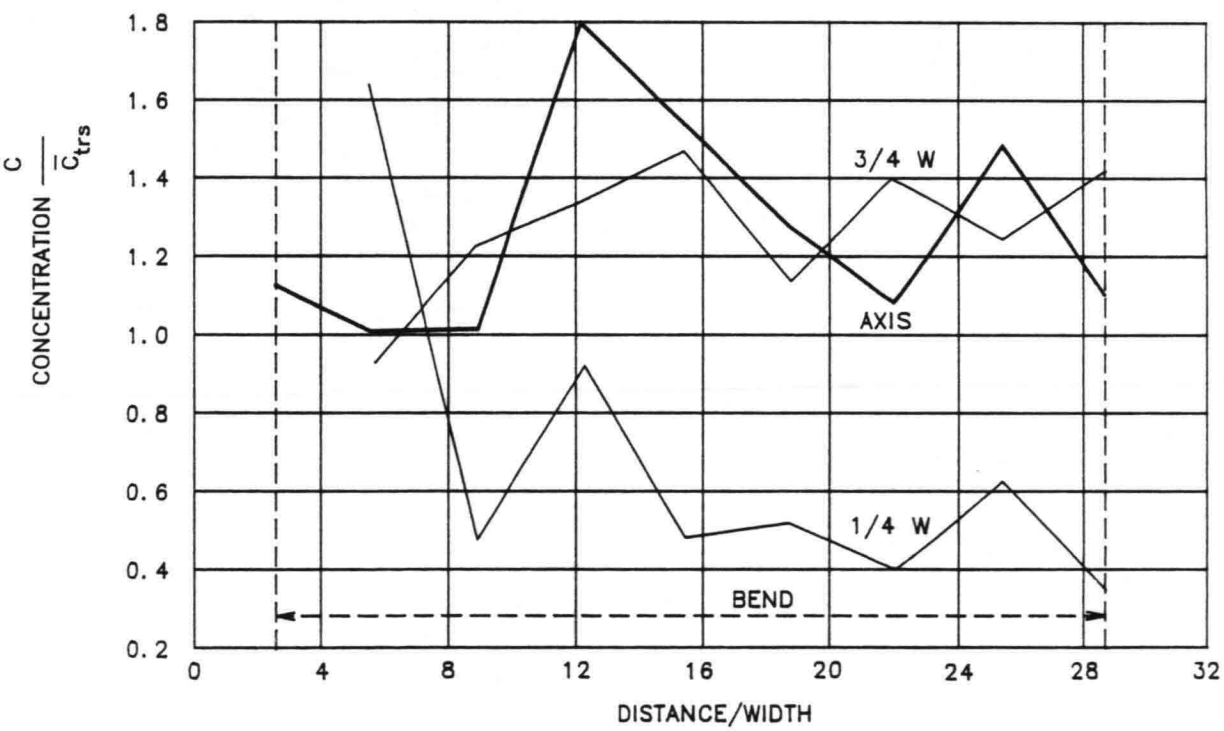

$\bar{c}_{trs} = 0.65\ \bar{c}_{tr}$ $z_r = 0.15\ a$

DEPTH AVERAGED CONCENTRATION FIELD

FIG. 12

DELFT UNIVERSITY OF TECHNOLOGY

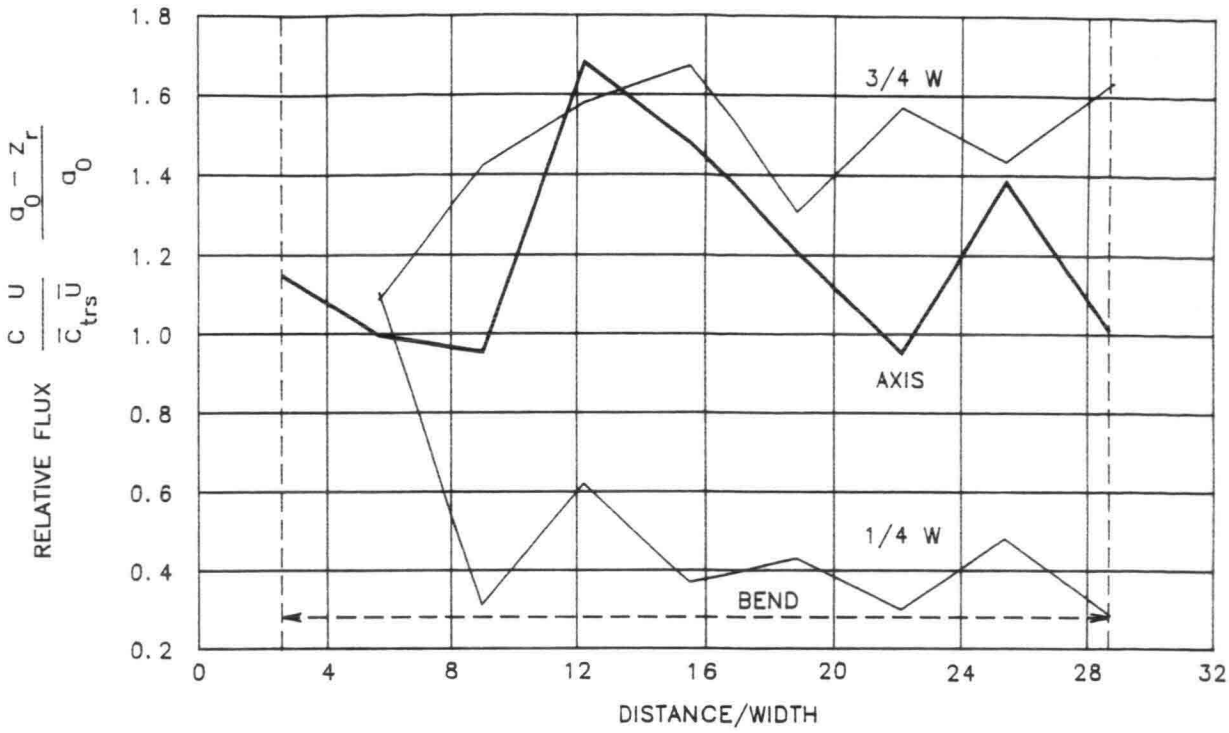

13a DEPTH AVERAGED SUSPENDED TRANSPORT IN S-DIRECTION

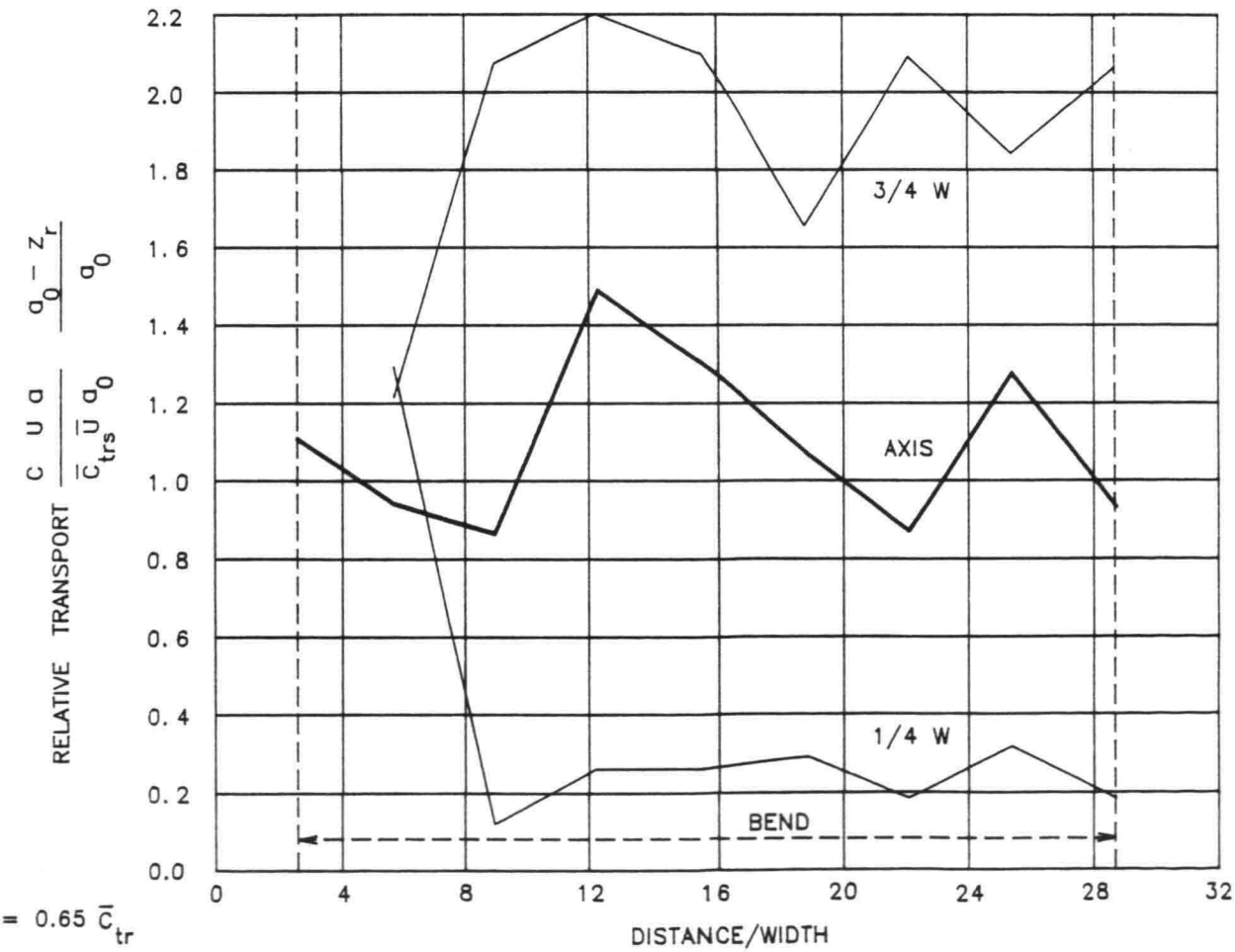

$\bar{c}_{trs} = 0.65\ \bar{c}_{tr}$

$z_r = 0.15\ a$

13b DEPTH INTEGRATED SUSPENDED TRANSPORT IN S-DIRECTION

13a DEPTH AVERAGED SUSPENDED TRANSPORT IN S-DIR. 13b DEPTH INTEGRATED SUSPENDED TRANSPORT IN S-DIR.	FIG. 13a FIG. 13b
DELFT UNIVERSITY OF TECHNOLOGY	